INSTYTUT FIZYKI PLAZMY I LASEROWEJ MIKROSYNTEZY
IM. SYLWESTRA KALISKIEGO

Advances in the development of gas detectors as plasma radiation diagnostic devices

Maryna Chernyshova on behalf of the Project Teams

HTPD 2024: 25th Topical Conference on High Temperature Plasma Diagnostics, 21-25.04.2024, Asheville, North Carolina

Outline

- Introduction: Principles of the GEM detector
- Design and status of the GEM detector for tomographic applications in the WEST project
- Radiation power measurement for DEMO
- GEM detector based imaging
- Use of the GEM detector for high-resolution SXR crystal spectroscopy at JET

Motivation

Looking for new technology for fusion reactors (the gas detectors appear to be among the most reliable and weakly degrading over time, unlike e.g. semiconductor or MCP detectors, whose sensitivity can drop several times over several years):

- ITER => decision to use advanced detectors for SXR system exhibiting high resilience to neutrons and gamma rays, such as gas-filled detectors,
- DEMO => metal bolometers expected to mutate, otherwise too low intensity behind the bioshield.

Imaging systems:

- Large plasma volume,
- Toroidal view.

Gas ionisation chamber

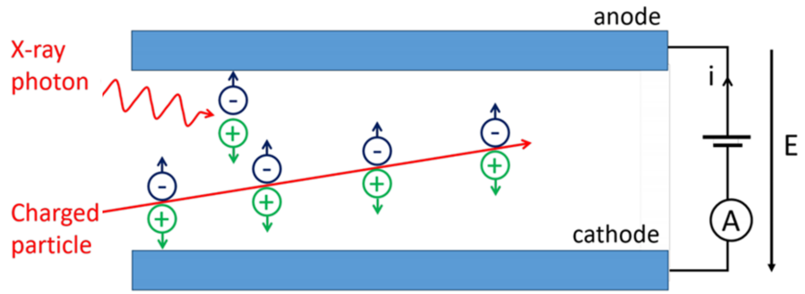

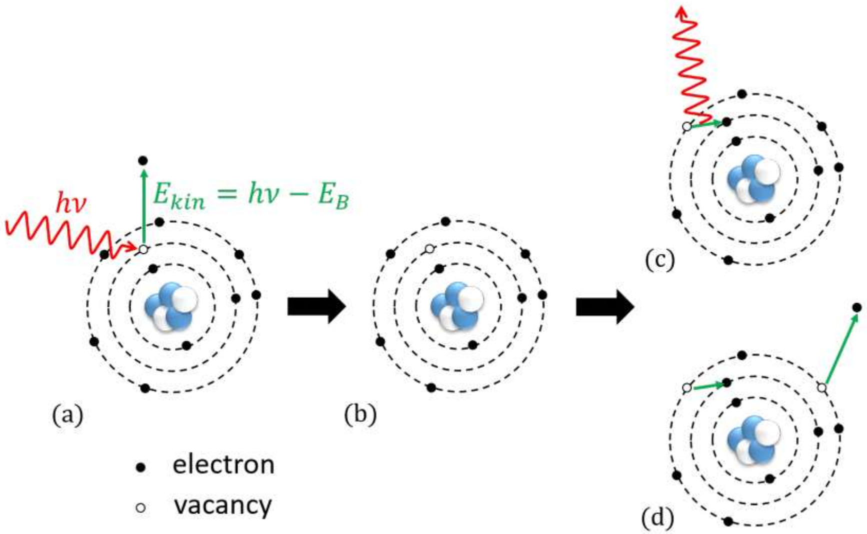

Different stages of the photoionization process:

(a) *absorption* of the photon, ionization of the atom, a bound electron with $E_{kin} = h\nu - E_B$, E_B - electron bound energy
(b) *excited ion,*
(c) *de-excitation* through X-ray fluorescence with a given probability P_f,
(d) *de-excitation* through Auger electron emission

X-ray fluorescence ($h\nu > E_X$), the lost charge $\Delta C_f = E_B/W$, W - the mean ionization energy of the gas => **escape peak** in the measured spectrum

Argon: P_f = 14%, E_X = 3.2 keV, E_B = 2.9 keV, W = 26 eV

D. Mazon et al., poster at EPS 2023

Gas Electron Multiplier (GEM) detector principle

GEM foils invented in the 90-s at CERN by Fabio Sauli

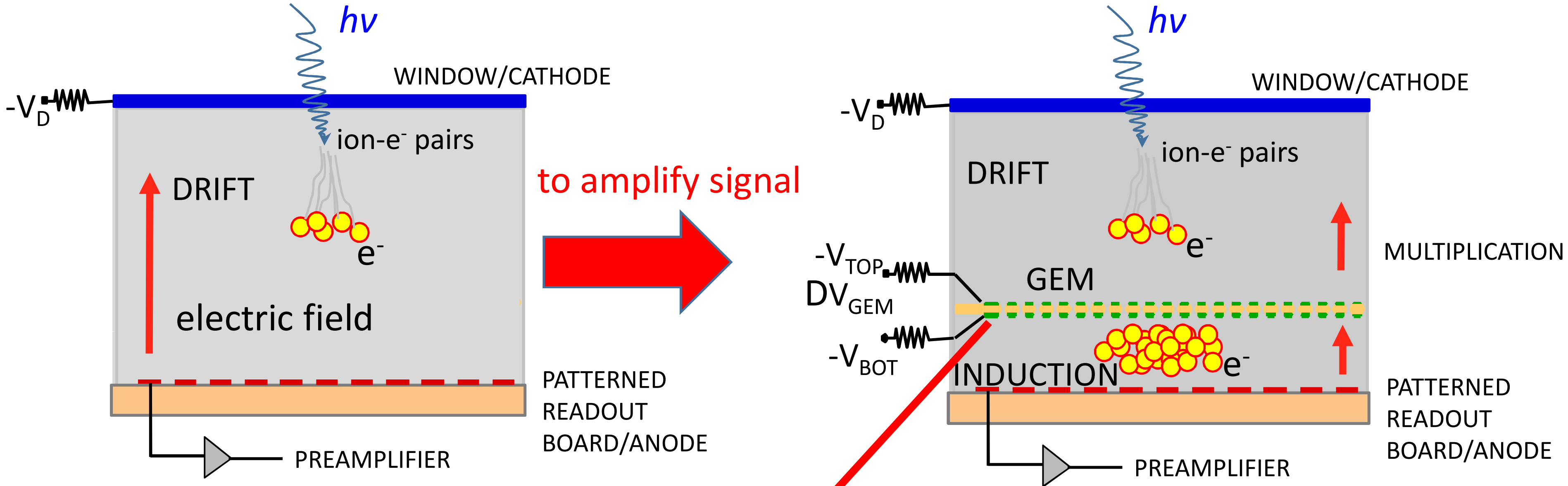

GEM foil

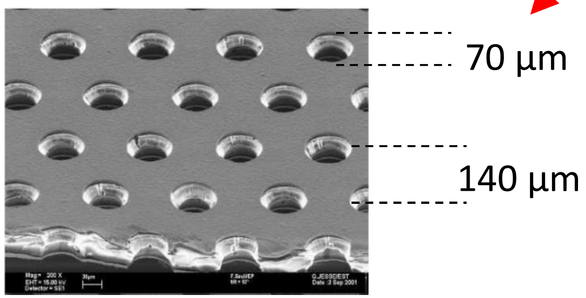

F. Sauli et al., Nucl. Instr. and Meth. A 505 (2003) 195

Gmsh/Elmer electric field distribution for HV values from drift to induction: 1500/360/700/360/700/360/ 900V

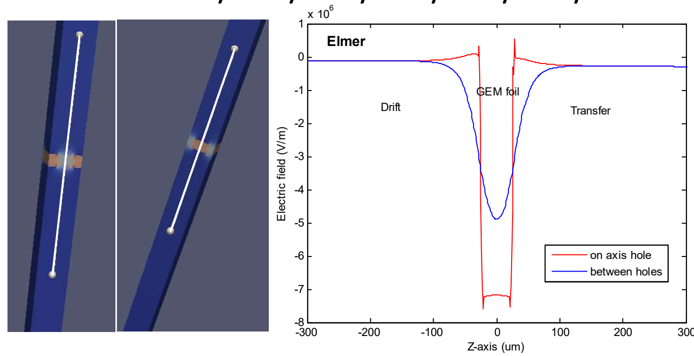

Gas Electron Multiplier (GEM) detector principle

GEM foils invented in the 90-s at CERN by Fabio Sauli

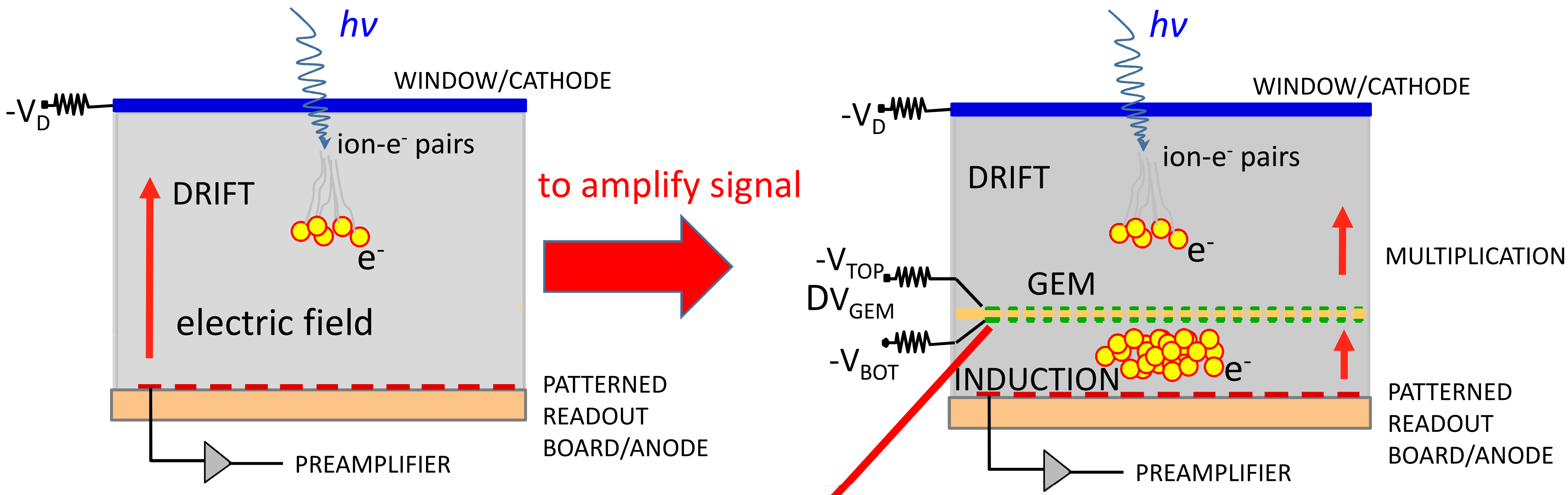

GEM foil

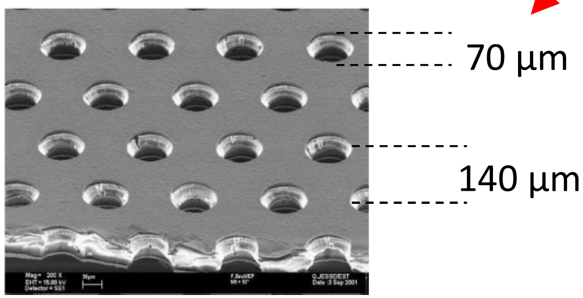

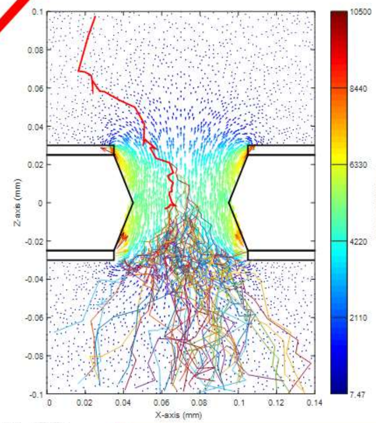

Vector plot of electric field in the GEM foil's hole (HV_{GEM}=360V) in XZ plane and calculated in Garfield++ example trajectory of the electron passing through the hole. In this case 98 electrons were produced, 43 of them formed a signal on the readout electrode.

F. Sauli et al., Nucl. Instr. and Meth. **A 505** (2003) 195

Triple-GEM: readout signals

A few micrometers thick mylar window with a thin, 0.2 μm, Al layer

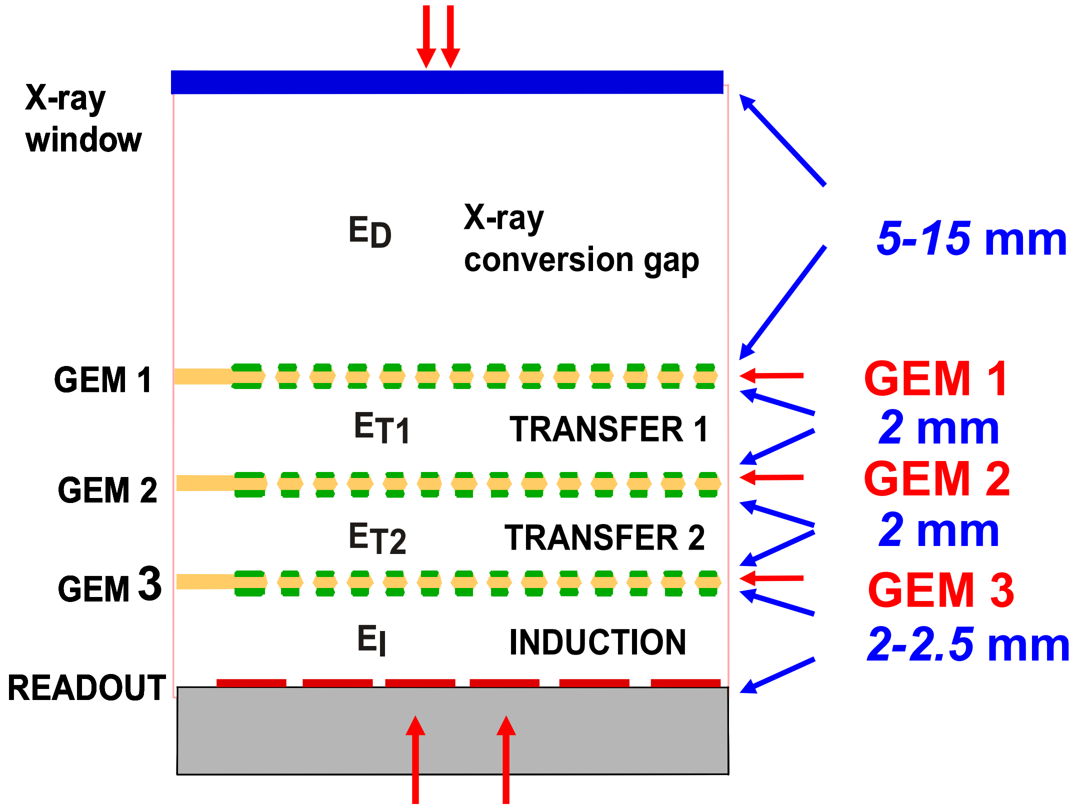

Readout plane with strip pitch

Single photon generates signal on a few anode pixels

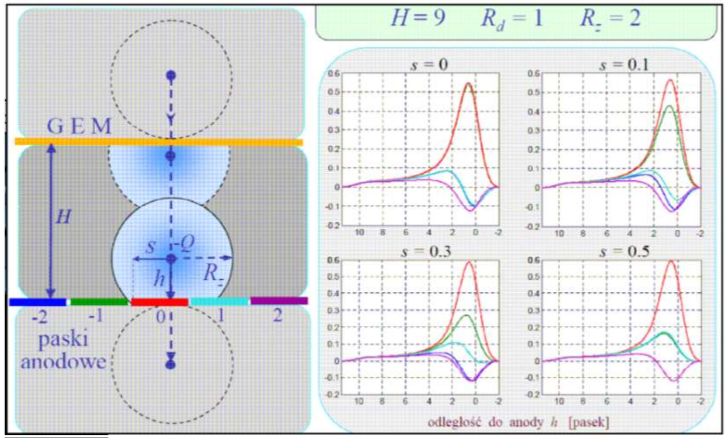

Triple-GEM: readout signals

Position reconstruction based on center of gravity among neighboring signals

^{55}Fe $\xrightarrow{\text{electron capture}}$ ^{55}Mn → E_γ = 5.9 keV

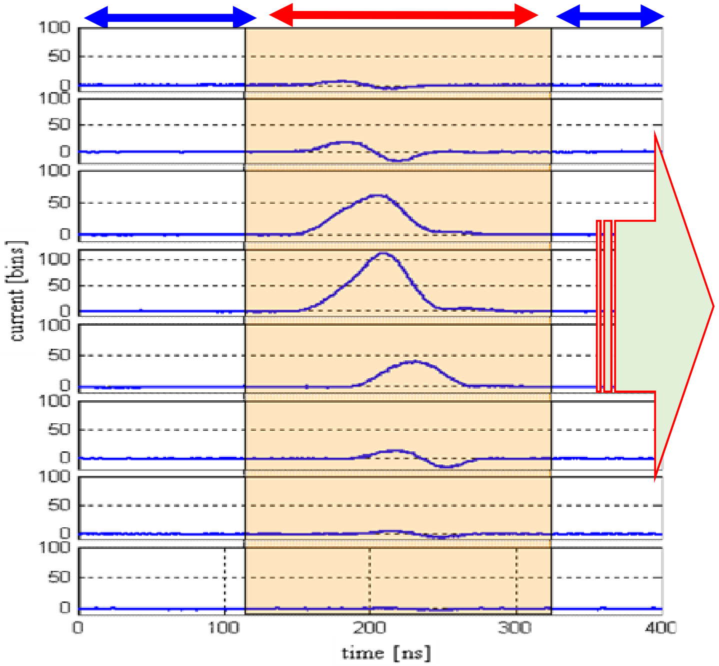

Anode current signals for 8 strips (without offset compensation) calculated within time of 200 ns (marked window)

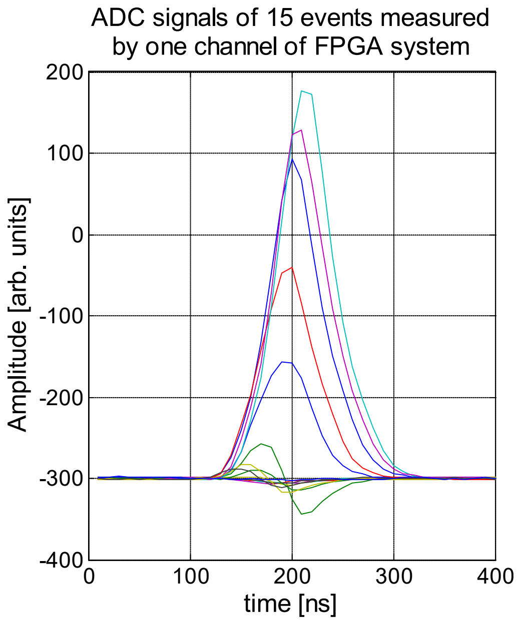

Example of digitized anode signals

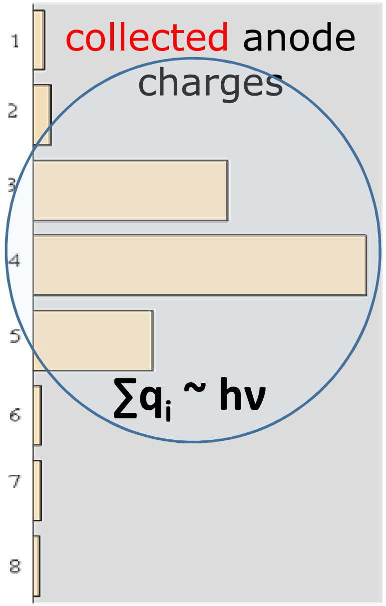

Corresponding relative charges (without offset compensation) calculated within time of 200 ns (marked window)

Total cluster charge ~ single photon energy

Triple-GEM: readout signals

Spatial resolution => cluster position => determined by pixel

- The cluster charge is dispersed within a number of pixels.
- Each pixel corresponds to a corresponding part of the detection area. The probability of finding an event in the part of the detector corresponding to a given pixel can be defined as the relative pixel charge of the corresponding cluster.
- The position of the cluster charge is considered to be scattered according to the relative charge values of the pixels.

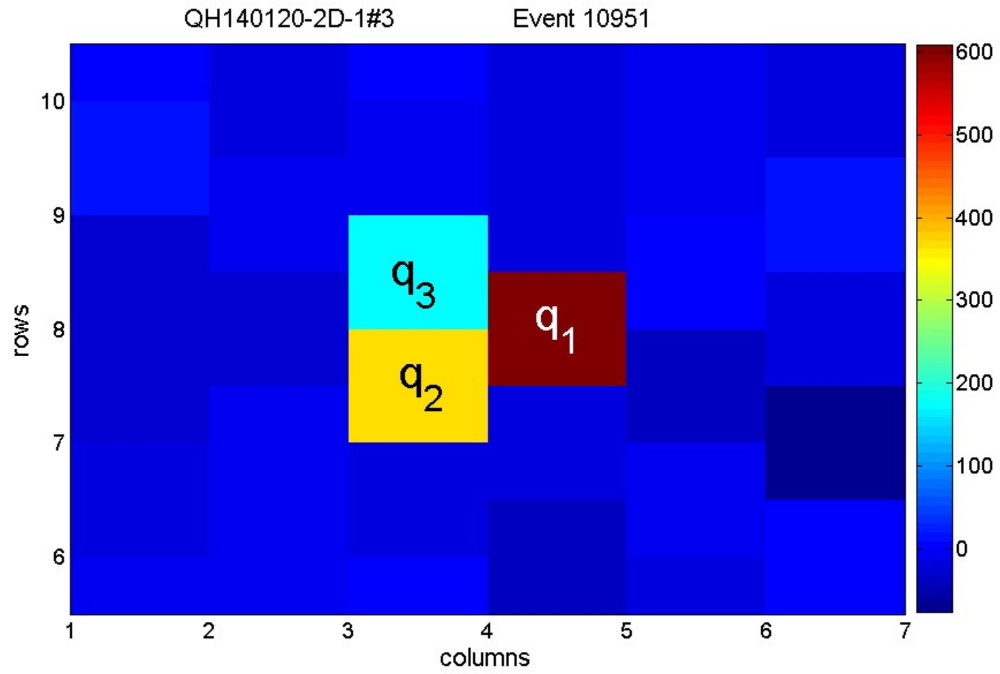

Pixel charges:

$Q_1 = 1215$ $Q_2 = 734$ $Q_3 = 350$

Cluster chargé:

$Q = Q_1 + Q_2 + Q_3 = 2299$

Pixel share for the cluster position:

$q_1 = Q_1/Q = 0.5285$

$q_2 = Q_2/Q = 0.3193$

$q_3 = Q_3/Q = 0.1522$

Spectral characteristics

Cluster charge distribution

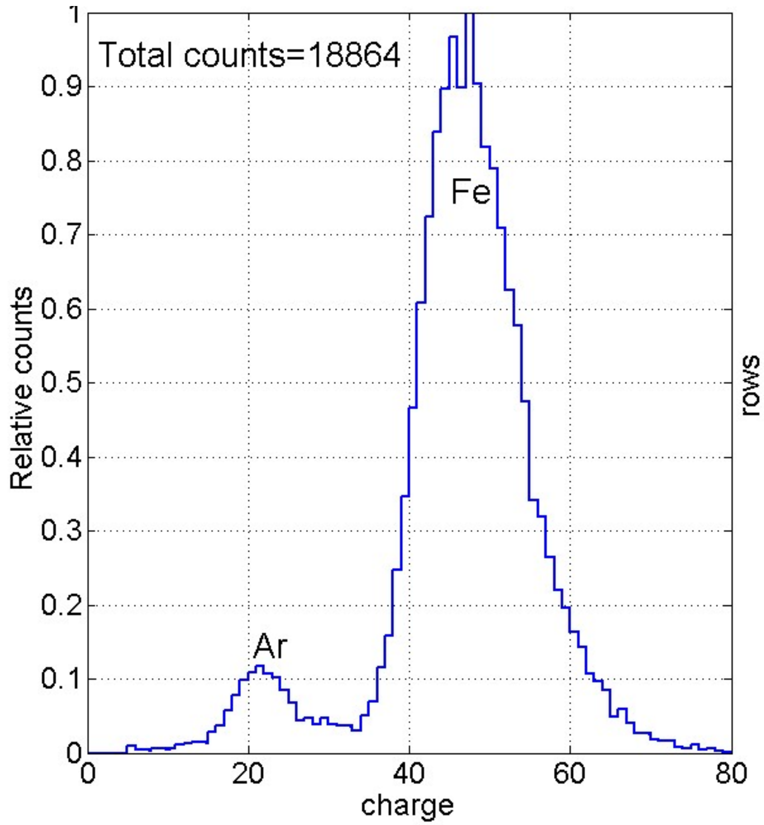

Cluster position distribution

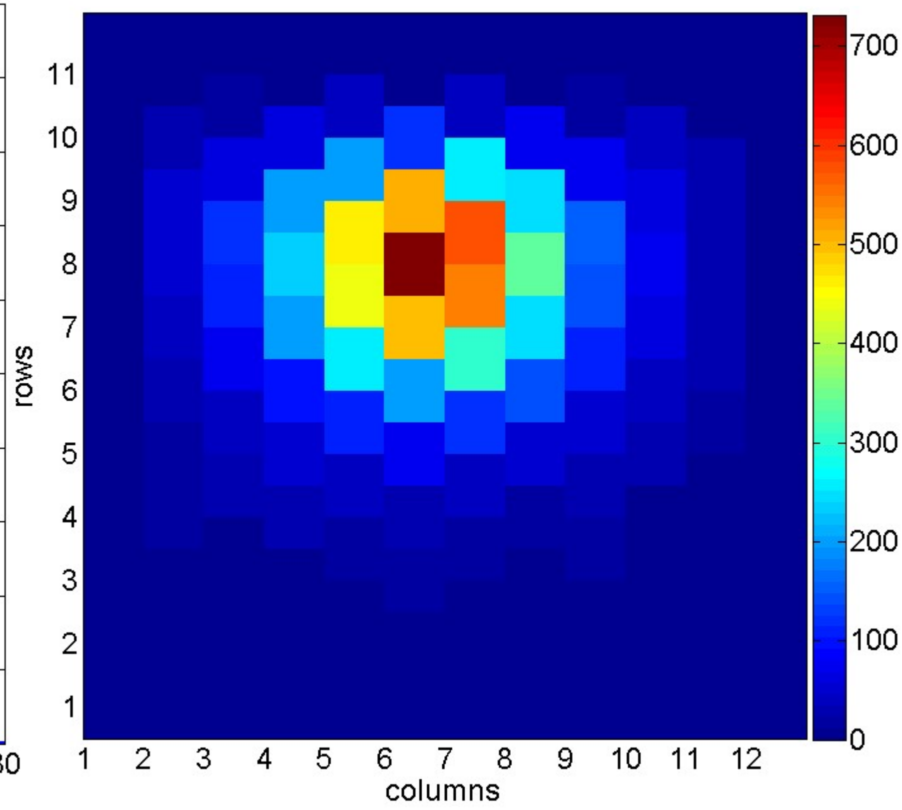

Measurements with ^{55}Fe source – energy/charge and spatial distribution of the radiation

Design and development for WEST tokamak

M. Chernyshova[1], K. Malinowski[1], T. Czarski [1], A. Wojeński[2], D. Mazon[3], E. Kowalska-Strzęciwilk[1], G. Kasprowicz[2], P. Malard[3], S. Jabłoński[1], D. Vezinet[4], P. Linczuk[2], F. Jaulmes[3], A. Ziółkowski[1], A. Jardin[3], B. Bieńkowska[1], R. Prokopowicz[1], W. Figacz[1], K. Poźniak[2], W. Zabołotny[2], A. Byszuk[2], P. Zienkiewicz[2], R. Krawczyk[2], P. Kolasiński[2], S. Eder[4]

[1]*Institute of Plasma Physics and Laser Microfusion, Warsaw, Poland*

[2]*Warsaw University of Technology, Institute of Electronic Systems, Warsaw, Poland*

[3]*Commissariat à l'energie atomique, Cadarache, France*

[4]*Max-Planck-Institut für Plasmaphysik, Garching, Germany*

Development since 2014

IFPiLM

Design and development for WEST tokamak

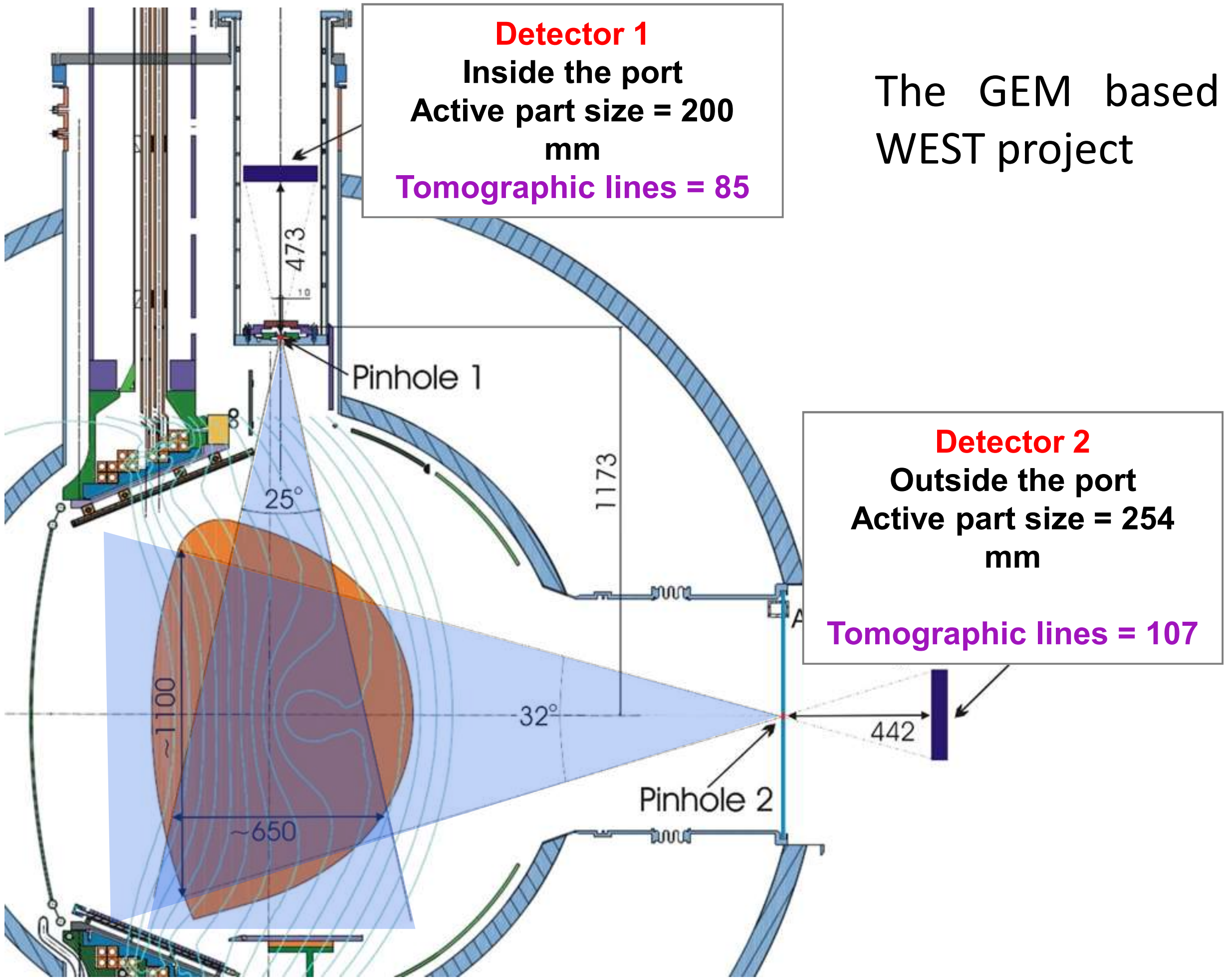

The GEM based tomography setup at the WEST project

M. Chernyshova et al., JINST 10 (2015) P10022

Design and development for WEST tokamak

Horizontal detector chamber

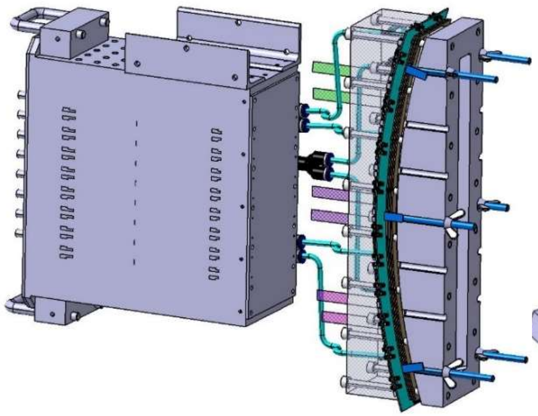

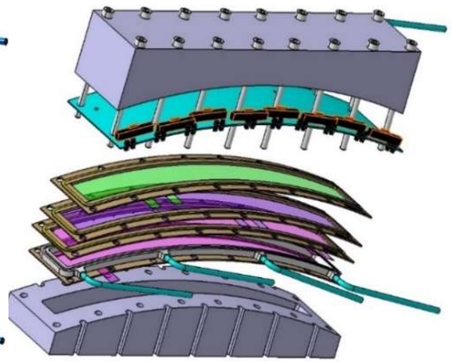

Vertical detector chamber

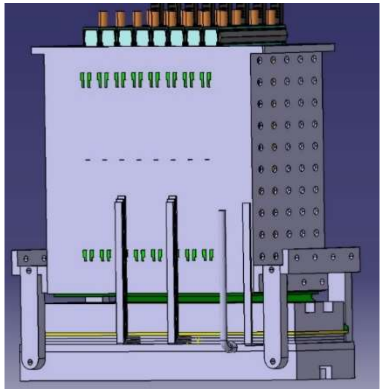

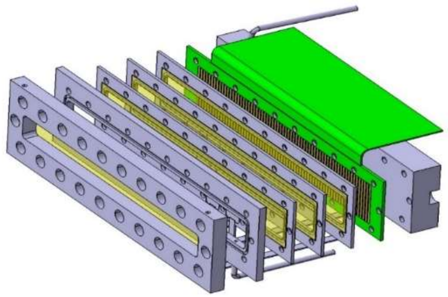

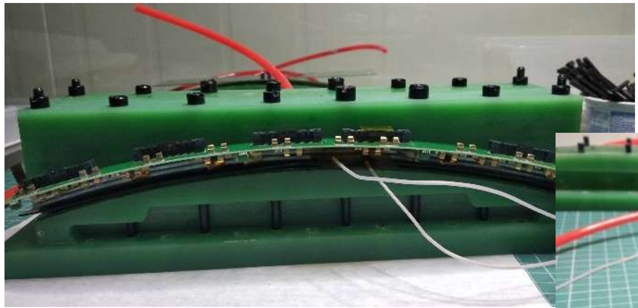

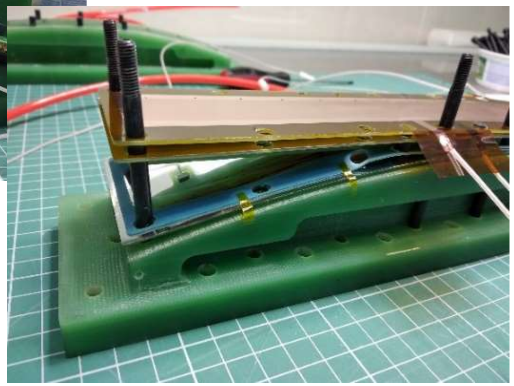

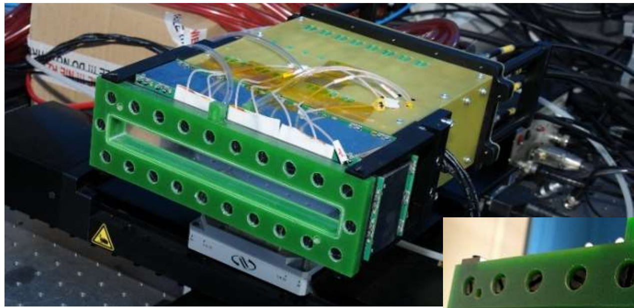

Acquisition system

Amplifiers, multiplexers, serializers, diodes, transistors => radiation tolerant to minimum of 50kRad

- The detector signals processing with 1 ms of real time resolution / full raw data acquisition for post-processing analysis down to 100 μs
- Wide bandwidth of analogue electronics module (80 MHz) => requires shielding against electromagnetic interference

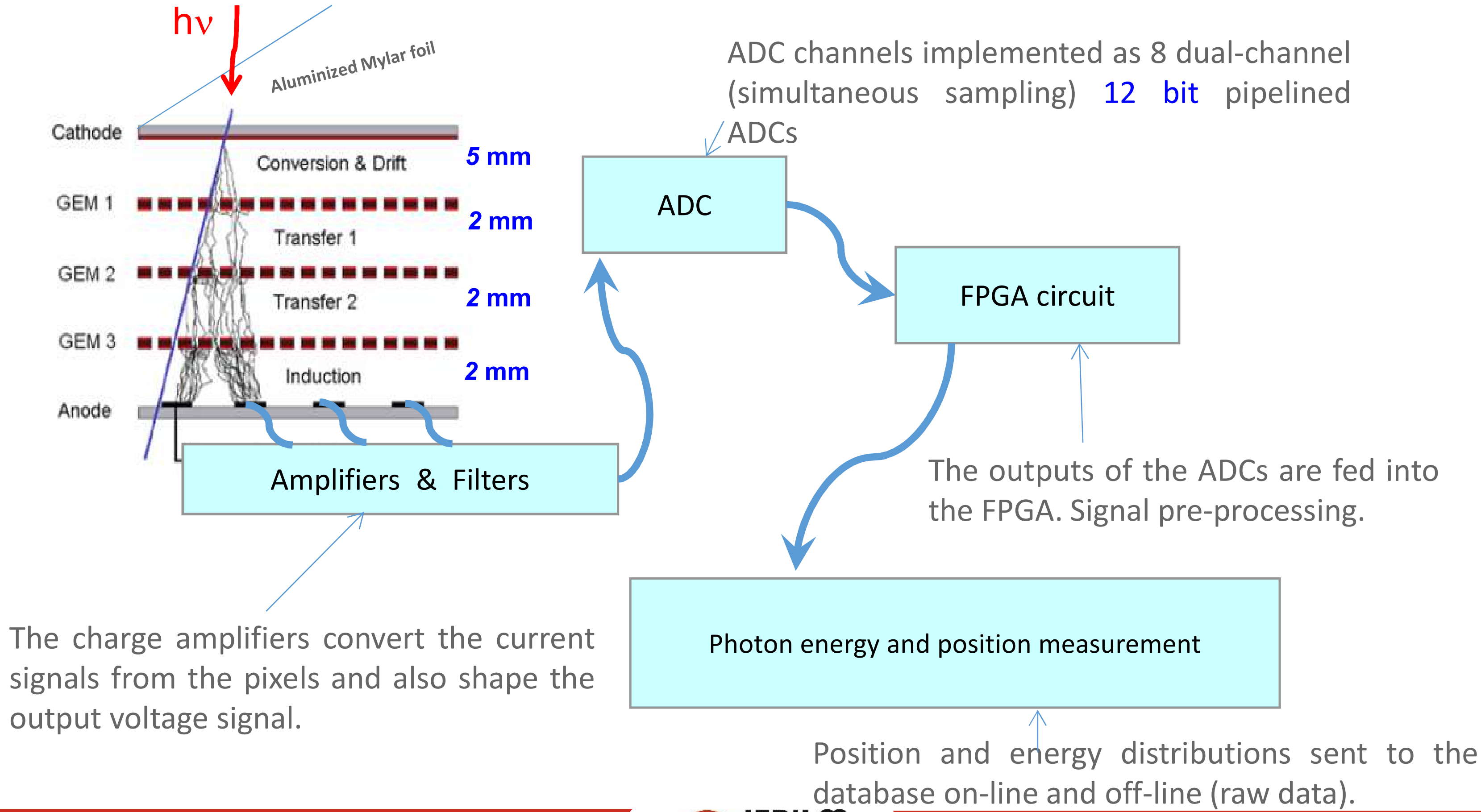

Magnetic field impact

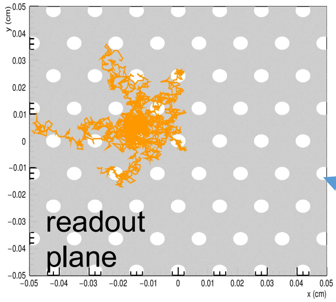

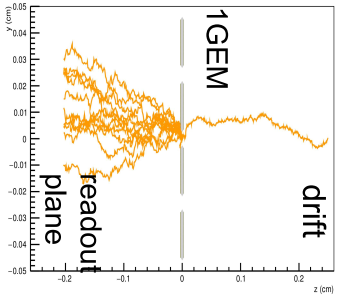

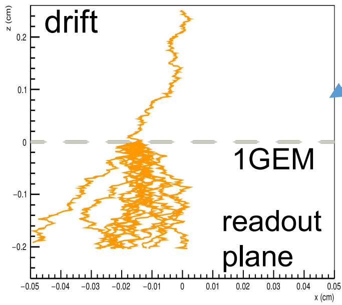

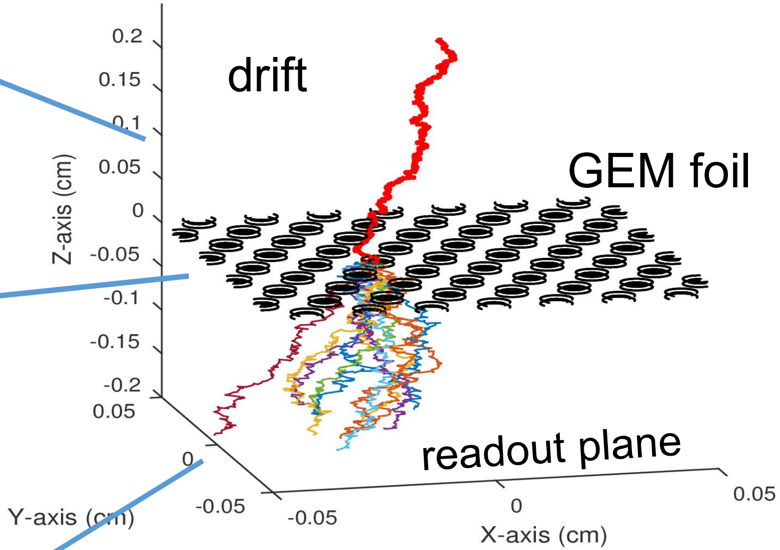

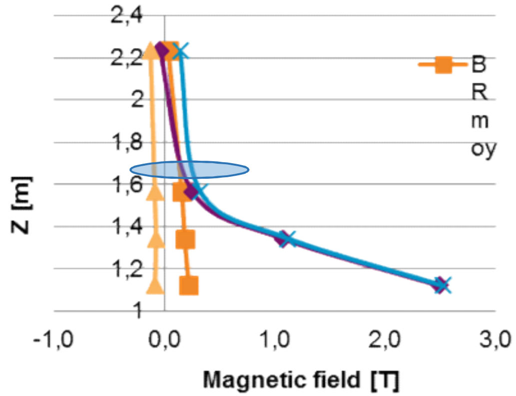

Magnetic field at the vertical detector location calculated by ANSYS code.

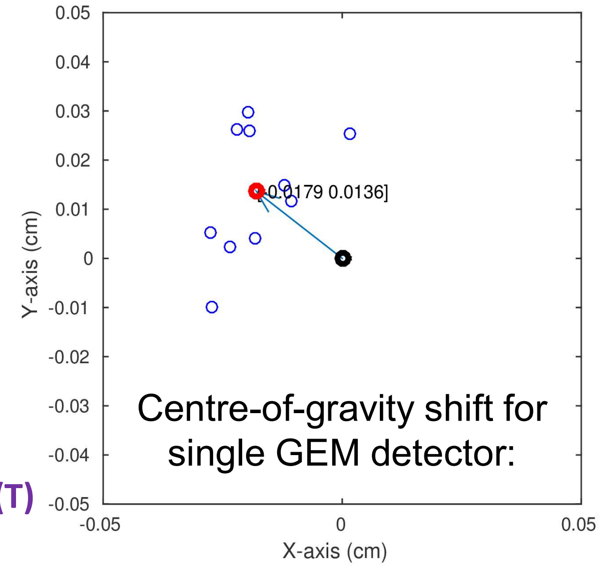

GARFIELD++ code simulations:

E_o= 0 eV; start at (0,0,0.25) cm

B_x=0.1494 B_y=0.0413 B_z=-0.090 (T)

Deflection limit - about 0.2 mm in (x, y) plane

Vertical detector

- Complete system for the vertical port with 85 LOS (103 DAQ channels),
- Permanent access, control and data acquisition through Control Room over internal network,
- Operation with the global trigger acquisition mode,
- Connected, verified and working external trigger from WEST tokamak for acquisition directly related with plasma cycle (start and stop), timescale is proper for comparison with other diagnostics,
- System measures plasma radiation during the experimental campaigns,
- First automatic acquisition mode was implemented for registration of ^{55}Fe and plasma without user operation
- Various configurational and arrangement works.
-

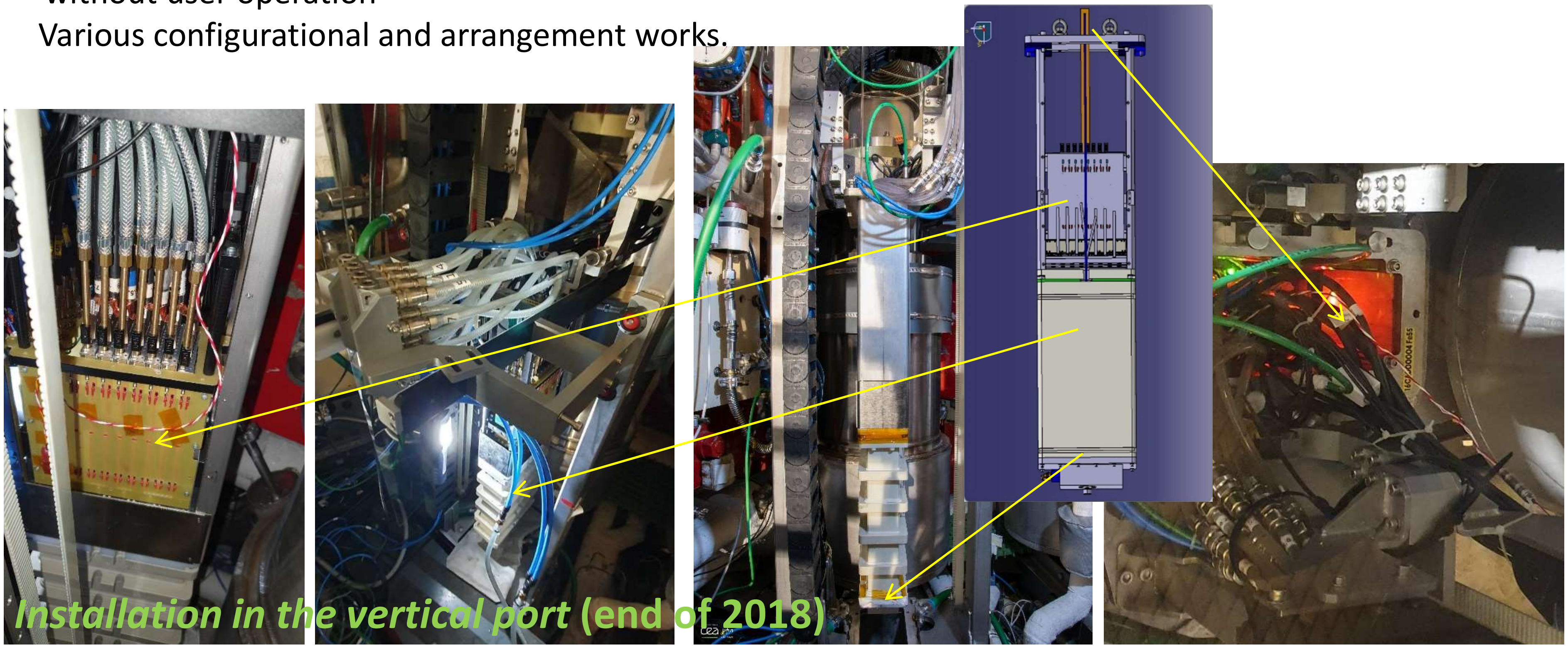

Installation in the vertical port (end of 2018)

Experimental setup for data validation

The diagnostic is undergoing various modifications concerning the acquisition mode, optimisation of numerical codes, improvement of diagnostic components and geometry layout, preparation for operation under long discharges conditions.

SXR diagnostics
GEM detector
Photon counting
Energy discrimination

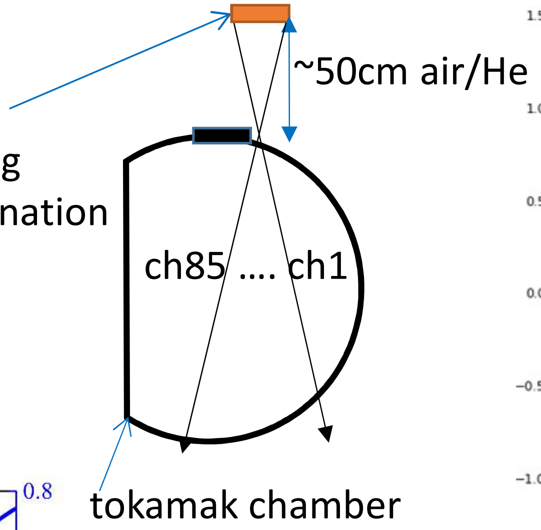

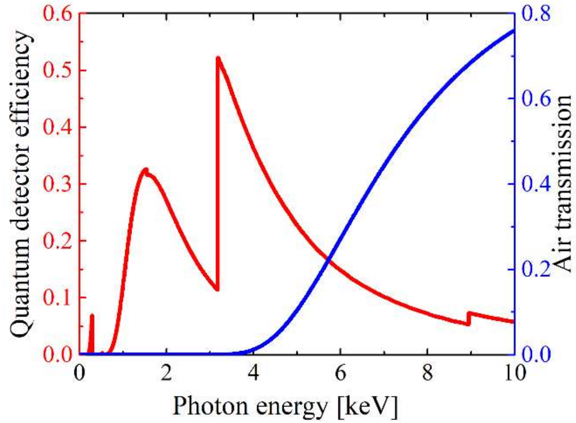

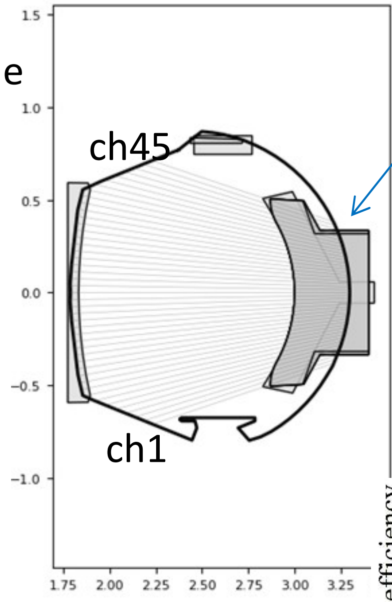

SXR diagnostics
DTOMOX (silicon diodes)
Current mode
Integrated SXR recording

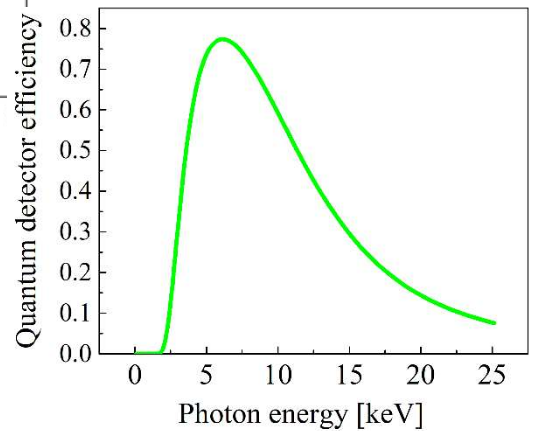

Validation and commissioning of diagnostics

Pulse #58327 parameters:

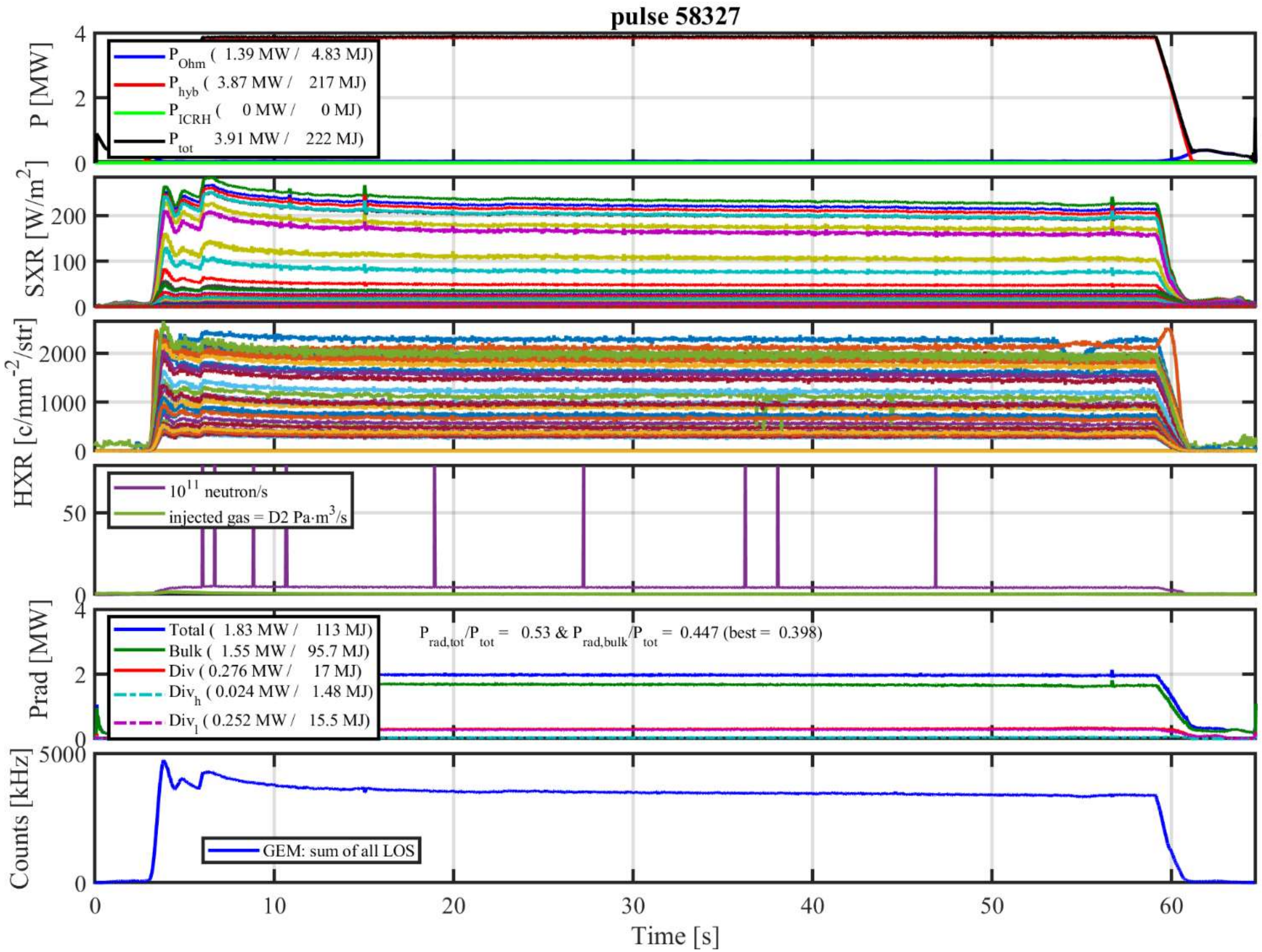

Validation and commissioning of diagnostics

c_W determination by SXR horizontal camera modeling:

$$\varepsilon_W^{\eta} = \int \eta(h\nu)\varepsilon_W(h\nu, T_e)dh\nu = n_e . n_W . L_W^{\eta}(T_e)$$

L_W^{η} : radiating function of W filtered by the detector

$$\boxed{c_W = 2 \times 10^{-4}}$$

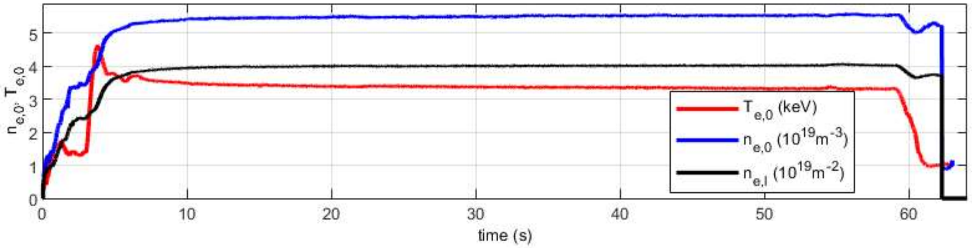

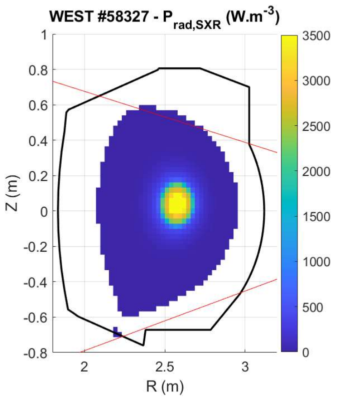

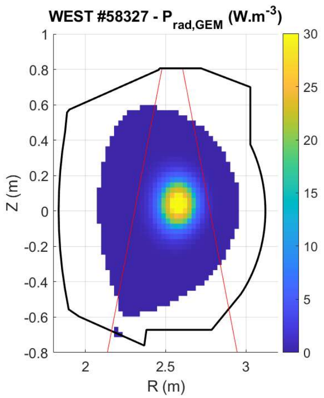

Radiative power modelling from SXR horizontal and vertical GEM cameras.

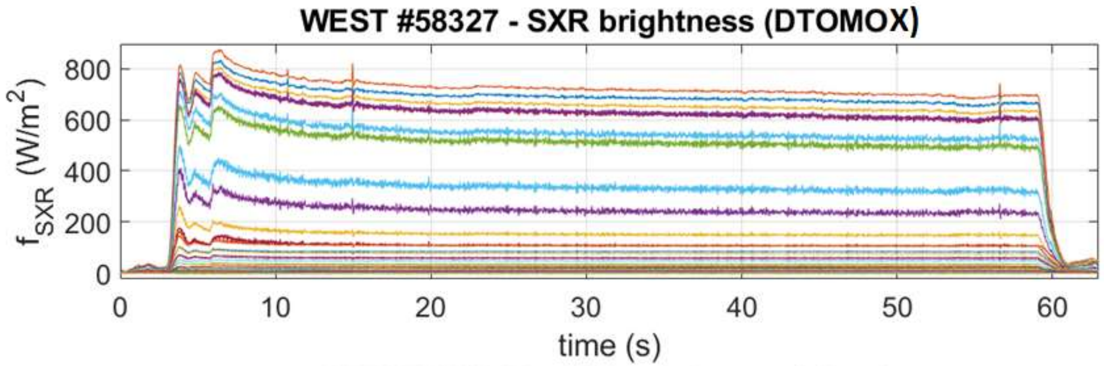

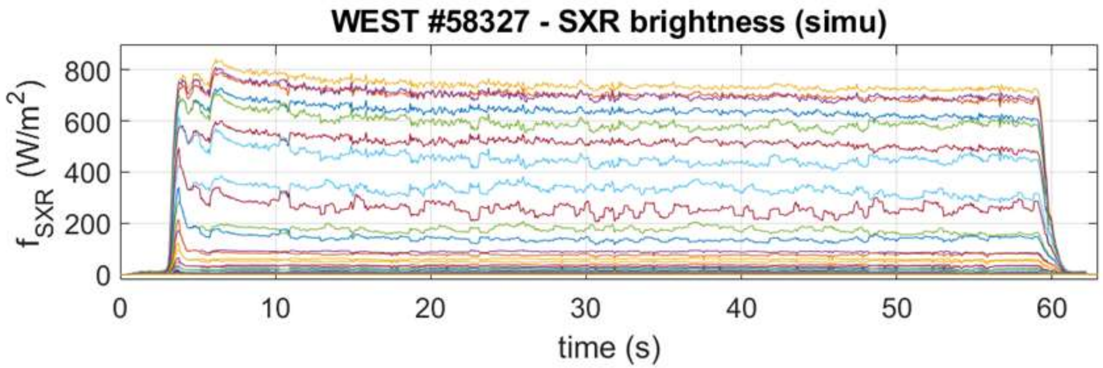

D. Mazon et al., poster at EPS 2023

Validation and commissioning of diagnostics

Modelling for vertical GEM camera

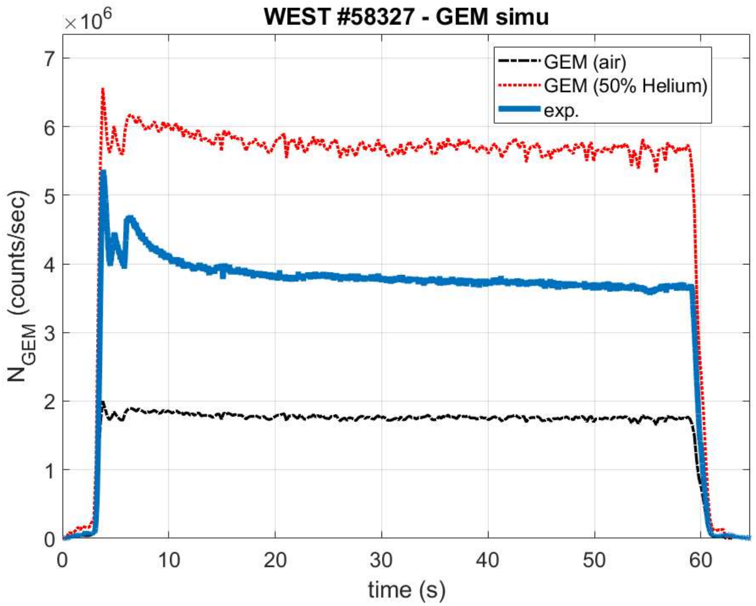

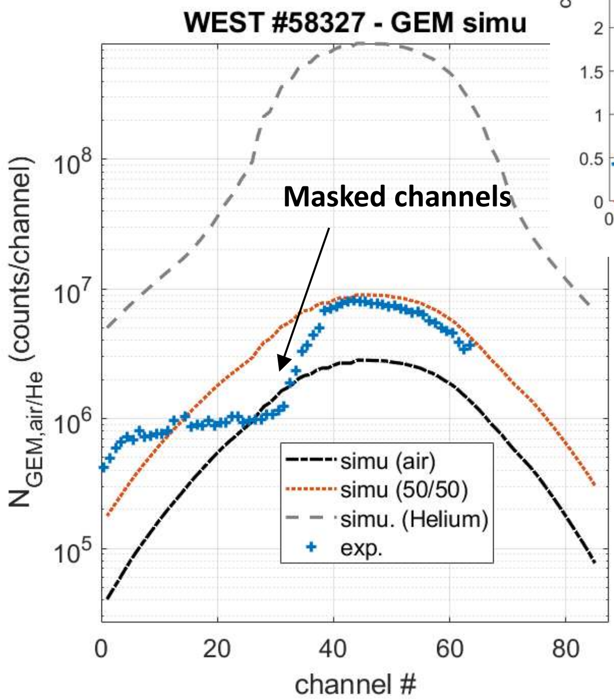

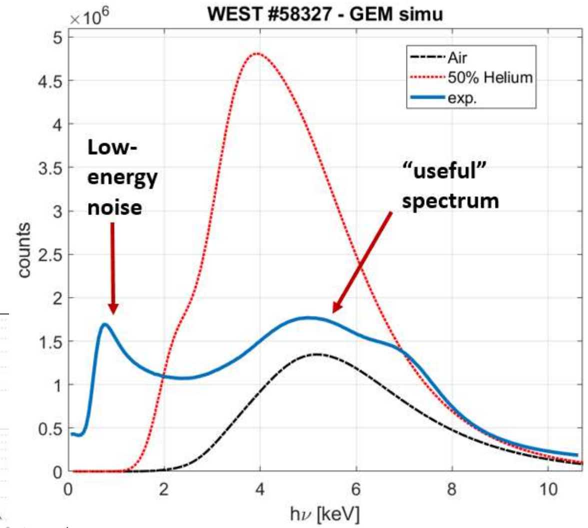

D. Mazon et al., poster at EPS 2023

Pulse #58327 time trace evolution of GEM total number of counts measured/modelled (left), GEM total counts per channels (middle), total measured/modelled spectra (right)

Validation and commissioning of diagnostics

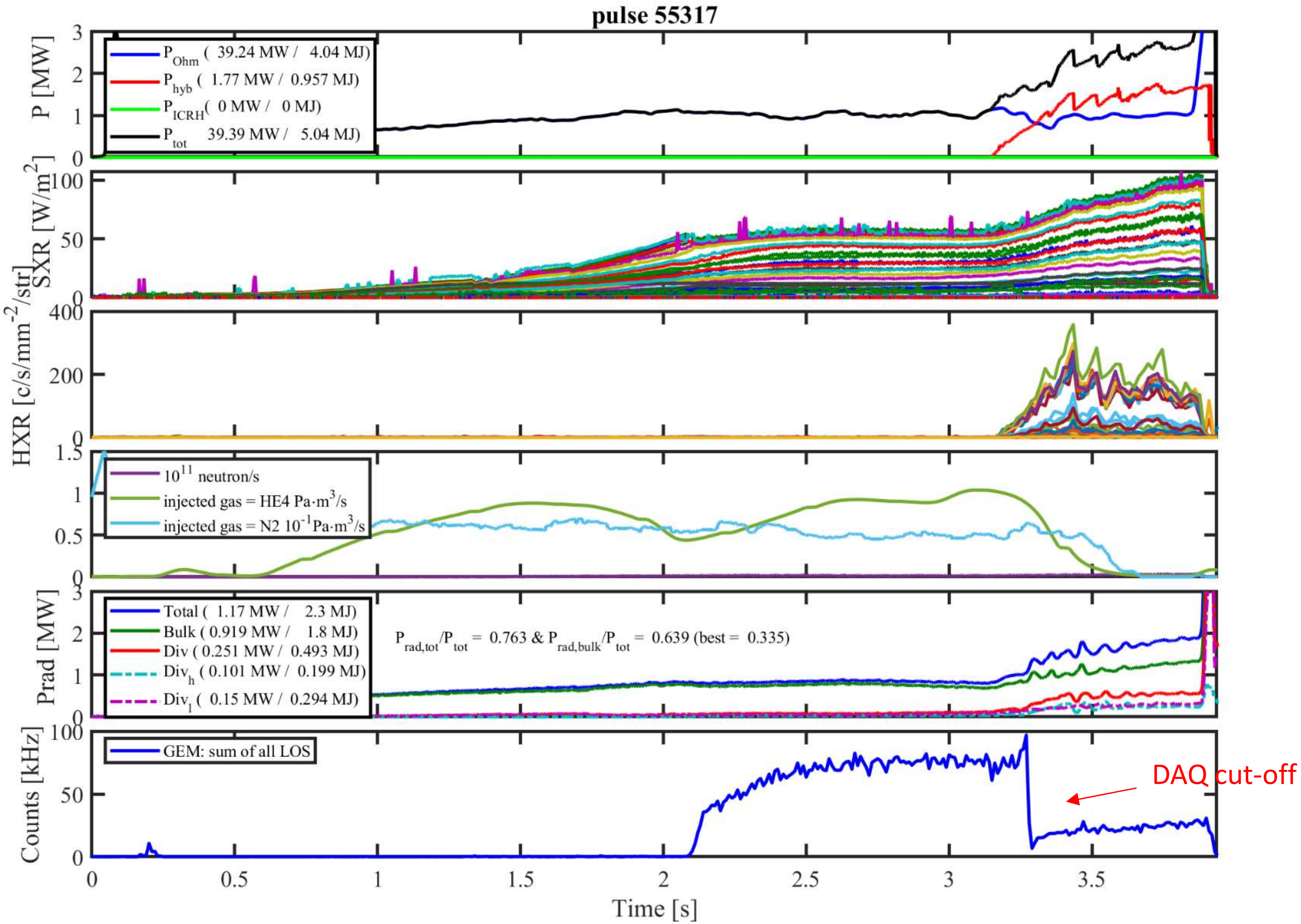

Validation and commissioning of diagnostics

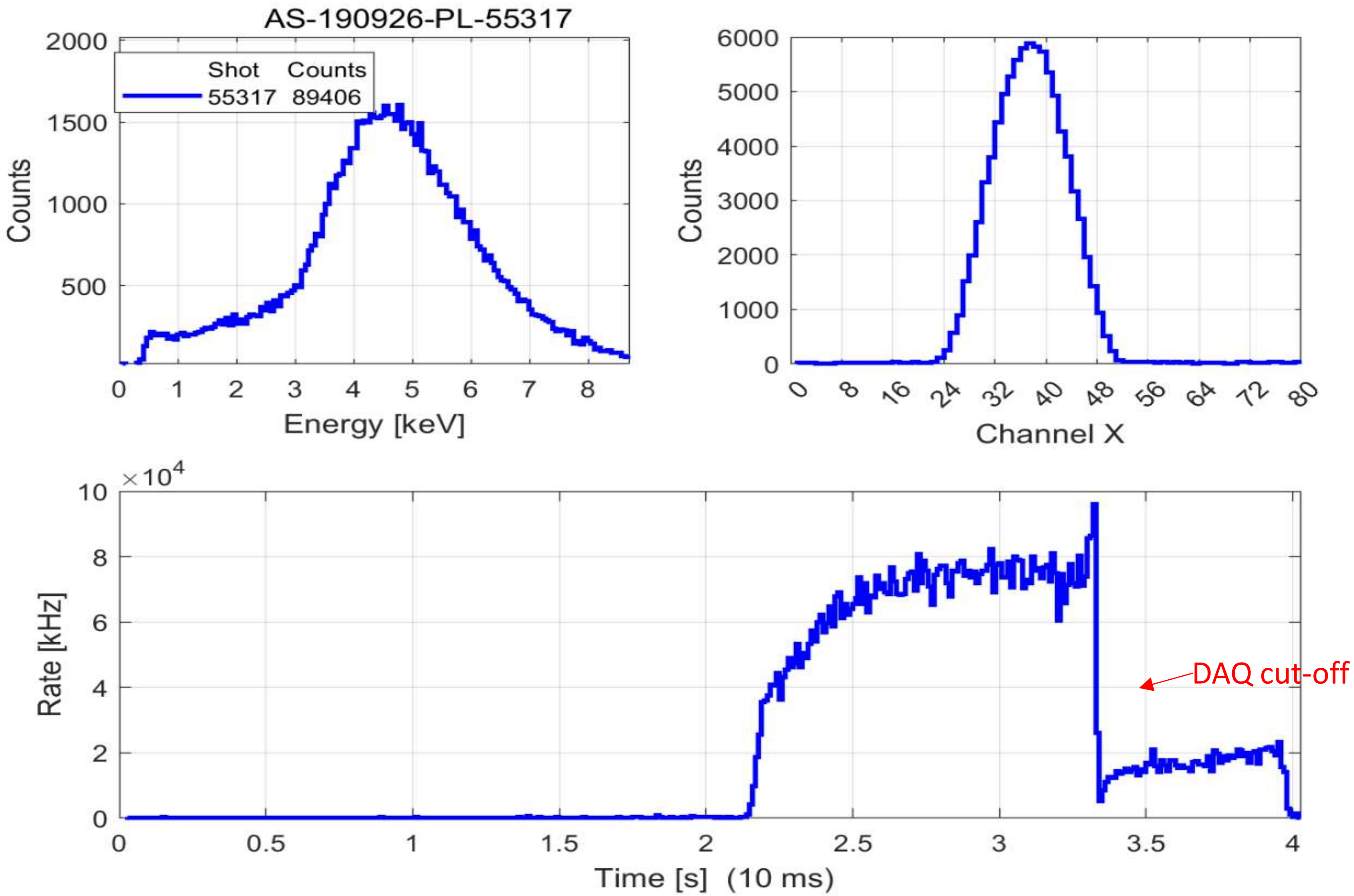

Validation and commissioning of diagnostics

Seeking answers and explanations for the experimental results:

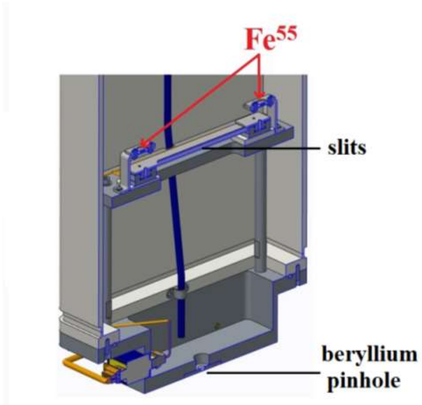

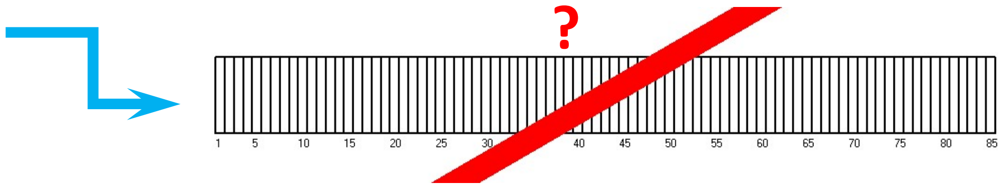

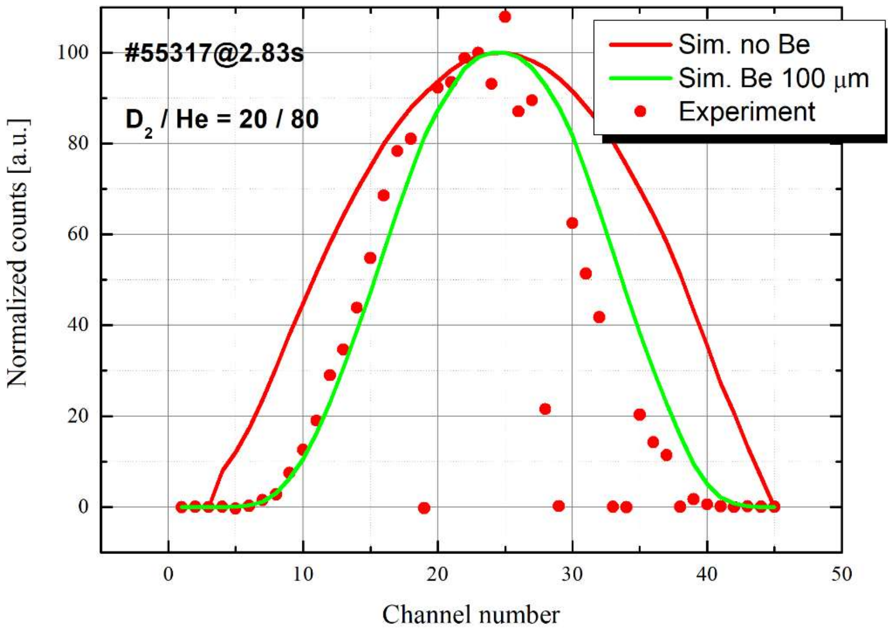

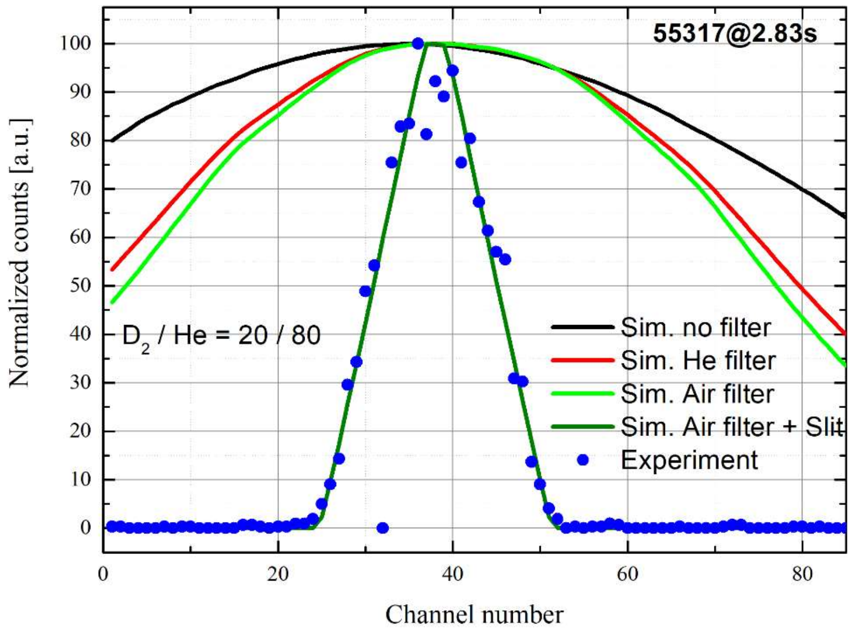

Validation and commissioning of diagnostics

- Simulated spectra for SXR region:

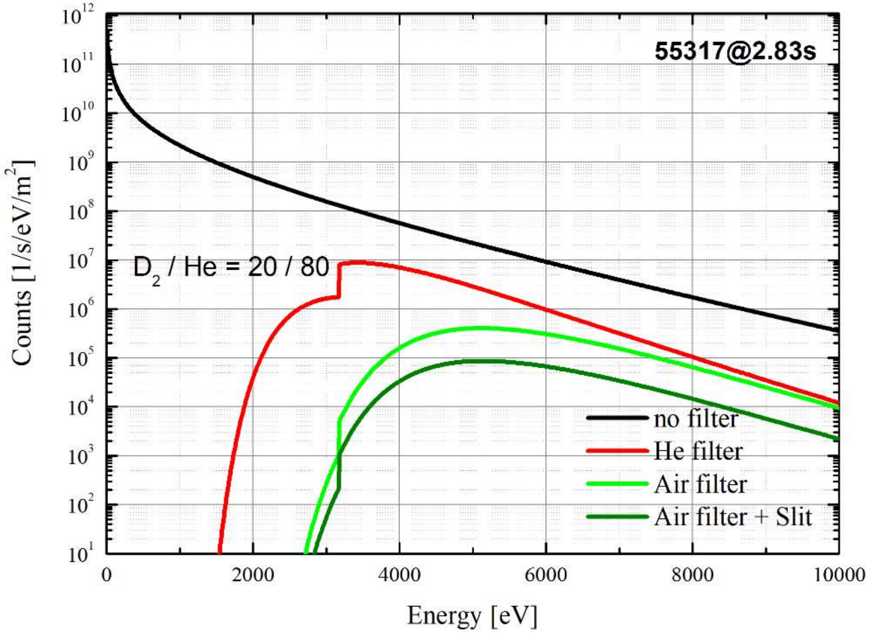

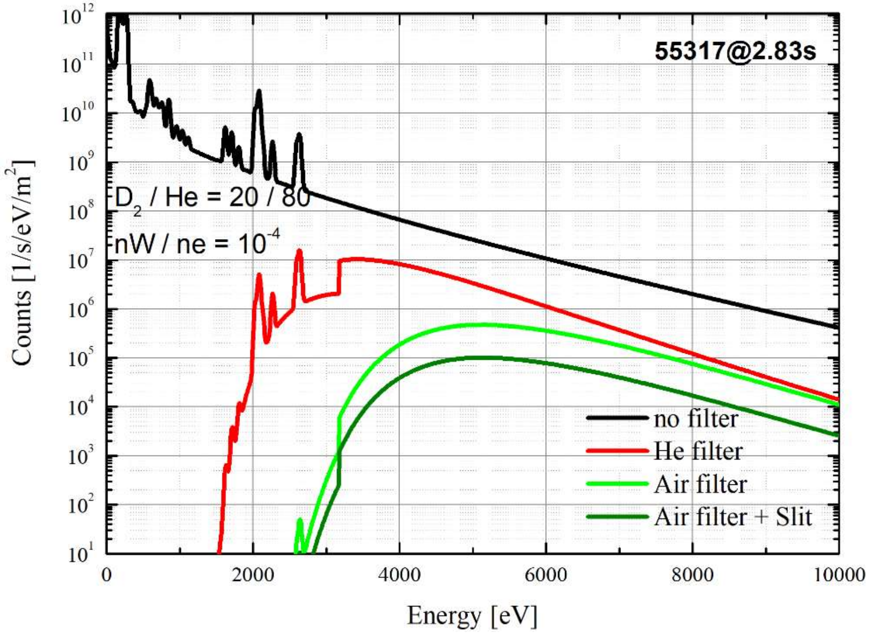

Validation and commissioning of diagnostics

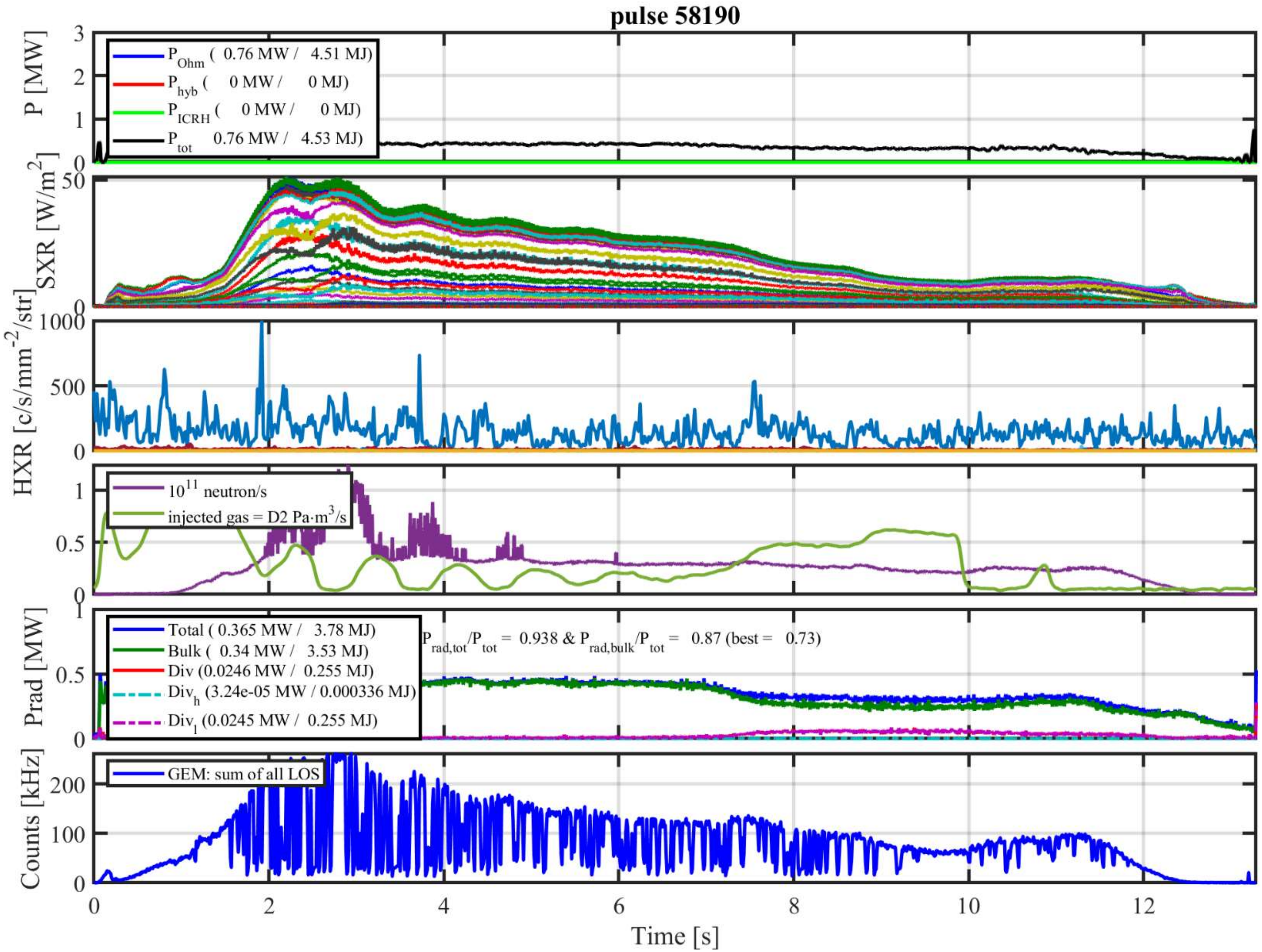

Validation and commissioning of diagnostics

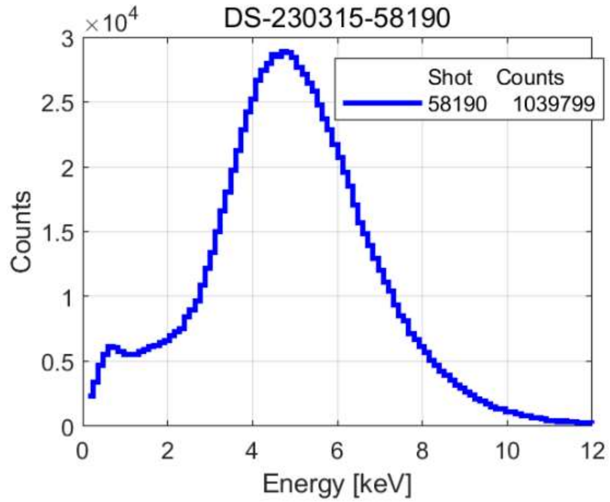

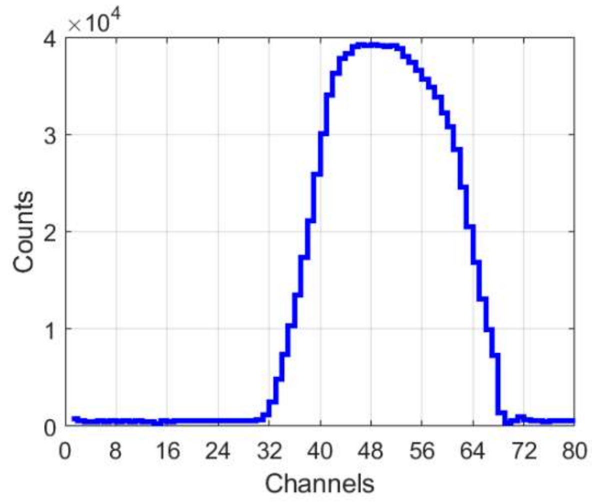

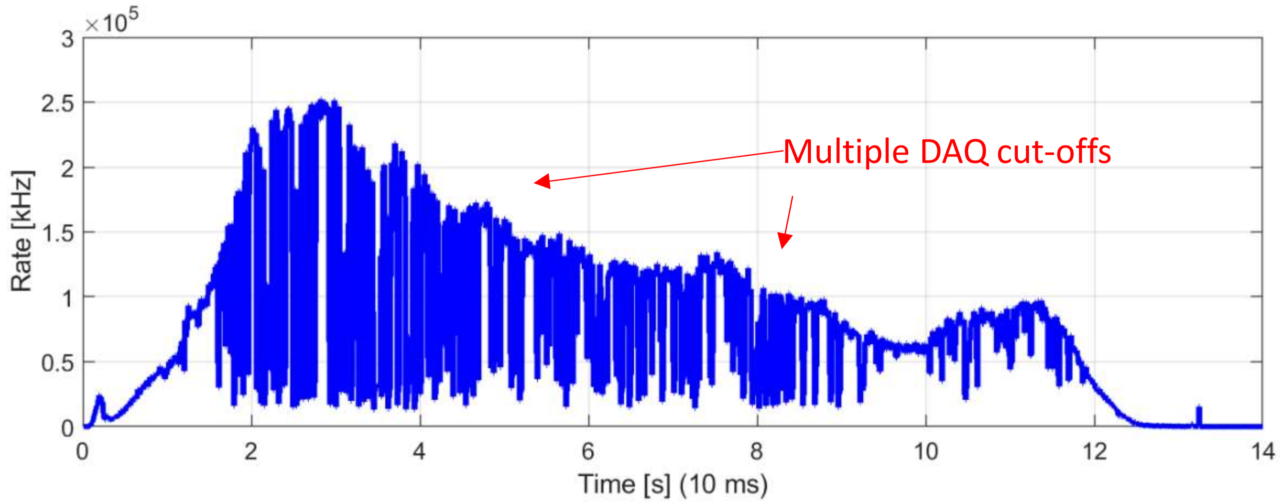

IFPiLM

Validation and commissioning of diagnostics

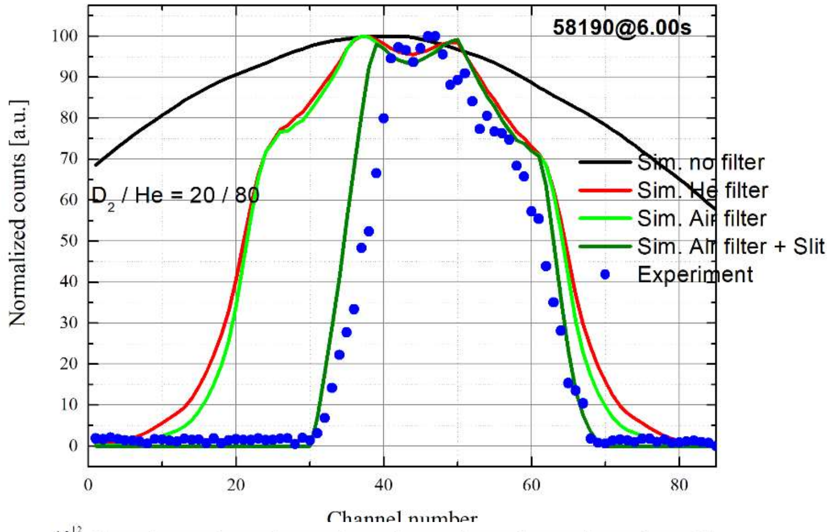

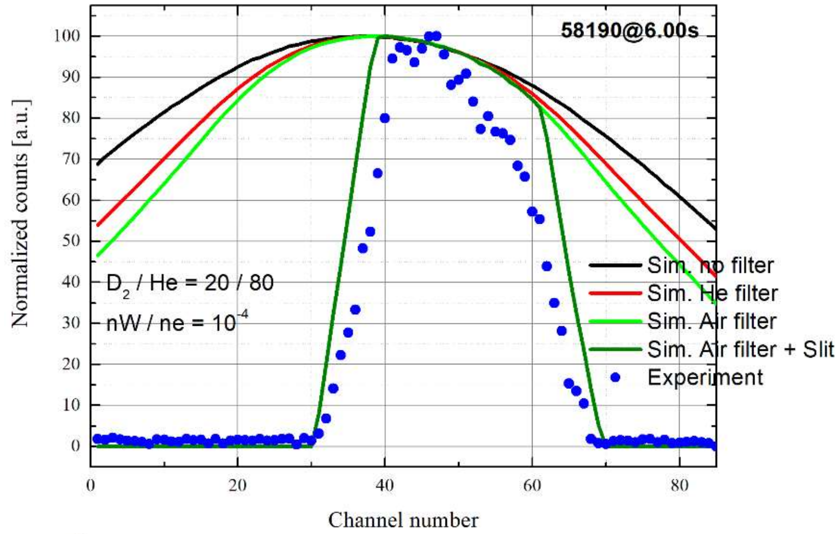

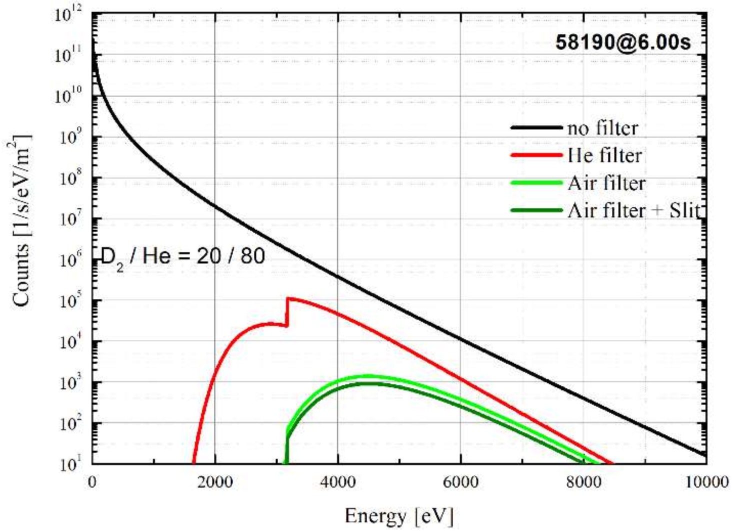

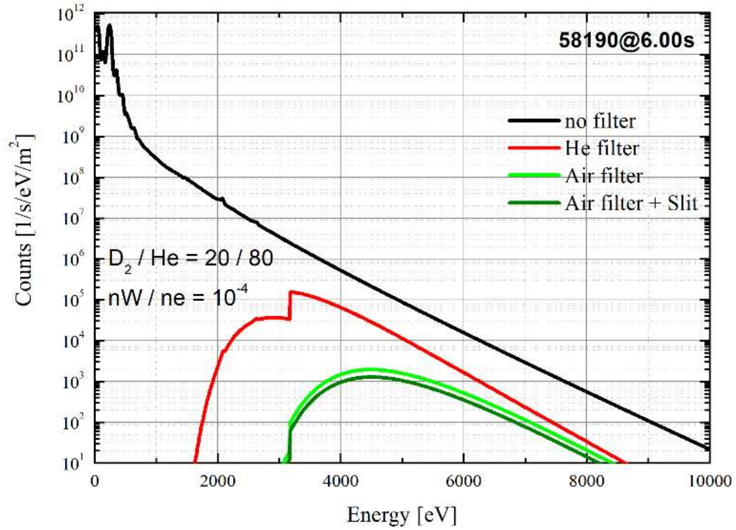

Validation and commissioning of diagnostics

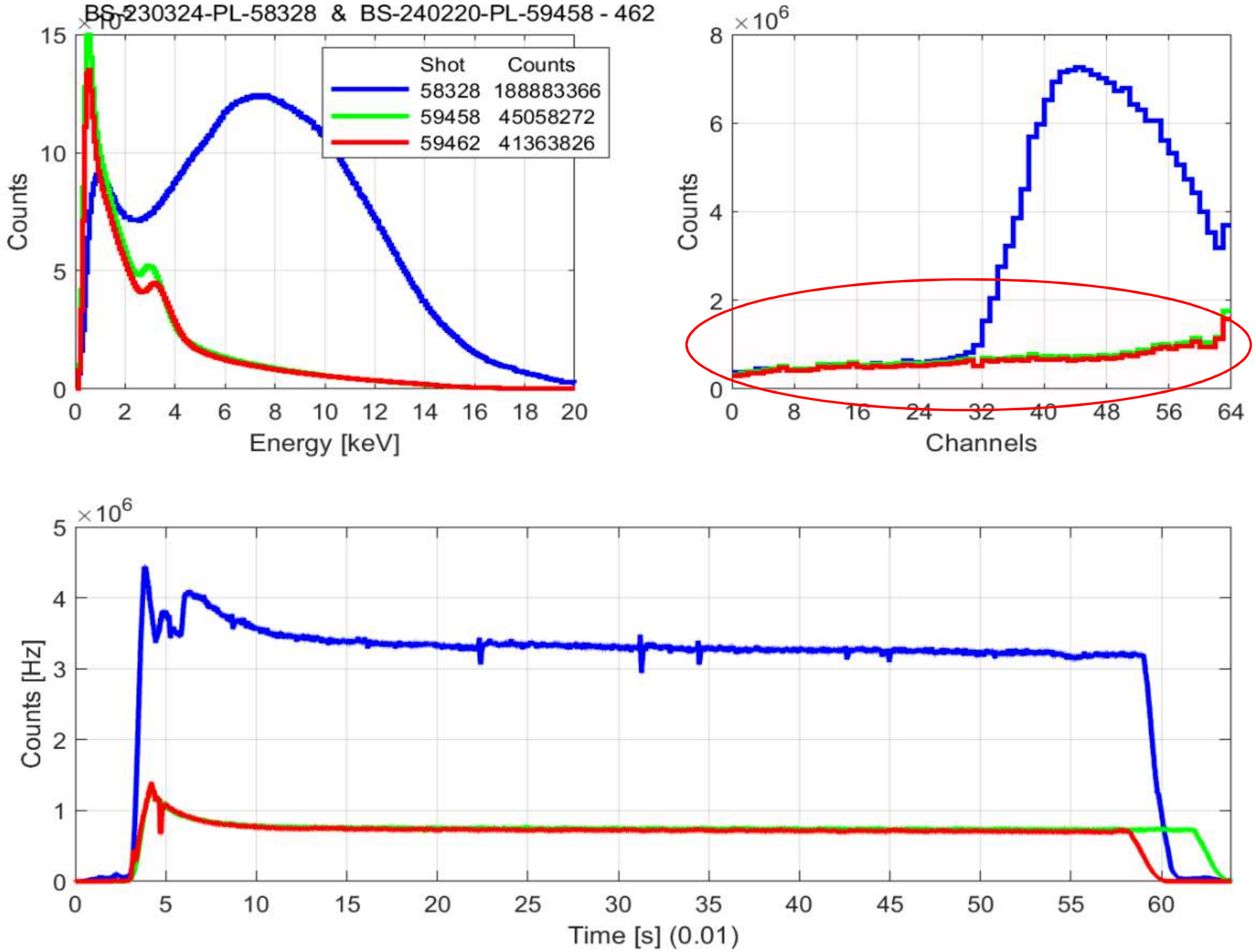

Validation and commissioning of diagnostics

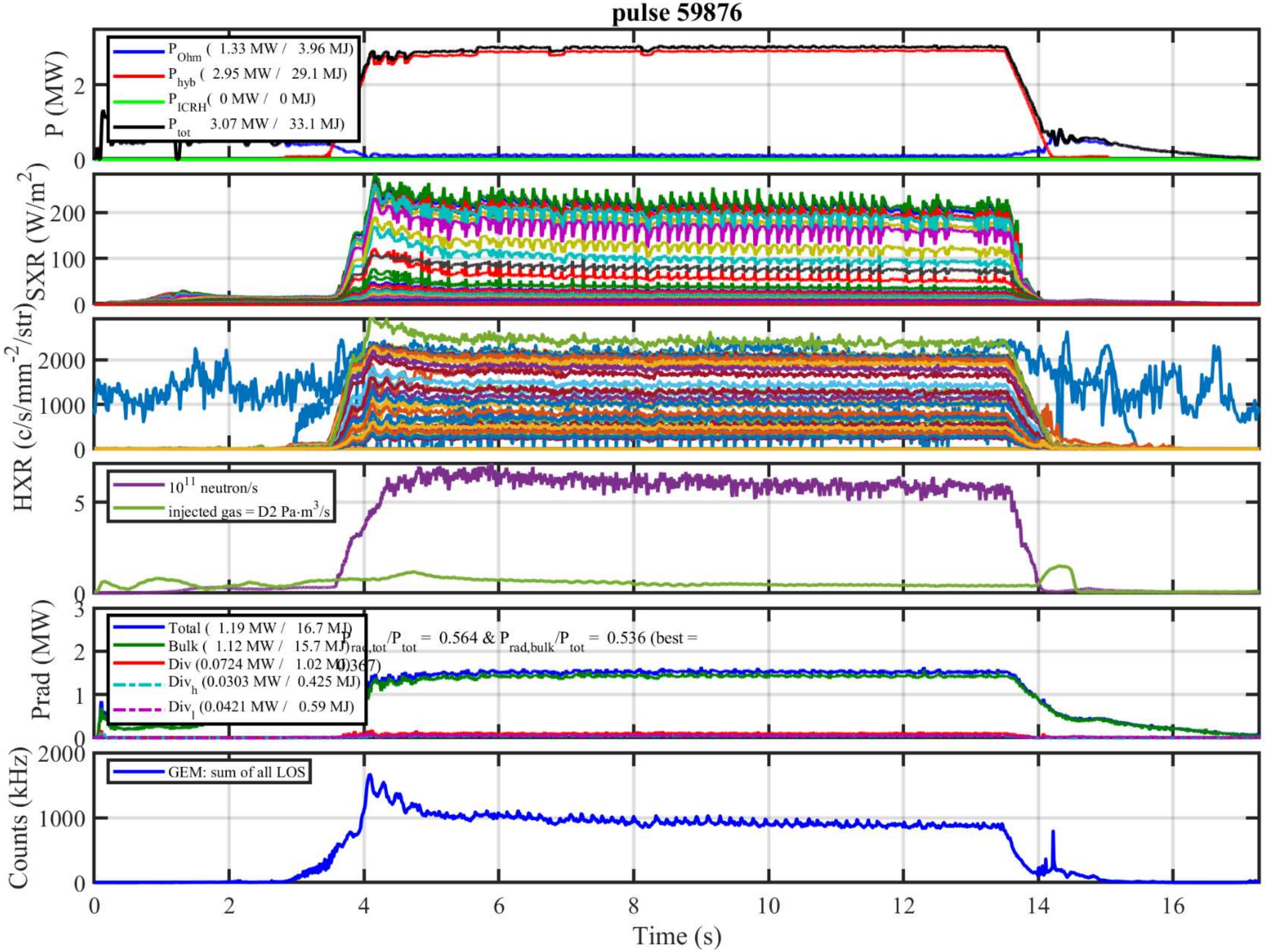

Validation and commissioning of diagnostics

Understanding spatial distribution => HEP(?) interaction

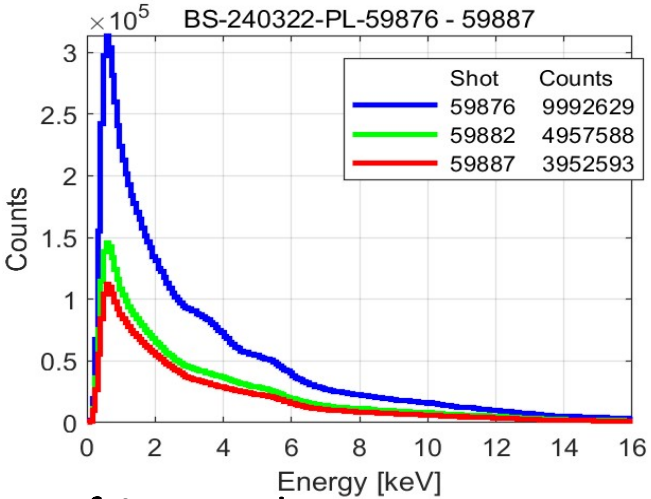

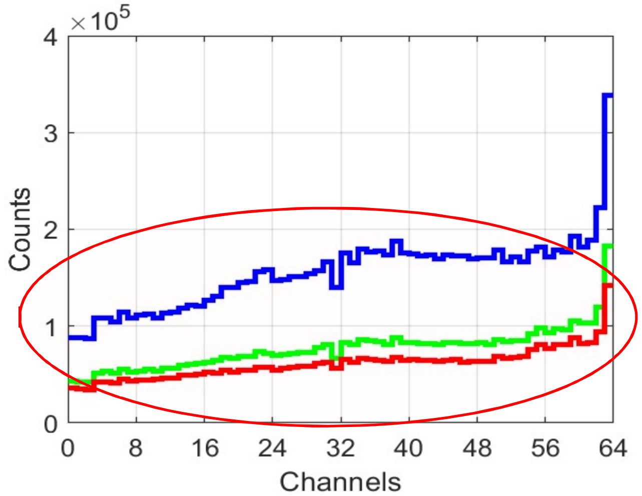

Superposition of SXR and HXR

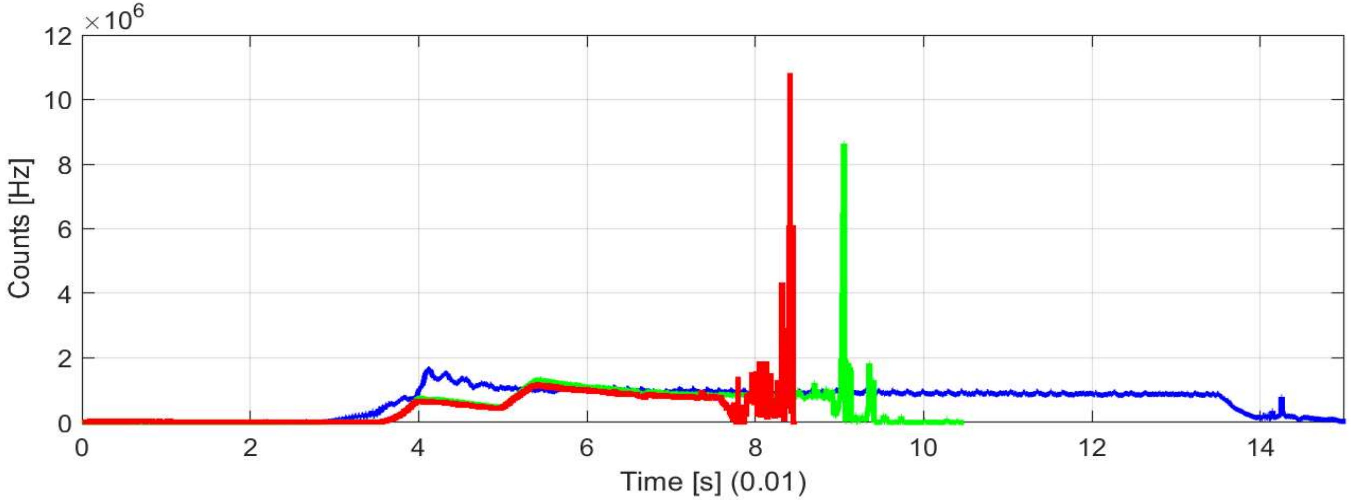

Validation and commissioning of diagnostics

GB data for very long WEST pulses => time to update DAQ?

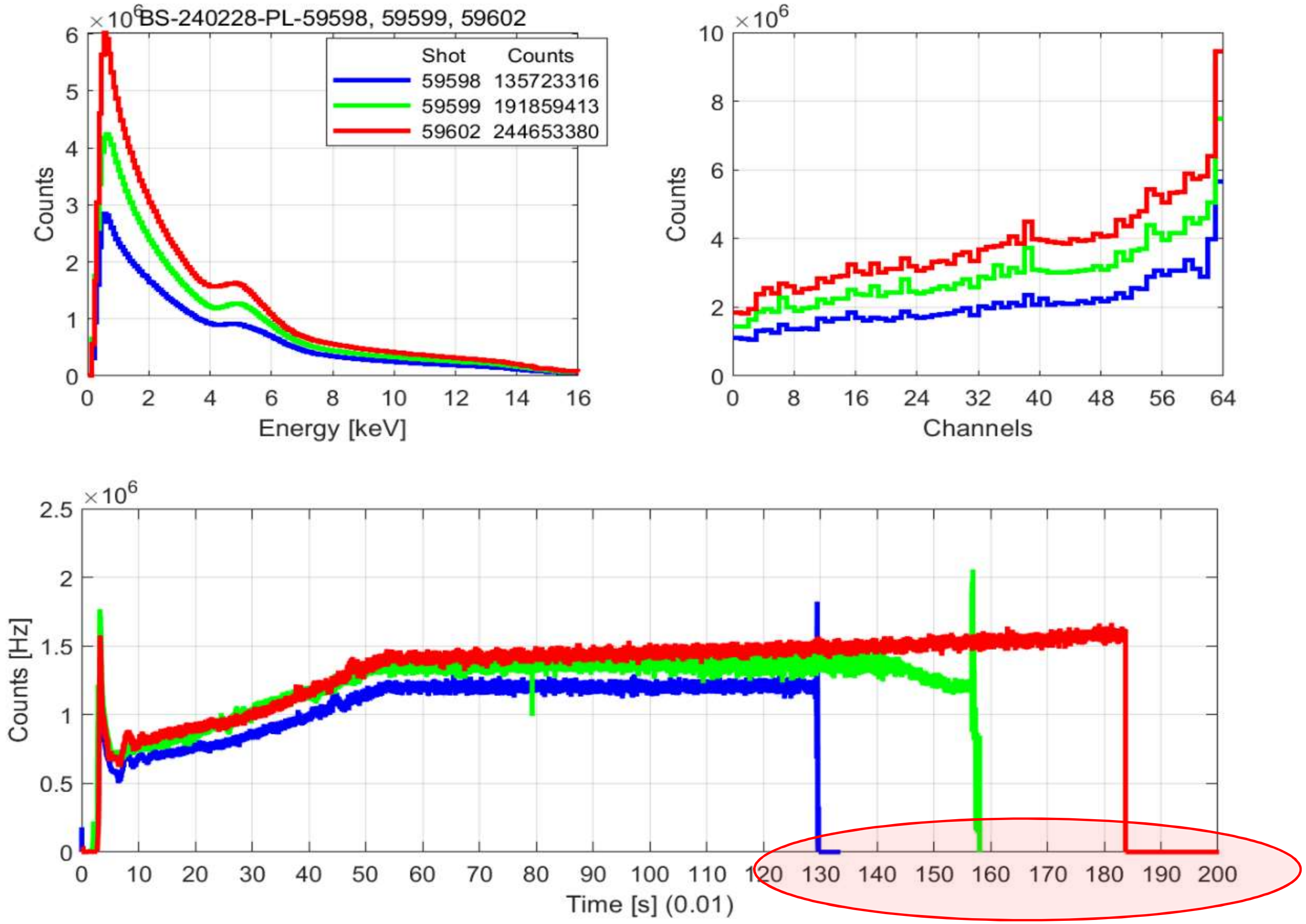

Complementary studies and tests

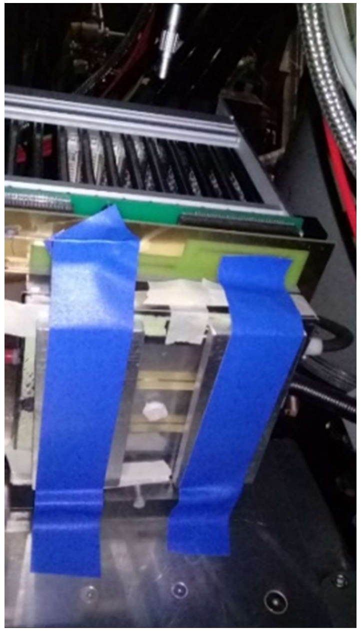

GEM detector window with two Al plates.

The detector has 128 hexagon pixels of 3.9 mm leg connected to independent fast electronics channels. It was installed in 13th AUG sector looking at the central plasma through a pinhole placed at about 35 cm distance from the detector.

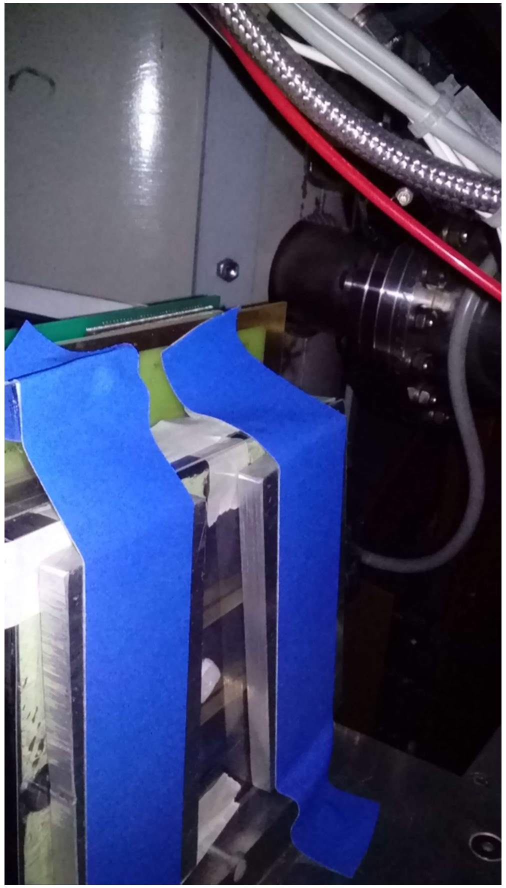

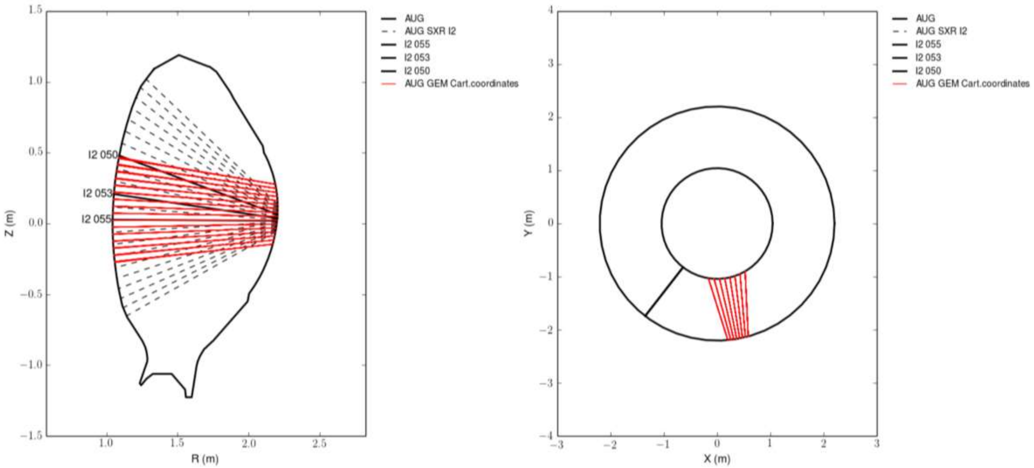

M. Chernyshova et al., RSI 87(11) (2016) 11E325

Distributions for exposed surface and shielded by Al and neutron attenuating plates were gathered.

Complementary studies and tests

SHOT 33464

Gases: D, total heating power: 2.931MW, L mode, N_2 injection

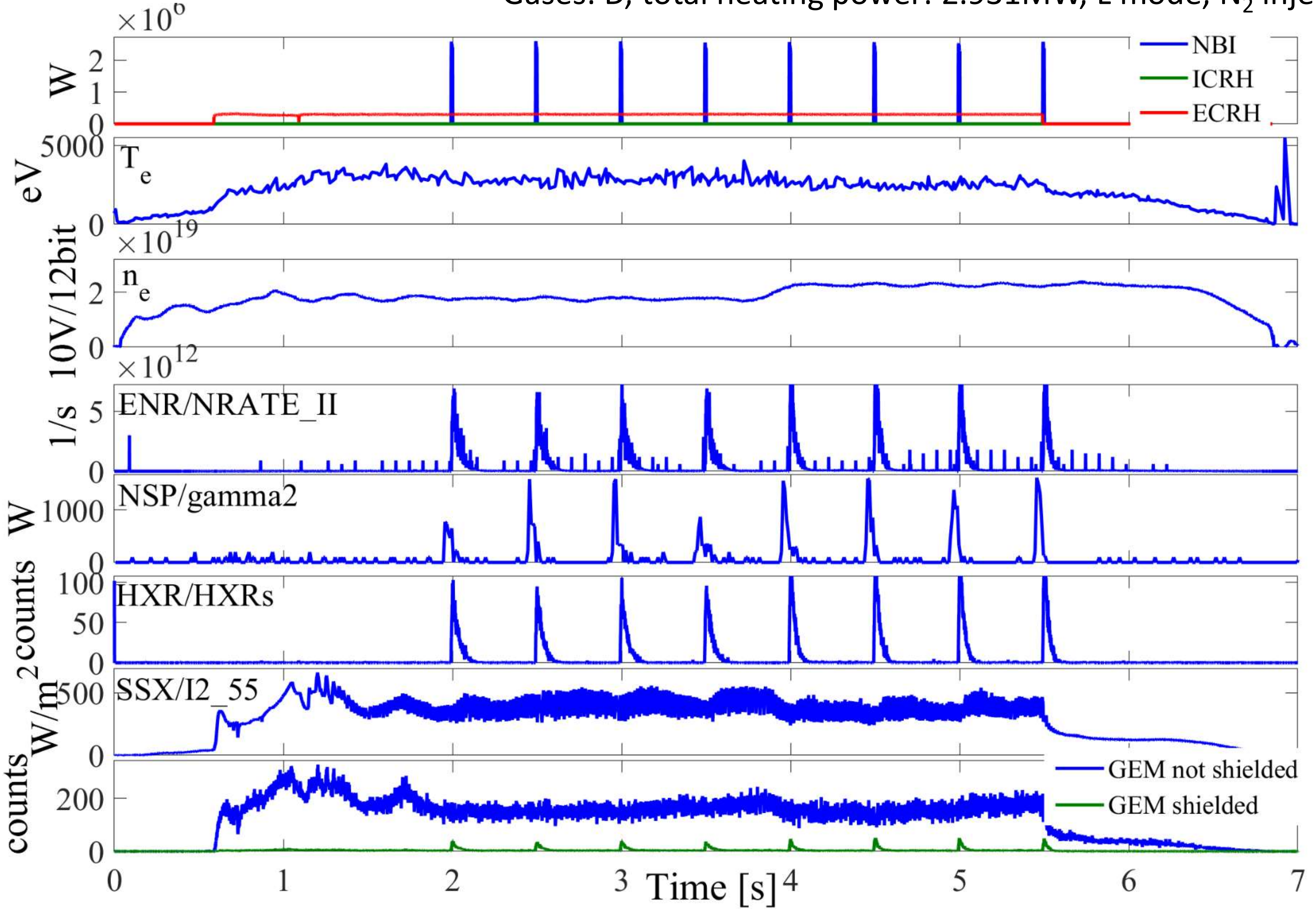

Complementary studies and tests

HEP interaction with matter:

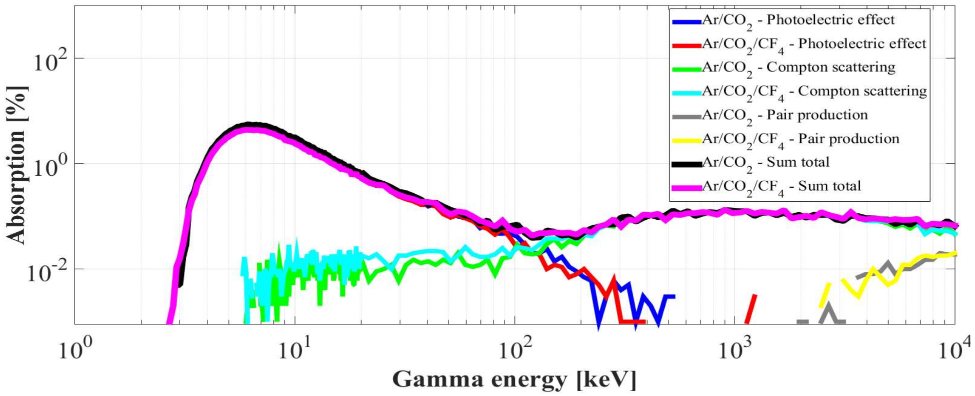

Gas: Ar 70% CO_2 30%
Drift/Transfer/Transfer/Induction: 5/2/2/2 mm
Window: Mylar 5um + Al 0.2um

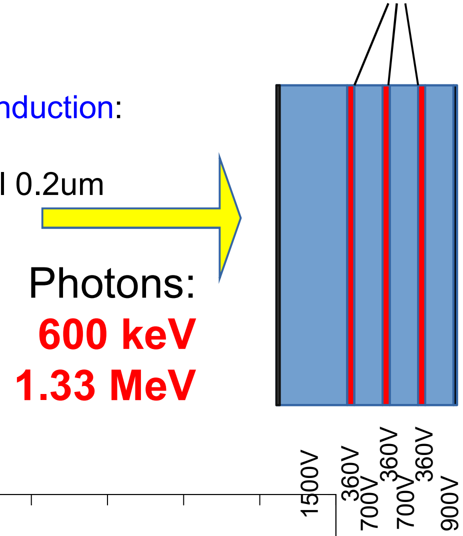

GEM detector photon detecting efficiency calculated using GEANT4 code for AUG set-up.

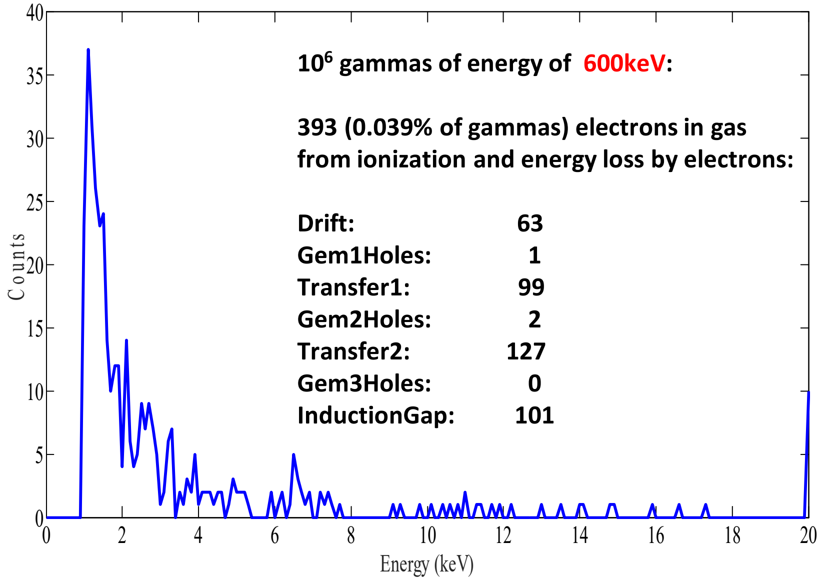

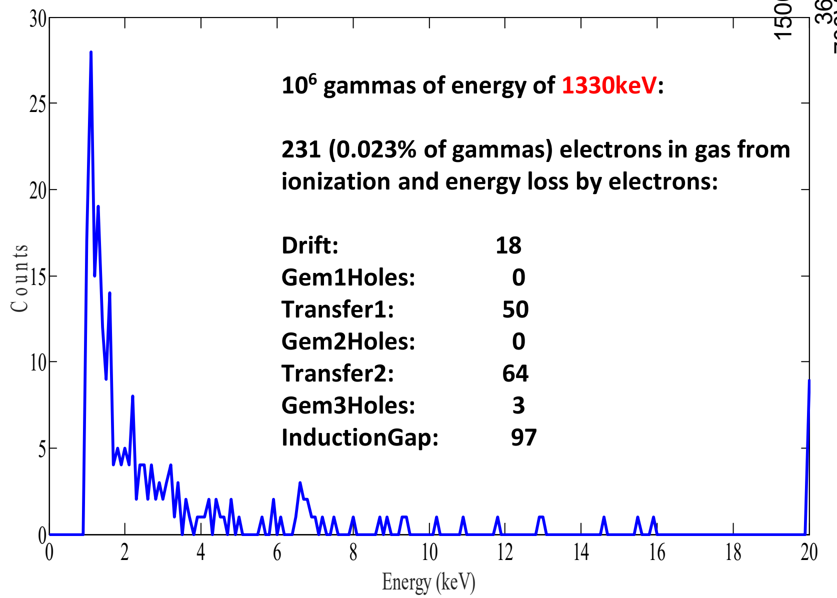

Complementary studies and tests

Intrinsic fluorescence, Cu vs. Al

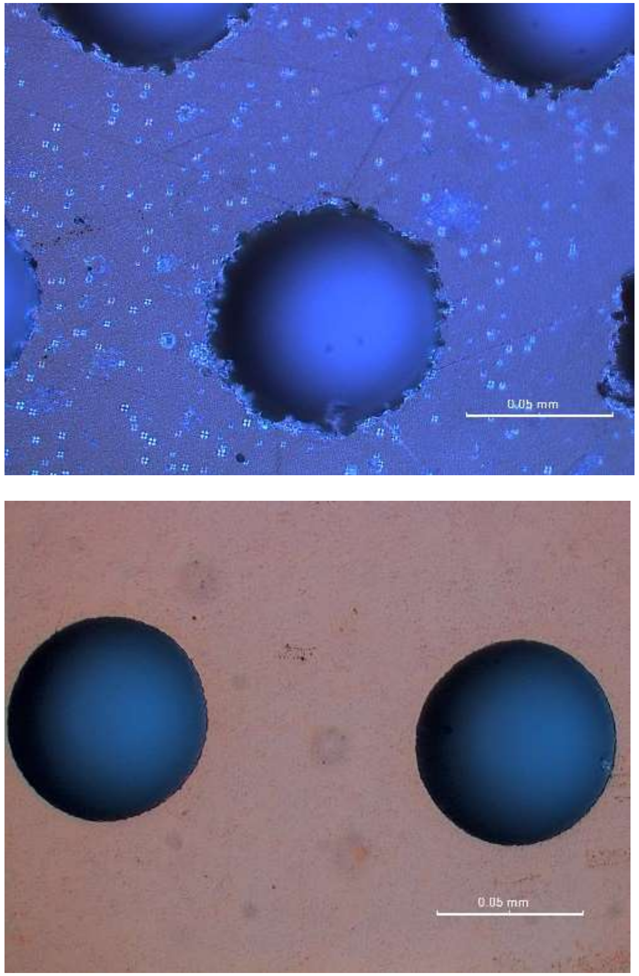

Optical microscope images of Al (top) and Cu (bottom) GEM foils

GEM detectors currently in use (CERN technology) => Cu covers both sides of a thin Kapton film.

The area of interest for SXR includes the excitation potential of Cu (~9 keV)
=> unwanted signal additional to the original spectrum

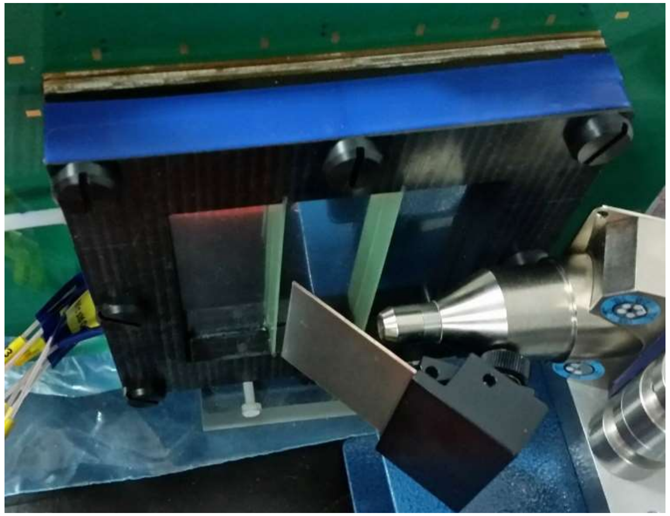

Experimental set-up.

M. Chernyshova et al., Fus. Eng. Des. 146 (2019) 1039

Complementary studies and tests

- **Al based GEM** technology for the first time for plasma diagnostics,
- Simulation results in agreement with the measured spectra, except the less signal from Al than expected from the simulations,
- Cr layer (adhesive layer) can affect the resulting spectrum if the energy of the incident photon is higher than the Cr excitation potential,
- For more effective elimination of the intrinsic detector lines, the Cr layer may be replaced by Ti one, which has slightly less radiative performance.

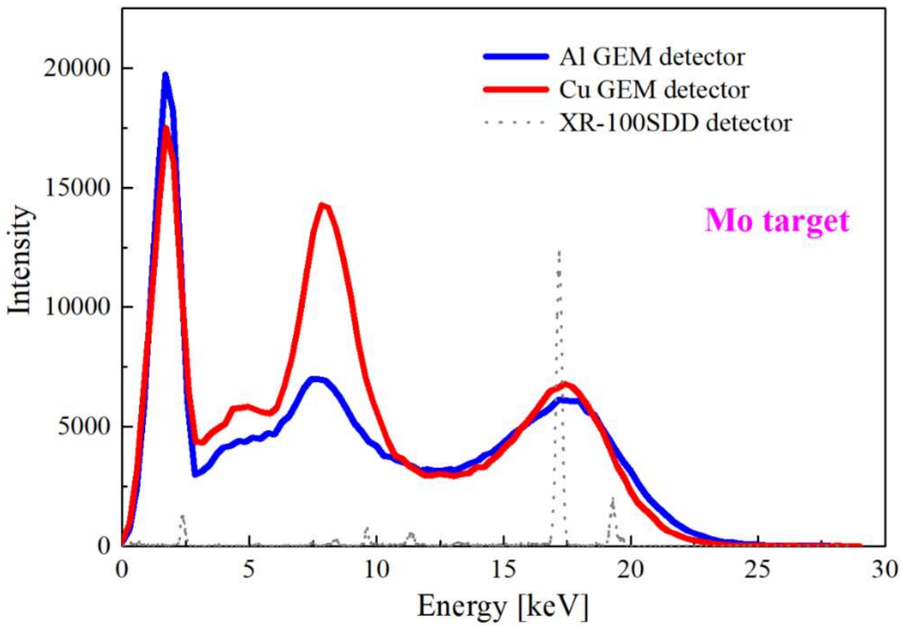

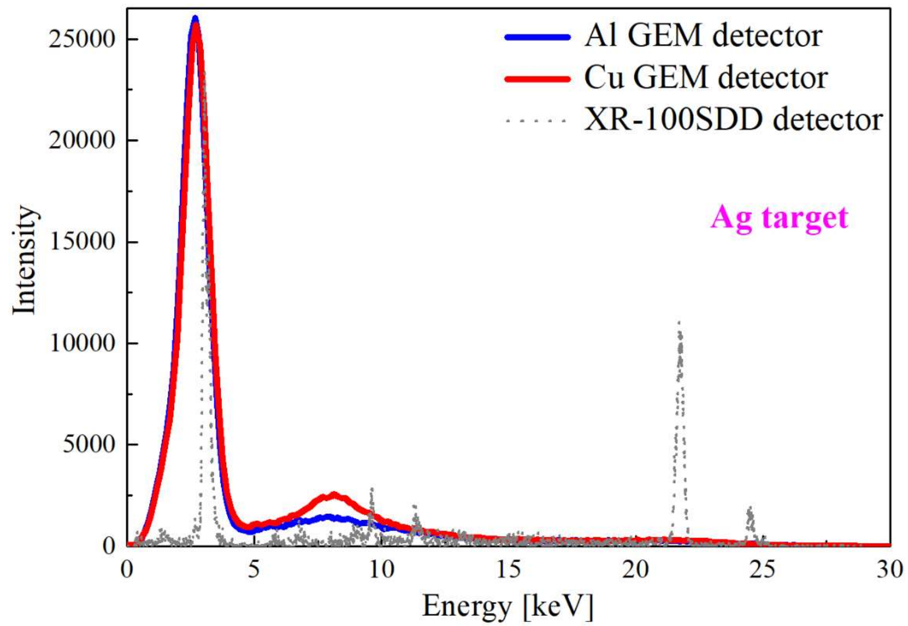

Design and development for DEMO

M. Chernyshova[1], K. Malinowski[1], S. Jabłoński[1], M. Jagielski [1], K. Mikszuta-Michalik[1], T. Czarski [1], B. Bieńkowska[1], S. Akbas[1], R. Prokopowicz[1], D. Makowski[2], T. Fornal[1], A. Izdebski[1], E. Kowalska-Strzęciwilk[1], A. Mielczarek[2], P. Perek[2], P. Nowak vel Nowakowski[2], B. Jabłoński[2], A. Krimmer[3]

[1]Institute of Plasma Physics and Laser Microfusion, Warsaw, Poland

[2]Lodz University of Technology, Department of Microelectronics and Computer Science, Lodz, Poland

[3]Forschungszentrum Jülich, Jülich, Germany

Development since 2021

Radiated power and core SXR diagnostics for DEMO

- **Goals:**
  - Measurement of the core plasma radiation power $P_{rad,core}$/core X-ray radiation profile to maintain the power loss across the separatrix above the confinement mode threshold, contributes to H-mode control as input to the calculation of the power crossing the separatrix;
  - MHD control (supplementary)
  - Impurity accumulation control (supplementary)
  - Plasma position control (supplementary)

- **Requirements (initial):**
  - Accuracy, spatial and time resolution (by November 2020):

    Latency - 0.01 s

    Time resolution – 100 ms

    Spatial resolution – 5 cm
  - Required relative difference – up to 3% (a relative „calibration" of $P_{rad,core}$ could be an option by monitoring contributions to P_{sep}, power flowing across the separatrix, during LH transition)
  - Initial photon range – 0.02–100 nm

Design and development for DEMO

- Measurement concept

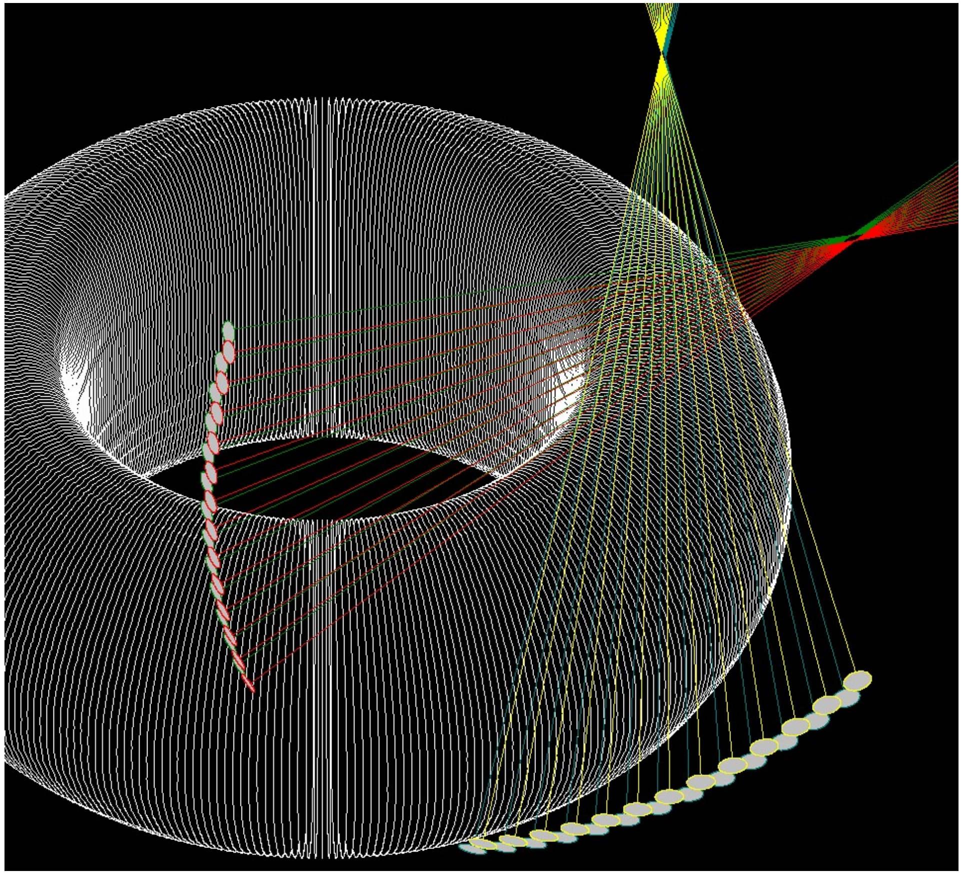

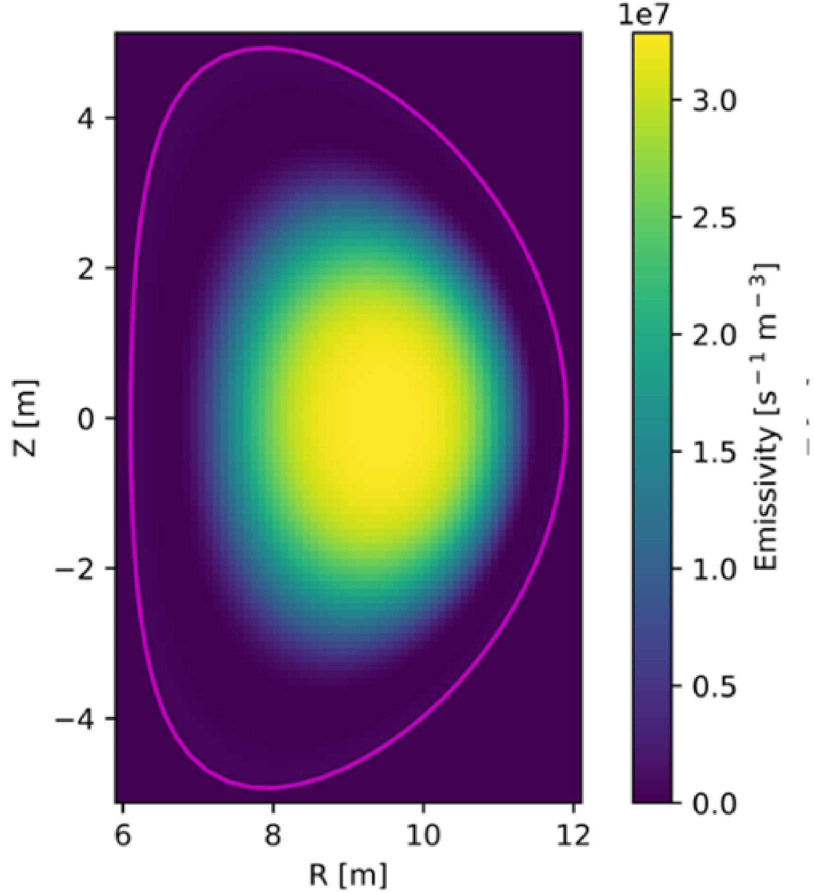

Power emission phantom prepared based on the EU-DEMO 2018 baseline in CHERAB.

Current positioning and geometry

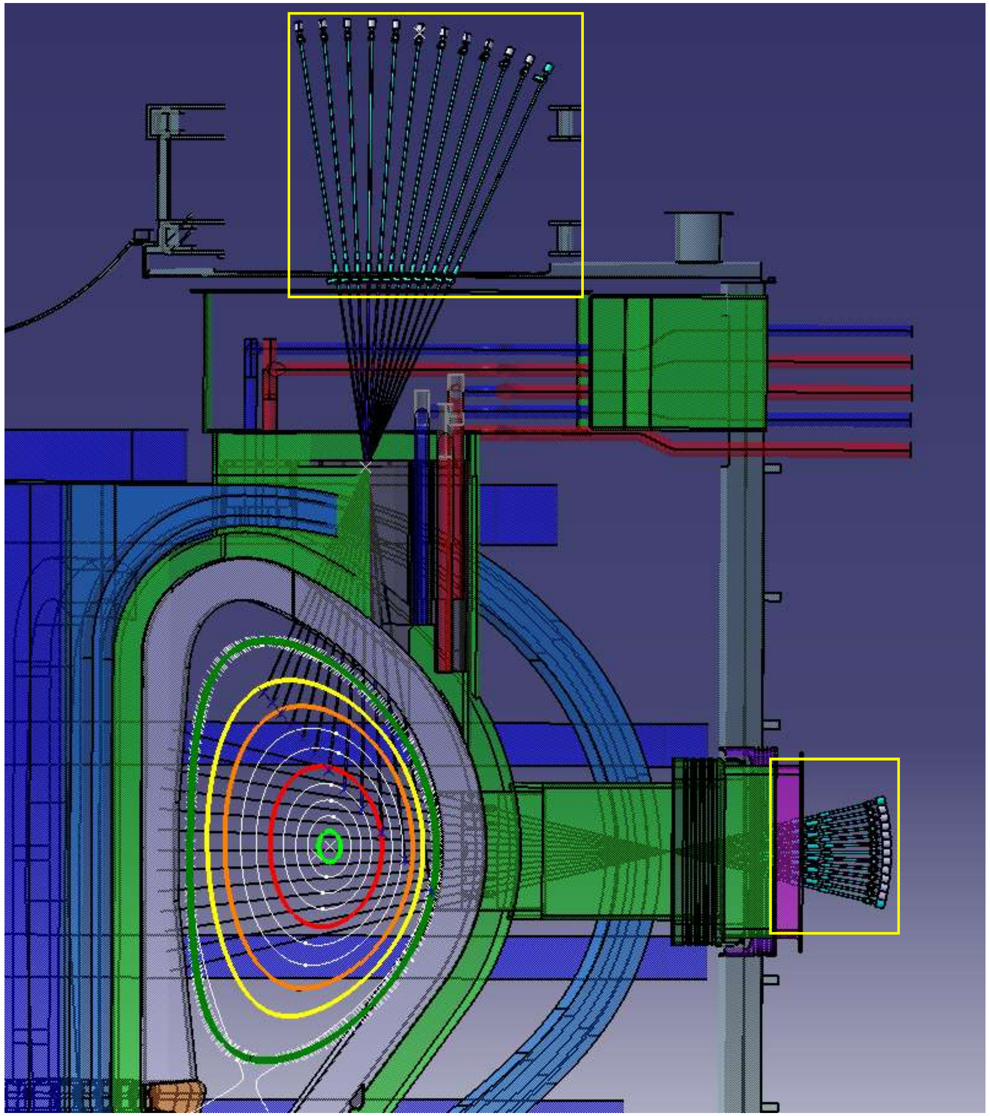

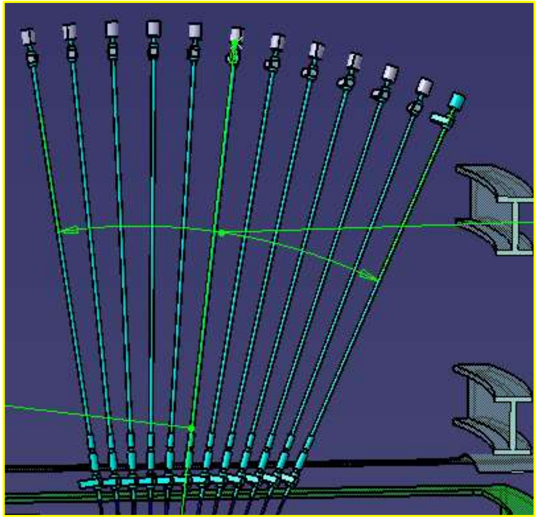

A set of collimators of initially 30 mm diameter for each LOS (13x2 raws in EP/UP)

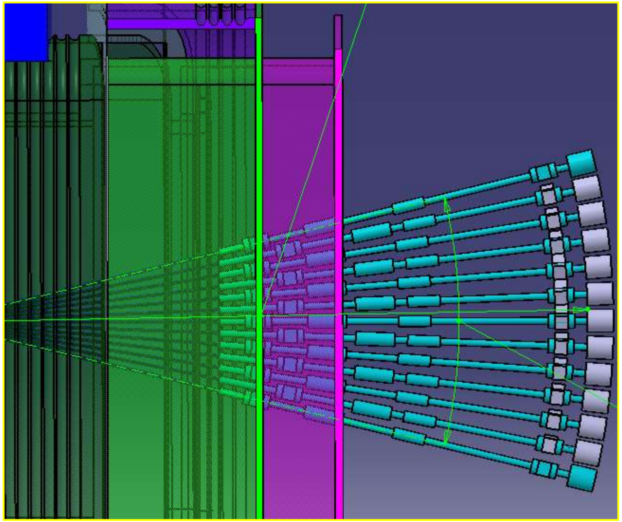

Estimation of the expected radiation load and range of interest

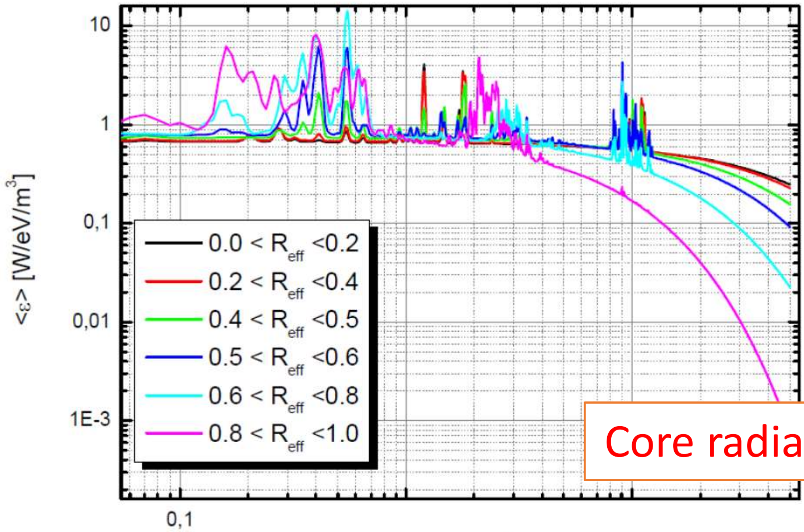

Core radiation from ab. 1 keV

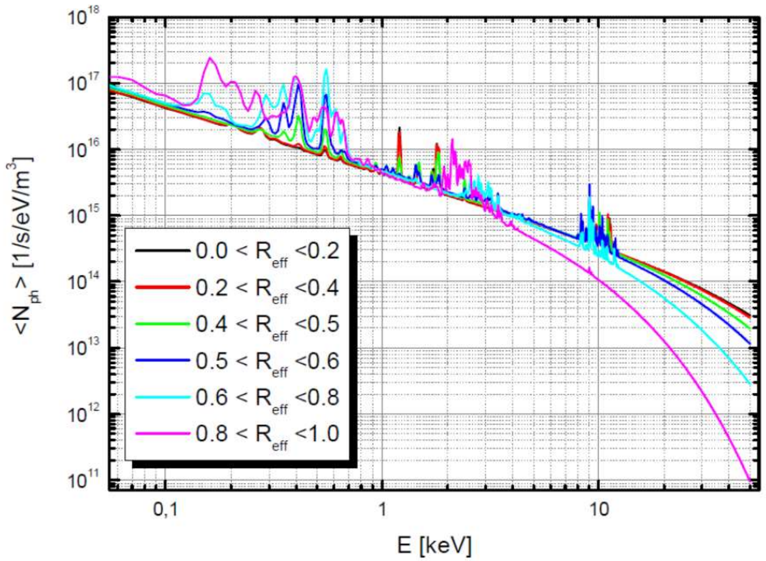

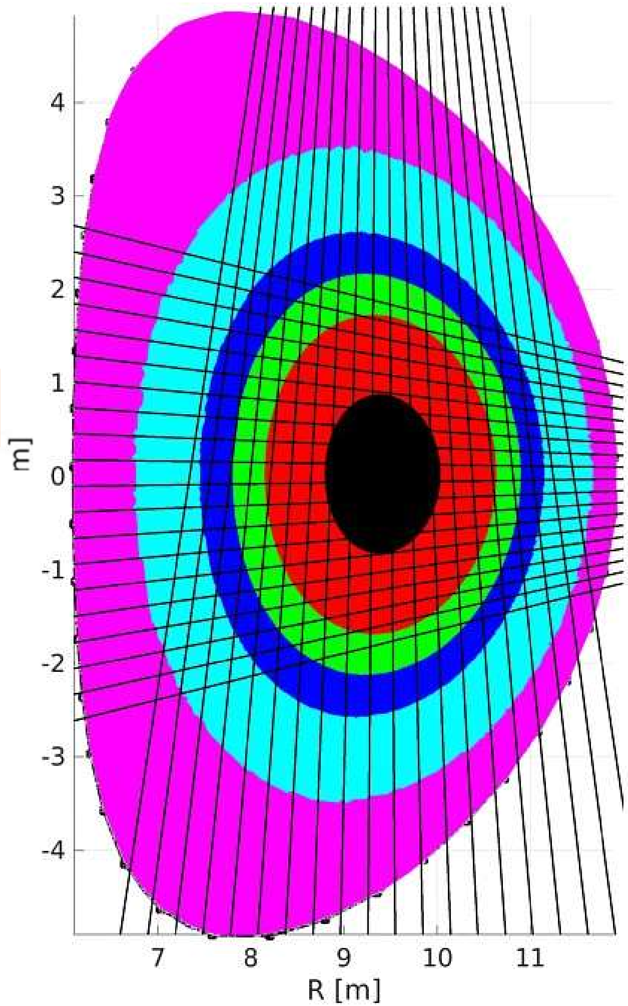

Concept of GEM detector based diagnostics

One or multiple (if needed) chamber could be exploited:

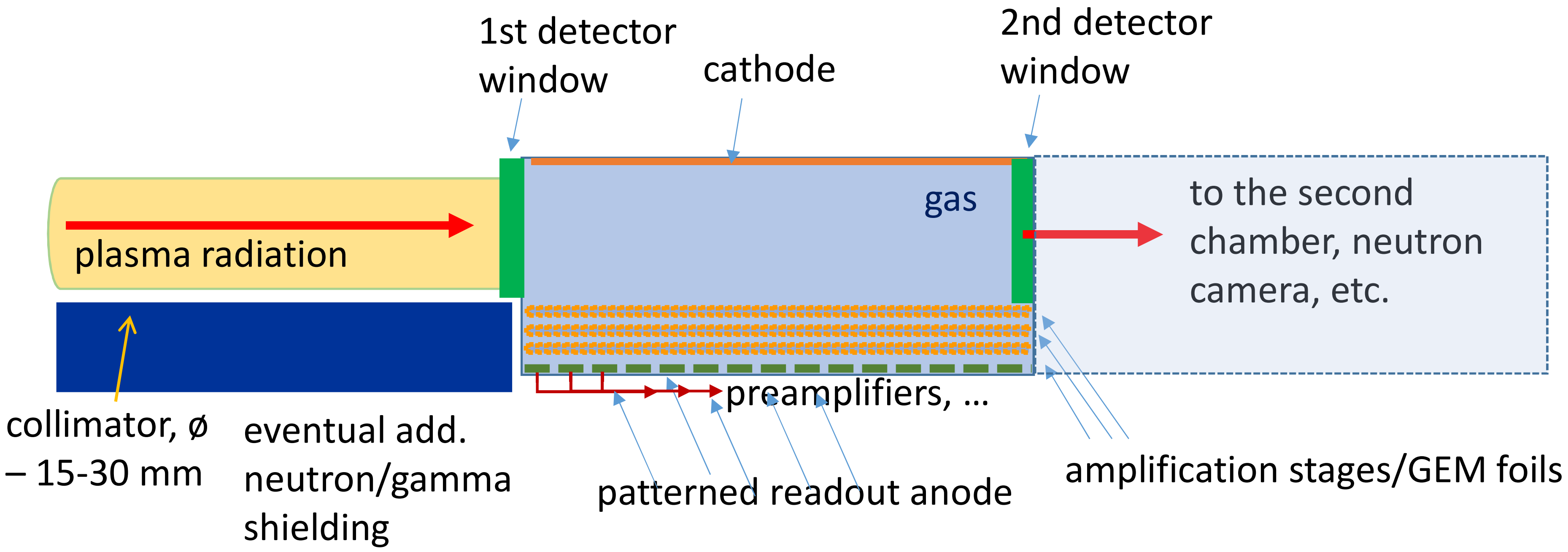

Model of the initial sensor concept => two gas chambers approach

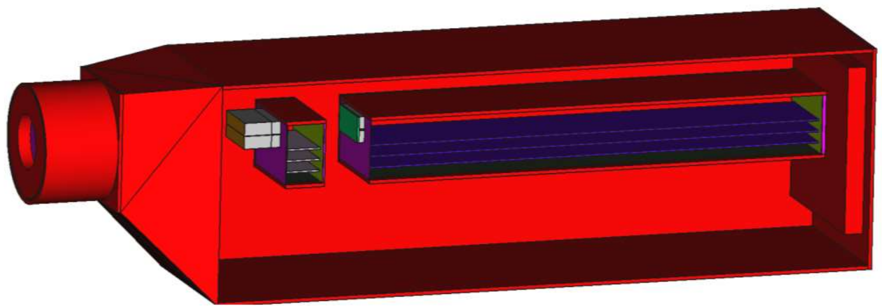

Design and development for DEMO

- Geant4 simulation results

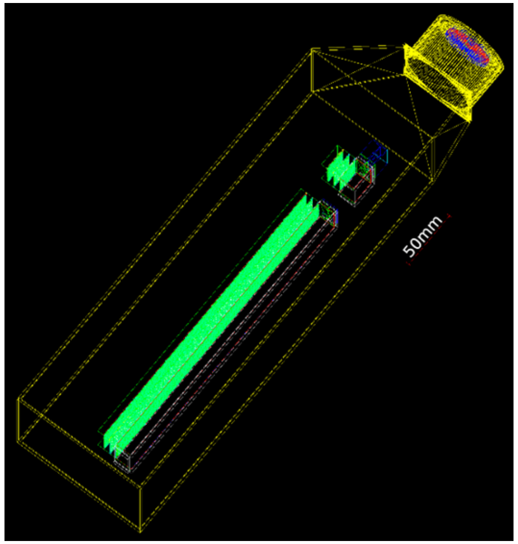

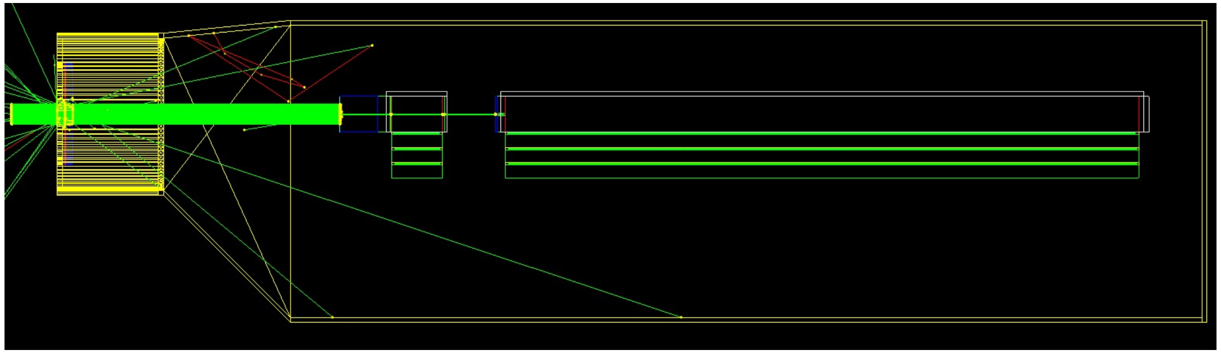

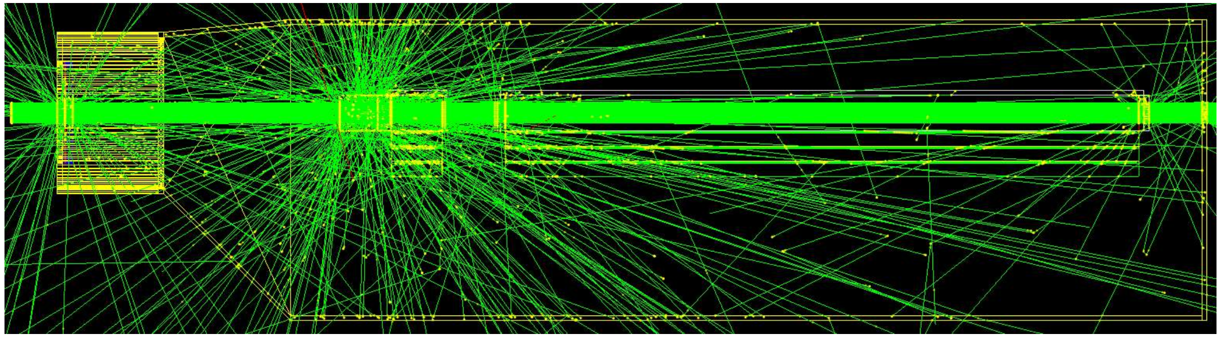

Illustration of the detector interaction with a photon beam of E=10 keV (top) and 100 keV (bottom), perpendicular to the direction of the electric field. Two gas chambers (2 cm and 25 cm long) with three GEM films in each chamber.

Relative measurement accuracy

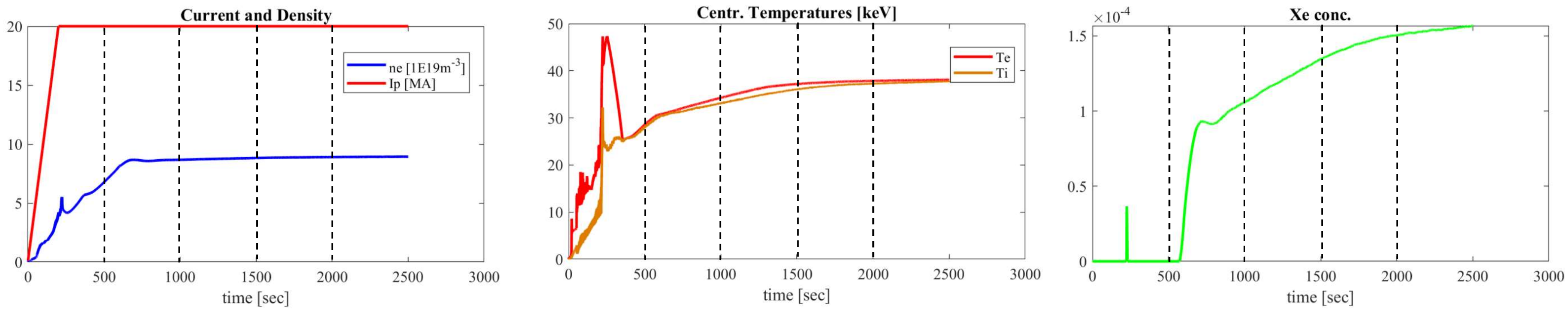

Initial plasma characteristics for DEMO ramp-up scenario and selected time points for analysis [http://idm.euro-fusion.org/?uid=2PFLML].

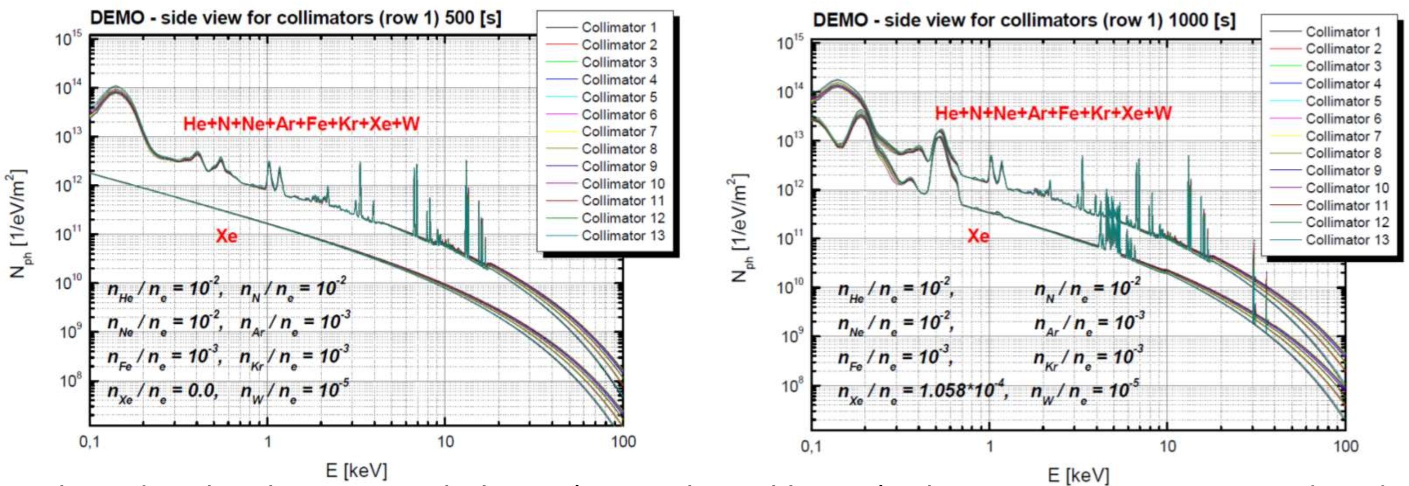

Calculated spectra based on local ionisation balance (coronal equilibrium). The impurities were considered to be either Xe only (marked as Xe) or the full set of considered for DEMO impurities (marked as He+N+Ne+Ar+Fe+Kr+Xe+W).

26 detectors are arranged in two rows, and each row covers the full field of view for the radial port location. The presented spectra refer to the detectors of row 1.

Relative measurement accuracy

- All energy of the primary quantum X_p is transferred to the electrons ($E_e=E_{Xp}$);
- The fluorescence takes away some of the energy, resulting in a decrease in the electrons' energy ($E_e=E_{Xp}-E_{Xf}$);
- All energy of the fluorescent quantum X_f is transferred to the electrons ($E_e=E_{Xf}$);
- Part of the X_f energy is taken by the secondary fluorescence quantum/quanta, resulting in a loss of energy for the electrons ($E_e=E_{Xf}-E_{Xf2}$).

The spectra from "white" radiation were obtained for the conversion region of both gas chambers: Drift1 (2 cm, Ne/CO_2 50/50 1 atm) and Drift2 (25 cm, Ar/CO_2 70/30 1 atm).

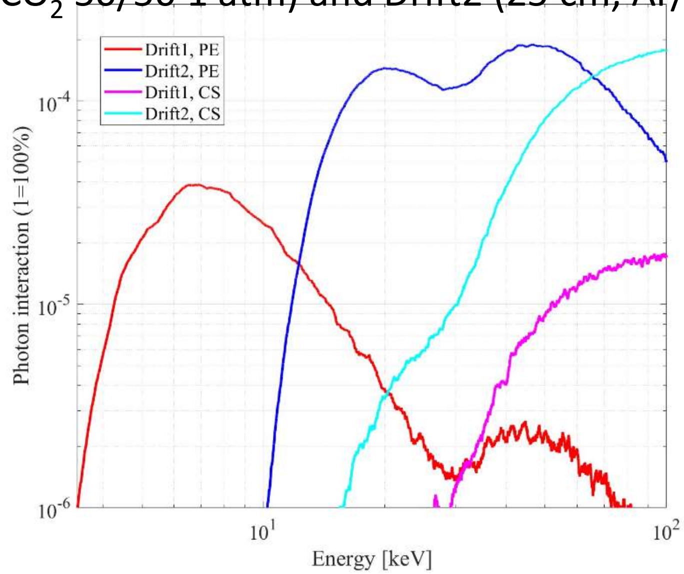

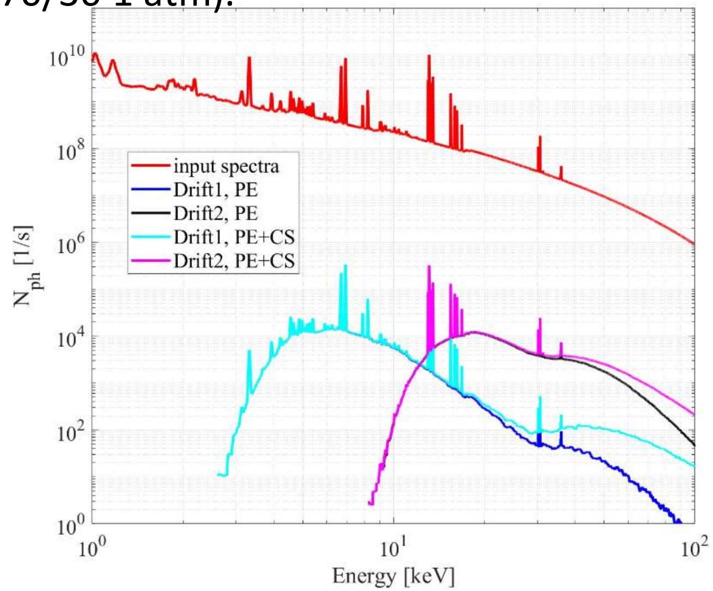

(left) Interaction of X-ray photons (white spectrum with 10^6/dE) with the regions of Drift1 and Drift2 through the photoelectric effect (PE) and Compton scattering (CS) (primary interactions). The results were smoothed over 100 points.
(right) Comparison of the input incident spectrum and result of its interaction with the detector in Drift1 and Drift2 through the photoelectric effect (primary interaction) and photoeffect plus Compton scattering.

Photoelectric effect spatial distribution

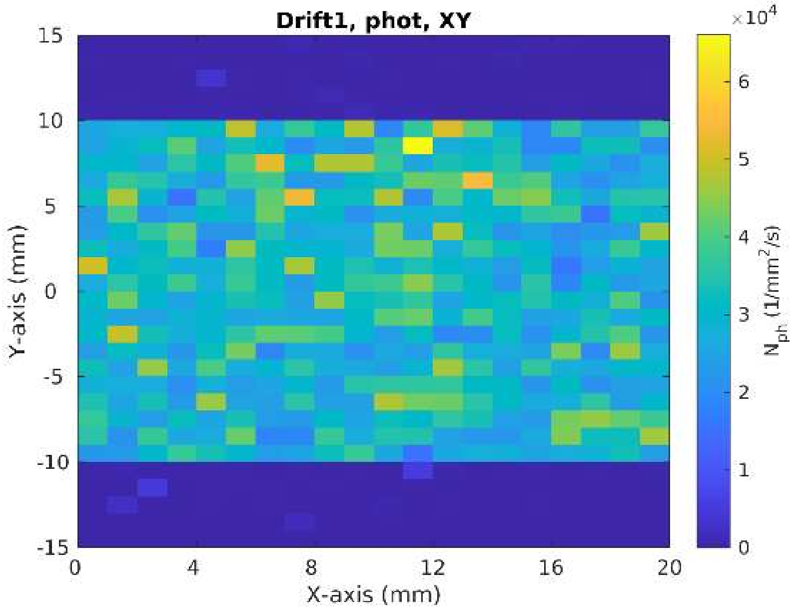

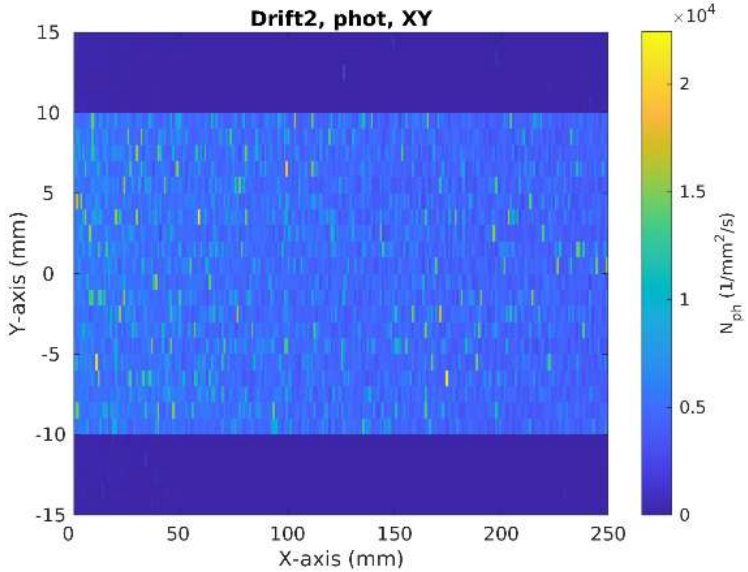

Density distributions of absorption (via photoelectric effect) on the readout plane (XY projection) of GEM1 and GEM2 detectors from the Drift area for the spectrum as above (for 12th detector in vertical port location).

Relative measurement accuracy

To determine the relative measurement errors => integrals/power of spectra ($\sum I_i \cdot E_i$) in the range from 1.5 keV to 100 keV.

For the total power values for the whole input spectra at times 500 s and 1000 s => relative difference is $(P_{1000s} - P_{500s})/P_{500s}$ = **0.0661 (6.6%)**.

The relative difference between the spectra simulated for two GEM gas chambers => $(P_{Drift12,1000s} - P_{Drift12,500s})/P_{Drift12,500s}$ = **0.0631 (6.3%)**.

Comparing the difference between the input spectra and the difference of the summed output spectra (Drift1+Drift2), there is a difference of <**0.5** percentage point (6.6%-6.3%).

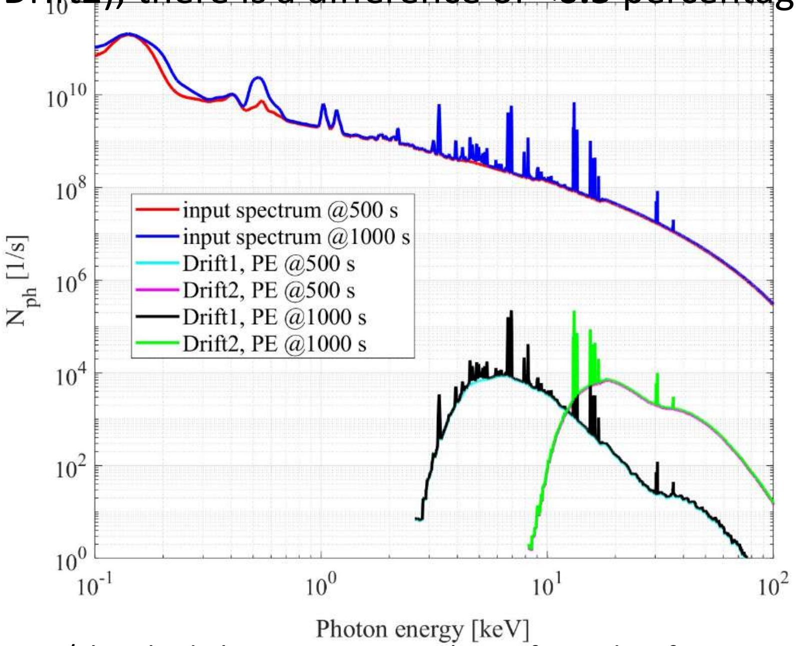

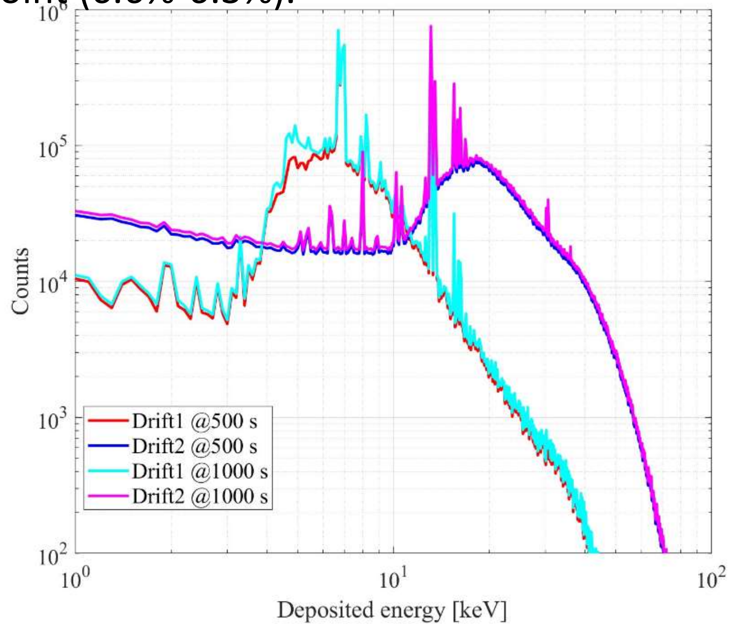

(left) Incidence/absorbed photon spectra in the Drift1 and Drift2 regions at 500 and 1000 s.

(right) The electron spectra obtained from the Drift1 and Drift2 regions for the incident spectra presented in the left panel.

Influence of the magnetic field

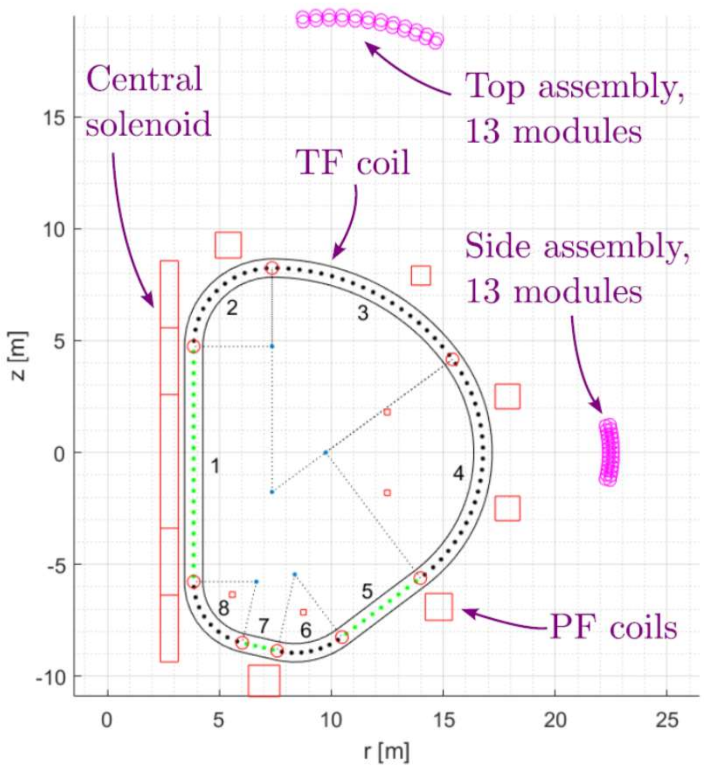

Diagram of evaluated field points with respect to DEMO field coils and solenoid. Assemblies were later revised to hold 26 modules each, but this configuration was used here.

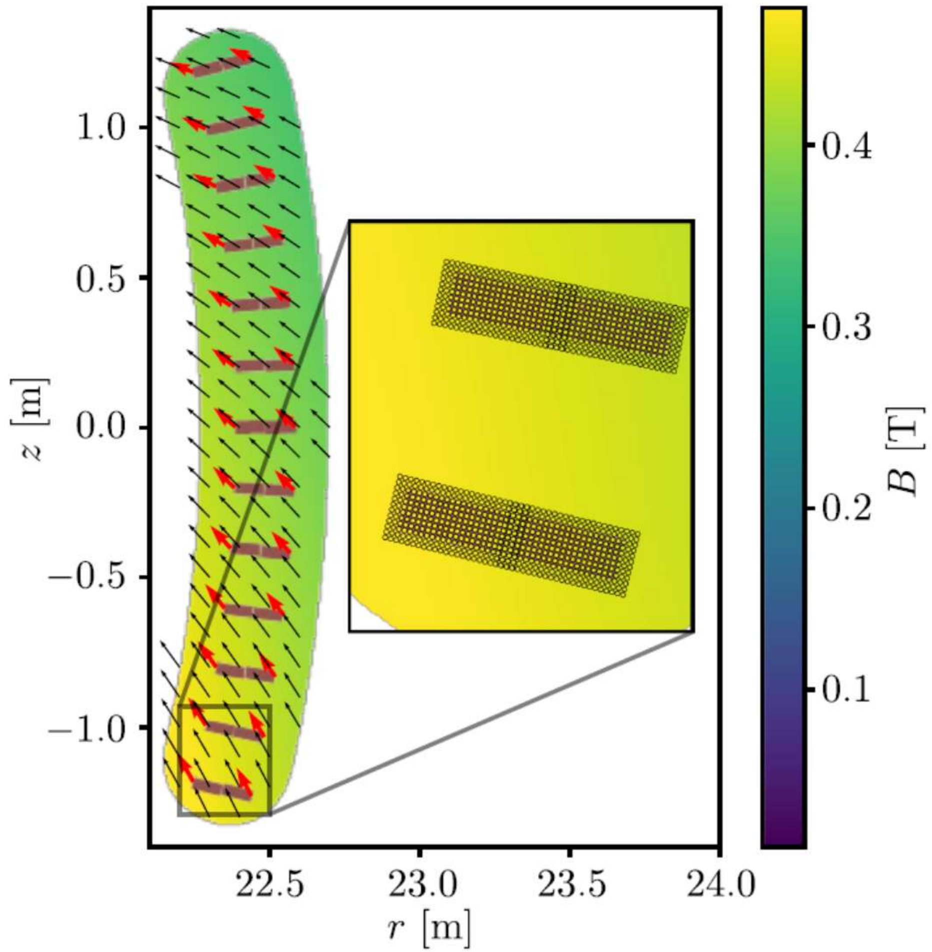

Magnetic field interpolation for the highest expected magnetic field.

M. Jagielski et al., to be published in PoP (2024)

Influence of the magnetic field

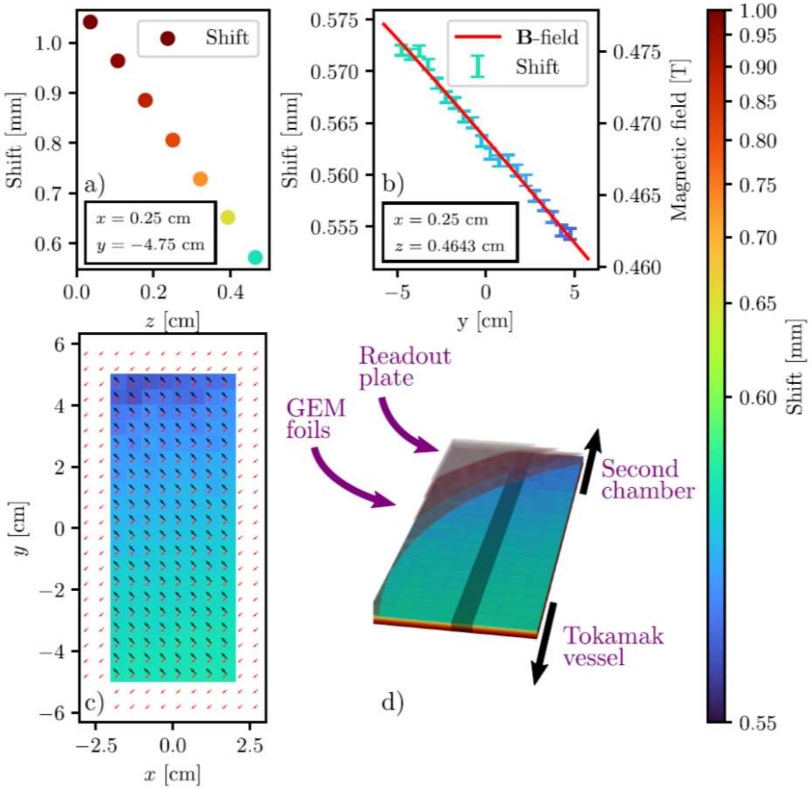

Distribution of average shifts of single electrons drifting in the standard GEM-based chamber. This case corresponds to the highest magnetic field. a) distribution of shift vector norms along z axis for specific x and y values. b) the change of shifts along y axis. Magnetic field norm is also shown. c) a colormap of the shift norms as well as vectors of magnetic field (in red) and shift (in black). d) a 3D voxel representation of the distribution of shifts inside drift region. Cells corresponding to values on (a) and (b) marked with darker color.

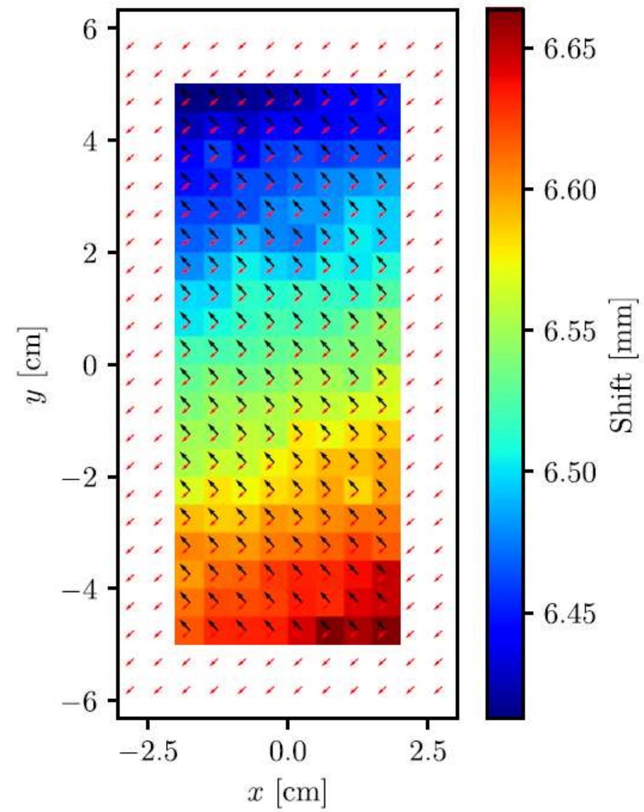

Shift map for furthest drift layer in the first chamber with THGEM cell configuration. The new shifts are up to around 6 mm in the worst case scenario.

Influence of the magnetic field

3 ns after ionisation: 150 keV photon

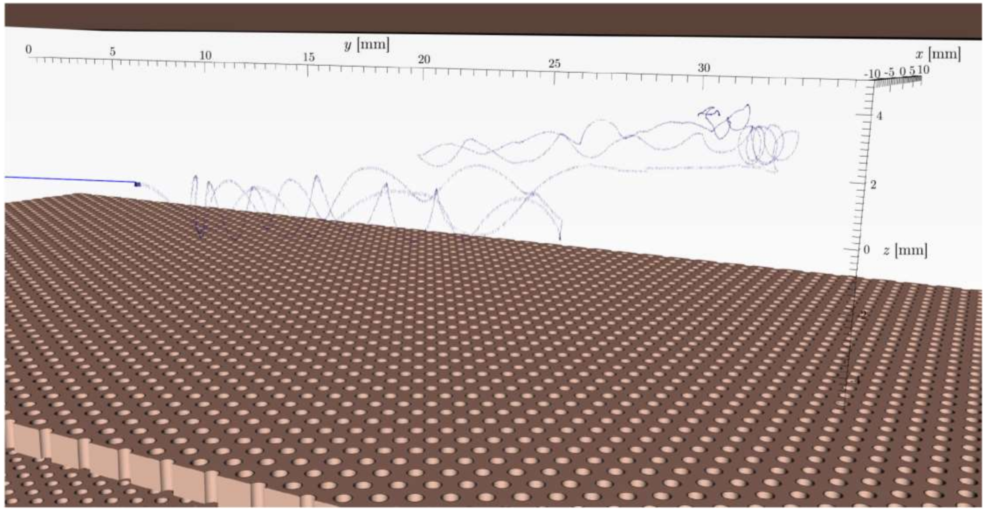

100 ns after ionisation: 150 keV photon

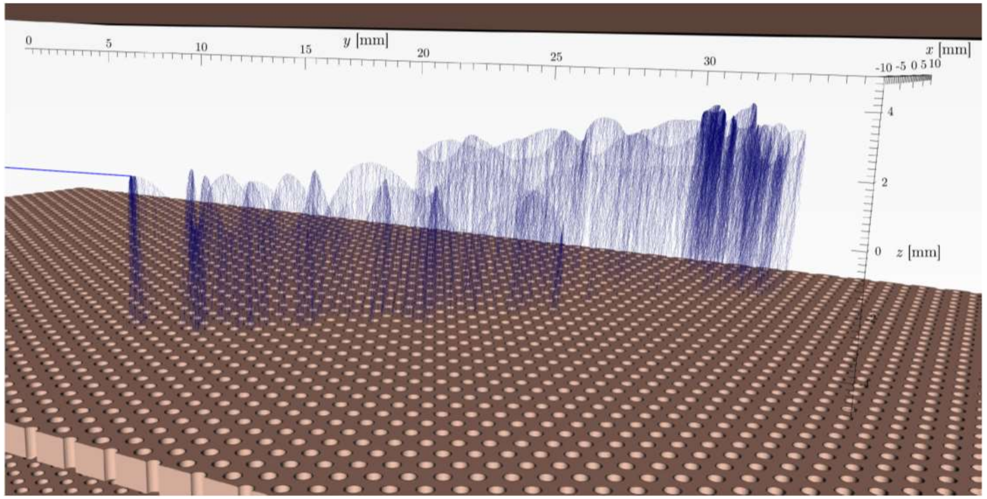

The deflection of the primary electron generated by an incoming 50 keV photon

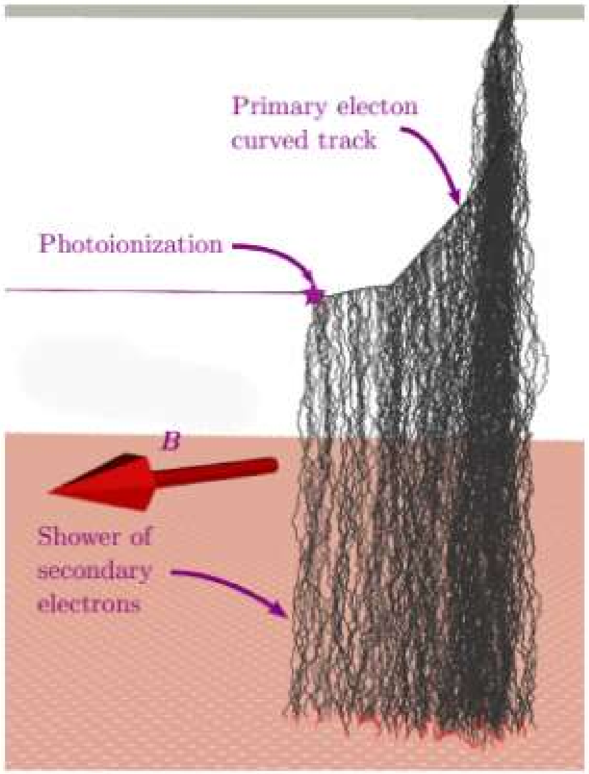

Neutron shielding of DAQ

The alternative materials offer better neutron shielding properties for the likely spectra in the bioshield plug, such as B_4C, W_2B_5, and WB_4, and could therefore be used to achieve thinner plugs with adequate shielding performance.

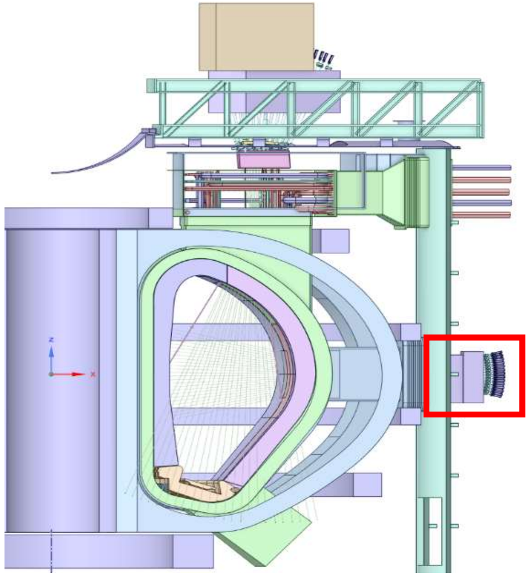

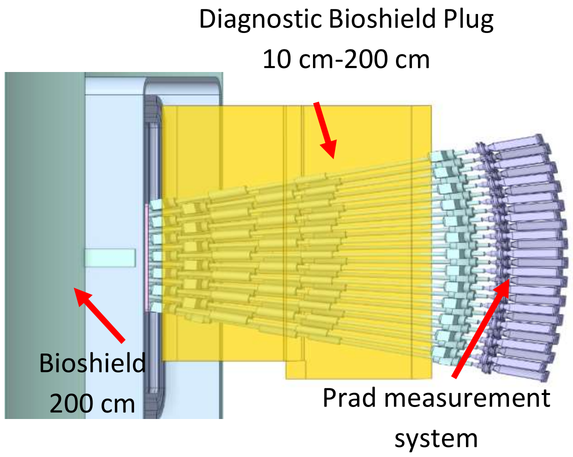

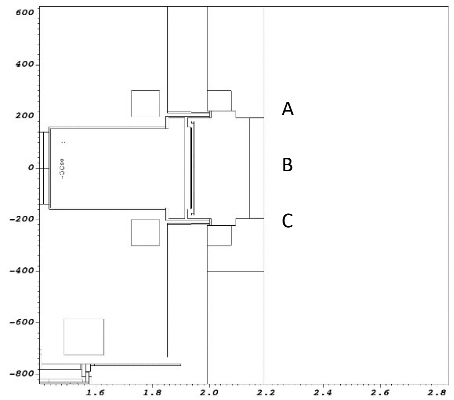

For each material, the bioshield plug thickness varied between 10 cm and 200 cm.

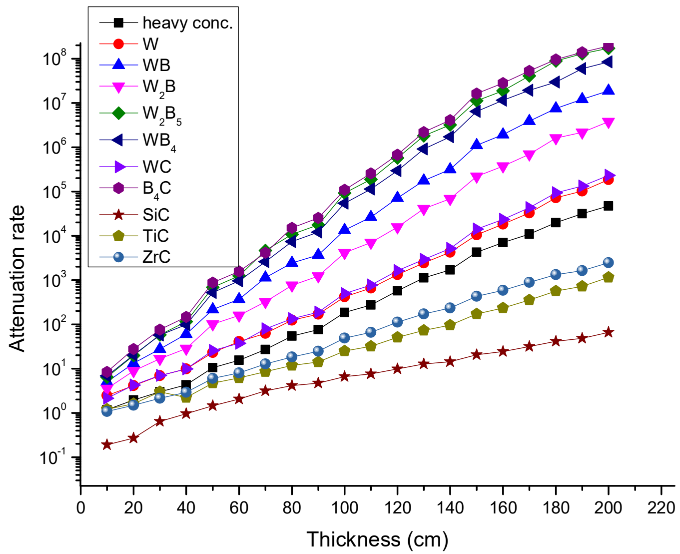

The neutron attenuation rate for selected materials with various thicknesses at B point.

S. Akbas et al., Phys. Plasmas 31 (2024) 033112

Design and development of imaging system (COMPASS Upgrade, TJ-II project)

M. Chernyshova[1], K. Malinowski[1], S. Jabłoński[1], A. Wojeński[2], T. Czarski [1], E. Kowalska-Strzęciwilk[1], G. Kasprowicz[2], T. Fornal[1], K.T. Poźniak[2], M. Kastek[1,2], P. Araszkiewicz[1,2], M. Imríšek[3], V. Weinzettl[3], F. Jaulmes[3], A. Alonso[4], K. McCarthy[4]

[1]*Institute of Plasma Physics and Laser Microfusion, Warsaw, Poland*

[2]*Warsaw University of Technology, Institute of Electronic Systems, Warsaw, Poland*

[3]*Institute of Plasma Physics of Czech Academy of Sciences, Prague, Czech Republic*

[4]*Laboratorio Nacional de Fusión, Madrid, Spain*

Development since 2020

Two-dimensional detector/toroidal camera

Objectives:

- 3D tomography of plasma, study of toroidal anisotropy;
- Additional 3D information to constrain 2D tomography;
- Direct imaging;
- Testing MHD simulations (synthetic diagnostics);
- Exploitation of the spectral resolution provided by the system can be used to constrain W transport codes, etc.;
- Supplementary to the identification of the magnetic axis (in case magnetic flux surface can be identified as isoemissive one);
- To test various properties of plasma with global imaging in photon counting mode;
- 3D phenomenon causing SXR emission connected with accelerated electrons, magnetic island dynamics and plasma disruption.

GEM detector imaging

XUV matrix readout structure of triangle pixels forming hexagon pixel. Pixels are characterised by optimal occupancy of the detecting area. While, the same detecting surface is kept for all acquisition planes. Detecting area size is 96 mm wide with 1.5 mm step between the pixels. This structure requires 3*128 very high speed channels. Pixel number - 18432.

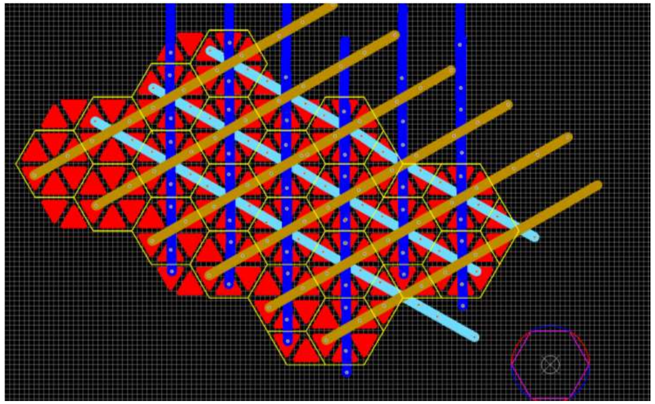

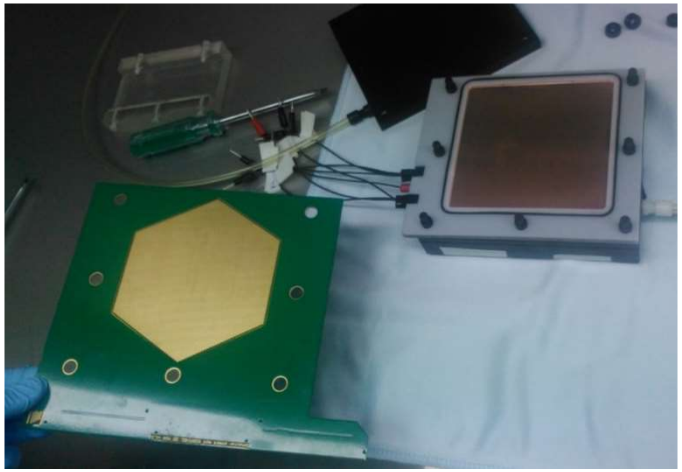

M. Chernyshova et al., poster at HTPD 2018

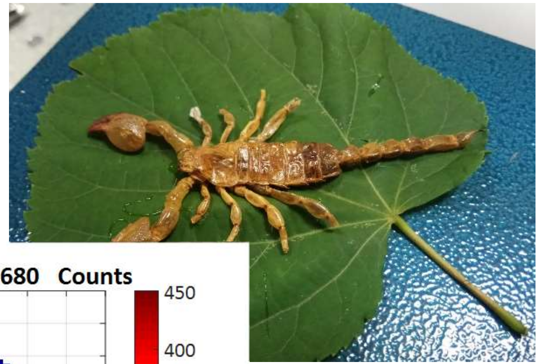

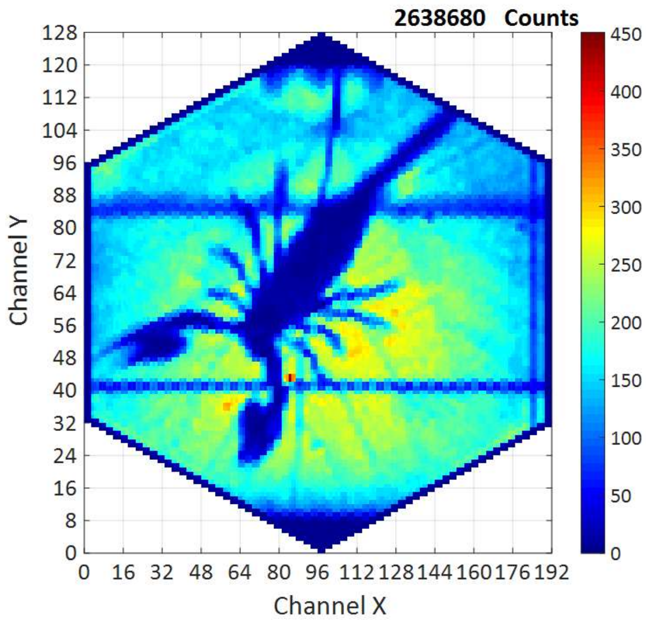

Planar distribution of X-ray tube radiation coming through scorpio.

Development of readout structure

The detector readout structure was chosen in the form of hexagon pixels of 0.35 mm side pitch. Sophisticated pixel interconnection proposed.

The **investigated readout structure UXYV.** Interconnected pixels to reduce number of electronics channels.

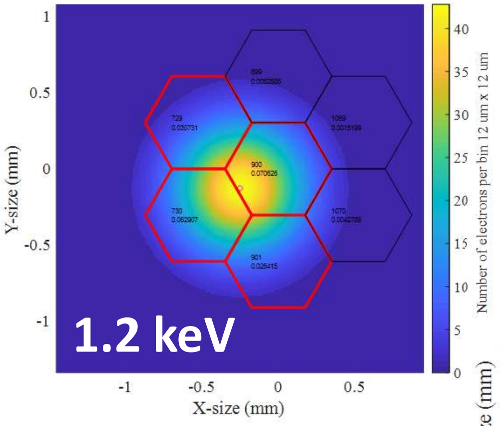

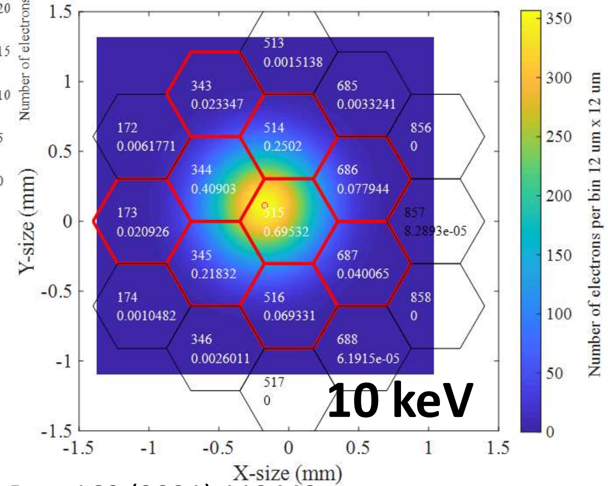

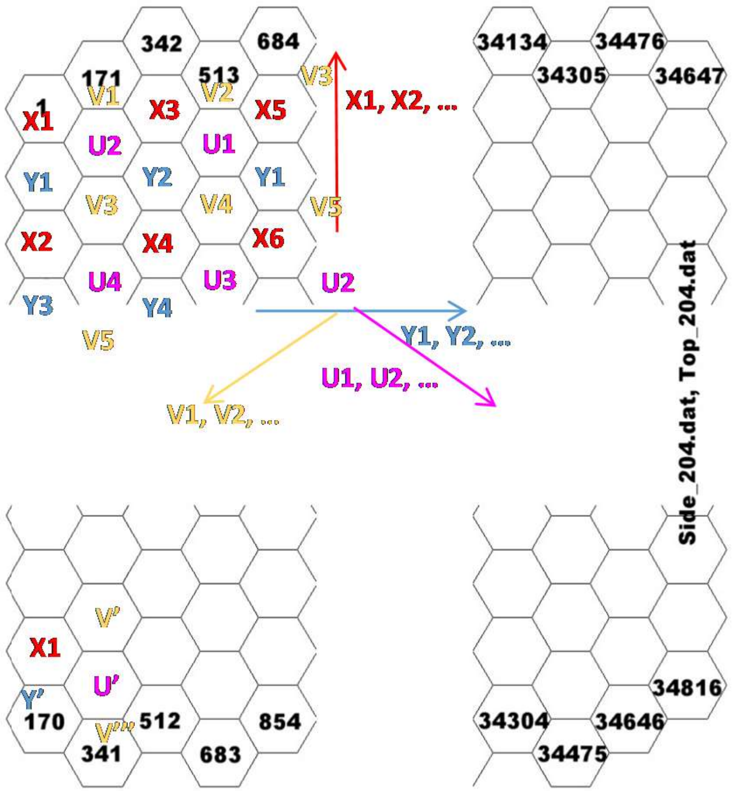

M. Chernyshova et al., Fus. Eng. Des. 169 (2021) 112443

Development of readout structure

(left) Average number of pixels that would register signals from a single X-ray photon, depending on the pixel size (hexagonal side). (right) Distributions of the number of signal pixels from a single electron avalanche, originating from X-rays with an assumed energy spectrum, for several selected pixel sizes.

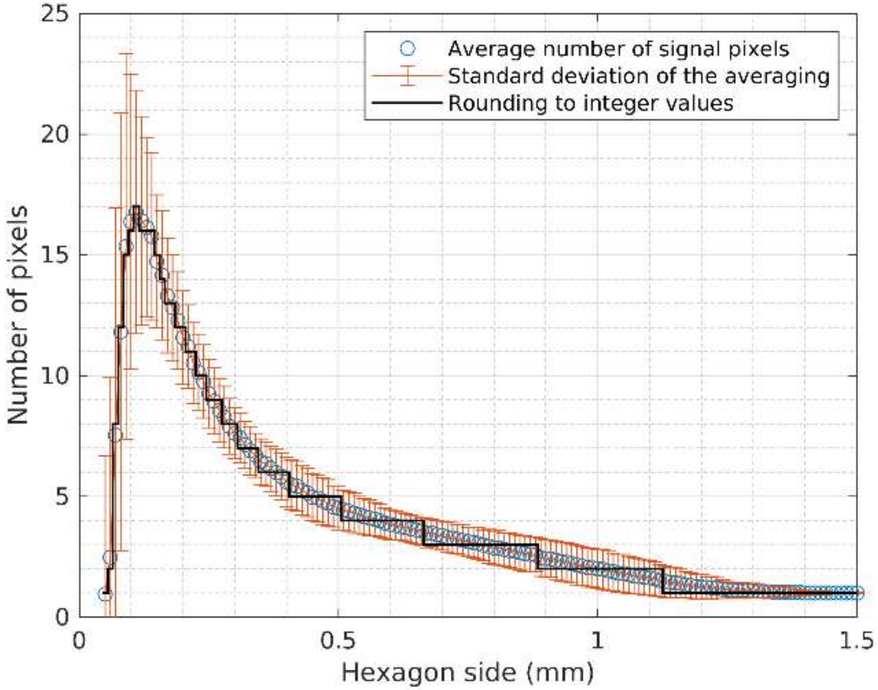

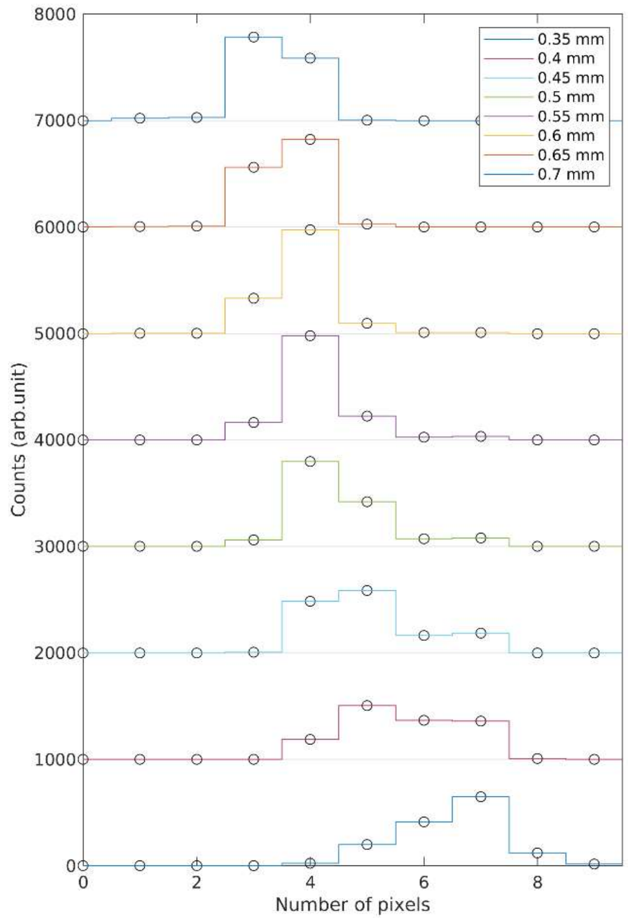

Optimised for 3072 individual channles (ab. **33k** pixels)

K. Malinowski et al., JINST 16 (2021) C11014

Amplification stage optimisation

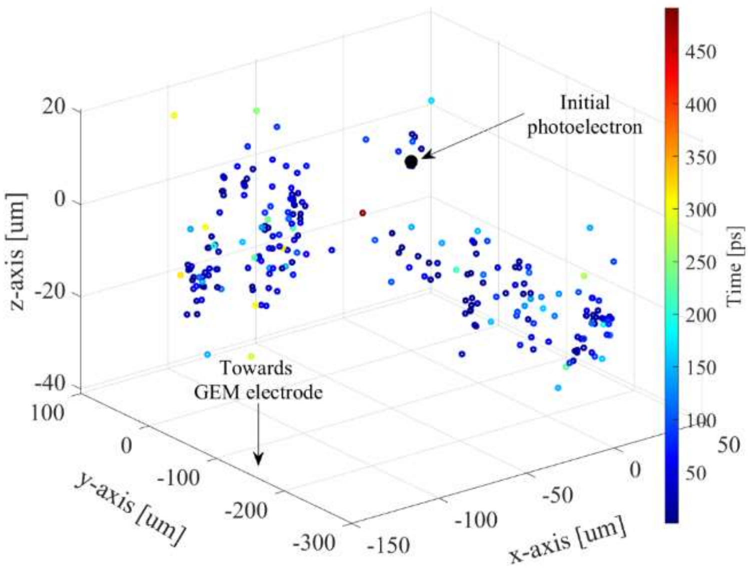

Spatial distribution of thermal (primary) electrons from absorption of 5.9 keV photon, including excitations, thermalized up to 2.0 eV energy in Ar/CO_2 at 2.4 kV/cm conversion field.

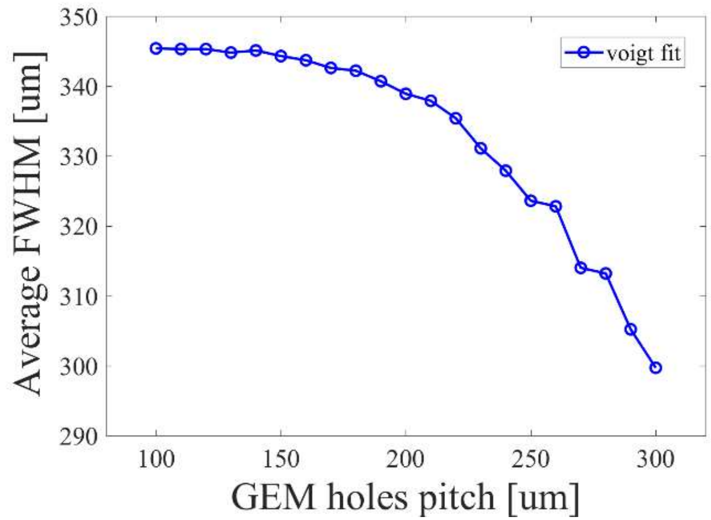

Average FWHM (Voigt fitting of single photon electron cloud shape) vs. GEM hole pitch for Single-GEM detector.

Electron spatial density distribution on the readout anode for GEM pitch: GEM1/GEM2/GEM3 pitch: 140/140/140 μm and 280/140/100 μm, 50 μm cylindrical holes.

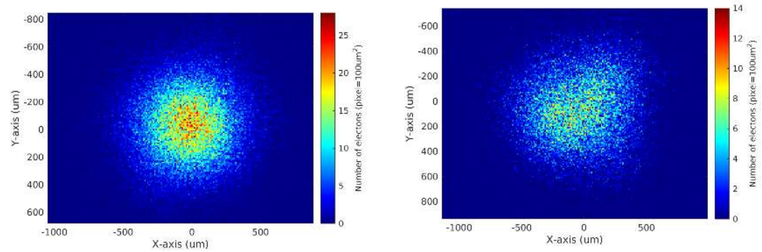

M. Chernyshova et al., NME 33 (2022) 101306

Amplification stage optimisation

Simulations of single GEM foil towards optimal spatial avalanche distribution

The most optimal case => 70d70c70t structure with hole pitch - 120 µm.

The mean electron gain of the GEM detector calculated for all cases studied.

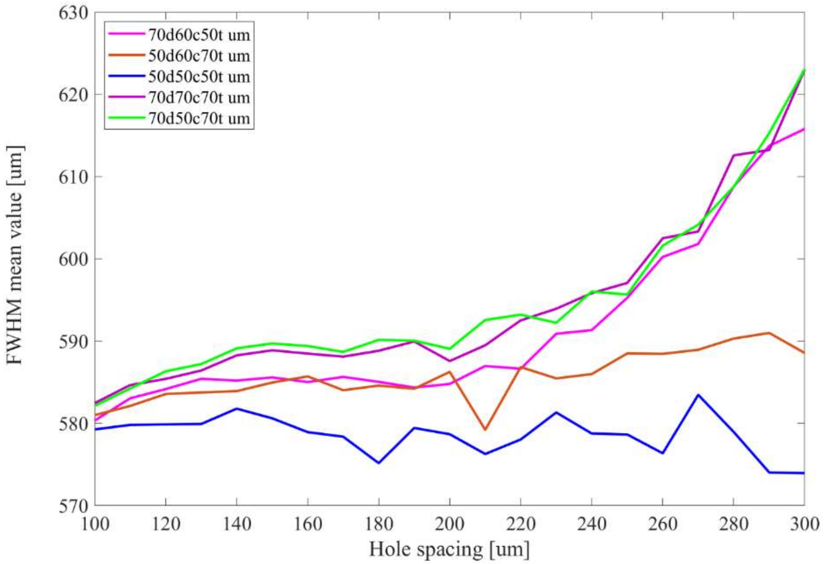

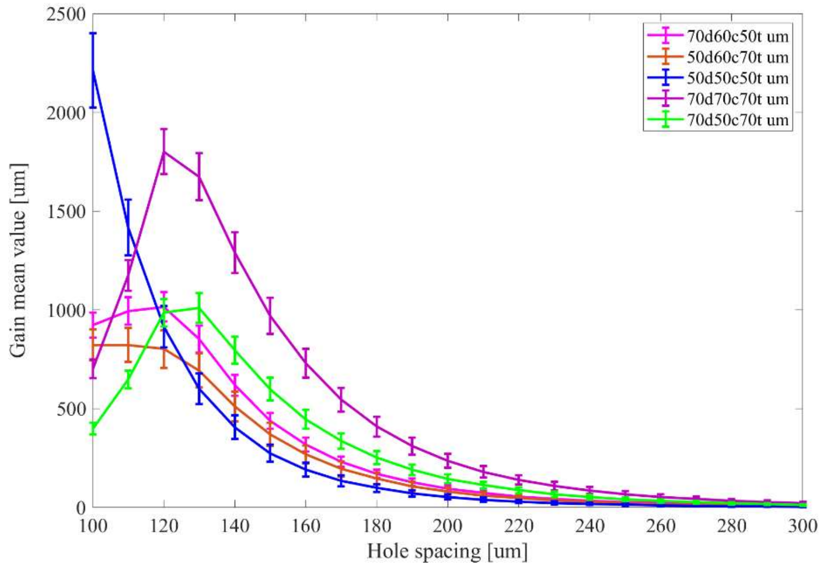

Distribution of FWHM values of electron avalanches on readout electrode for different GEM foil configurations (hole shapes and spacing).

K. Malinowski et al., to be published (2024)

Design and development of imaging system (COMPASS U, TJ-II)

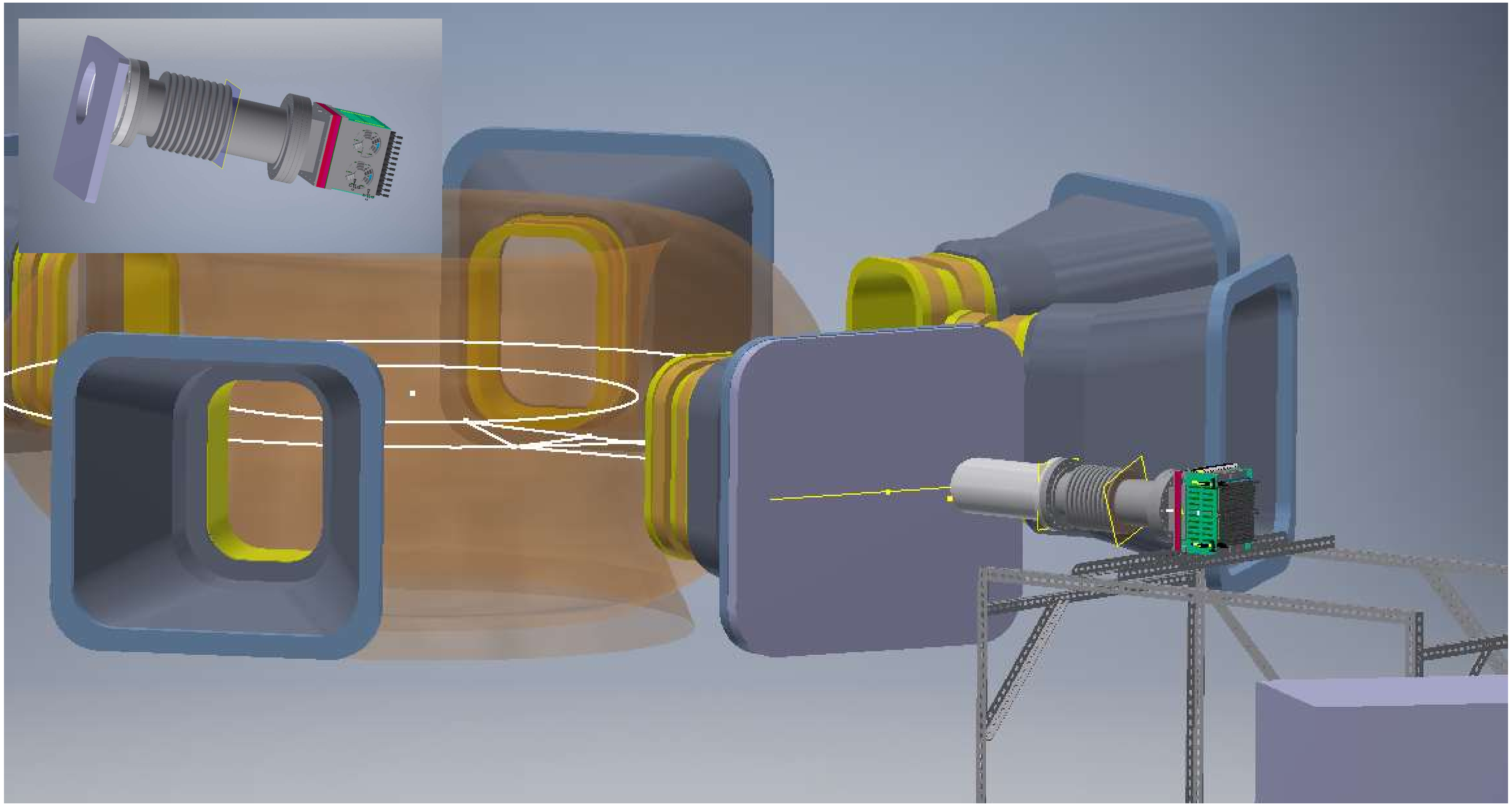

Design and development of imaging system (COMPASS U, TJ-II)

Initially, tests of the detector under construction are planned on smaller machines (COMPASS-U).

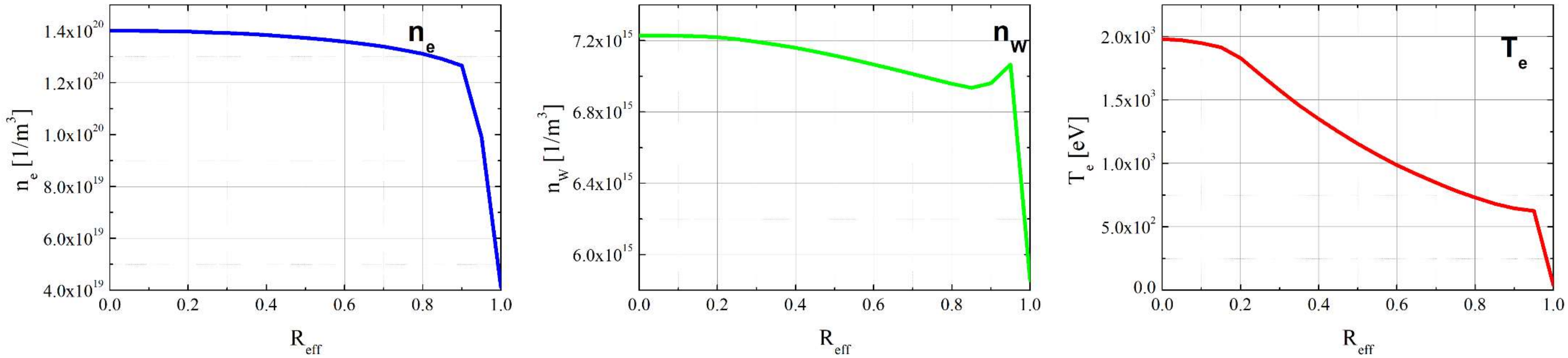

Outside port plug arrangement layout showing sensor and plasma contour, the red zone is the field of plasma volume view

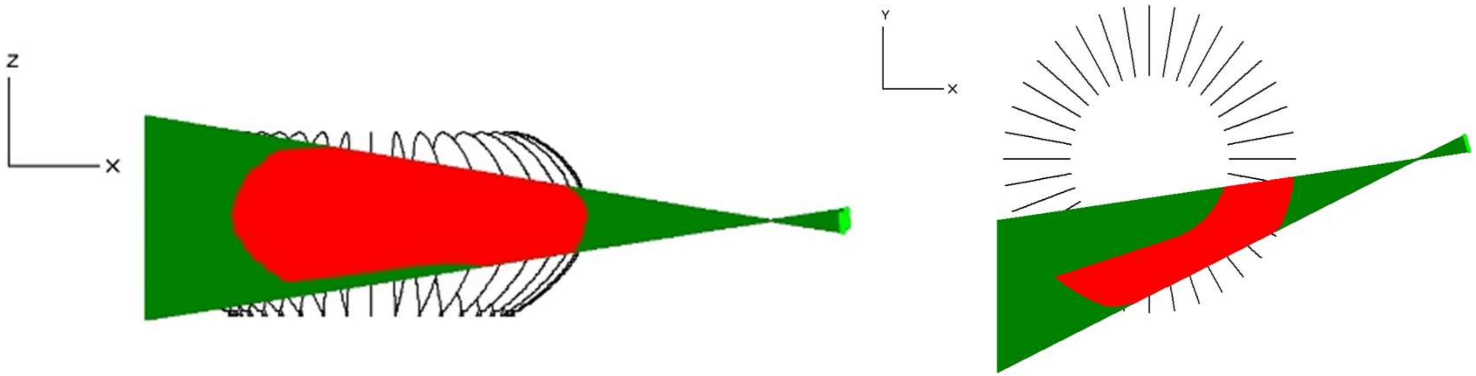

M. Chernyshova et al., NME 33 (2022) 101306

Design and development of imaging system (COMPASS U, TJ-II)

Simulations of SXR spectra for Phase 1 COMPASS U scenario #23400, t = 1.245 s

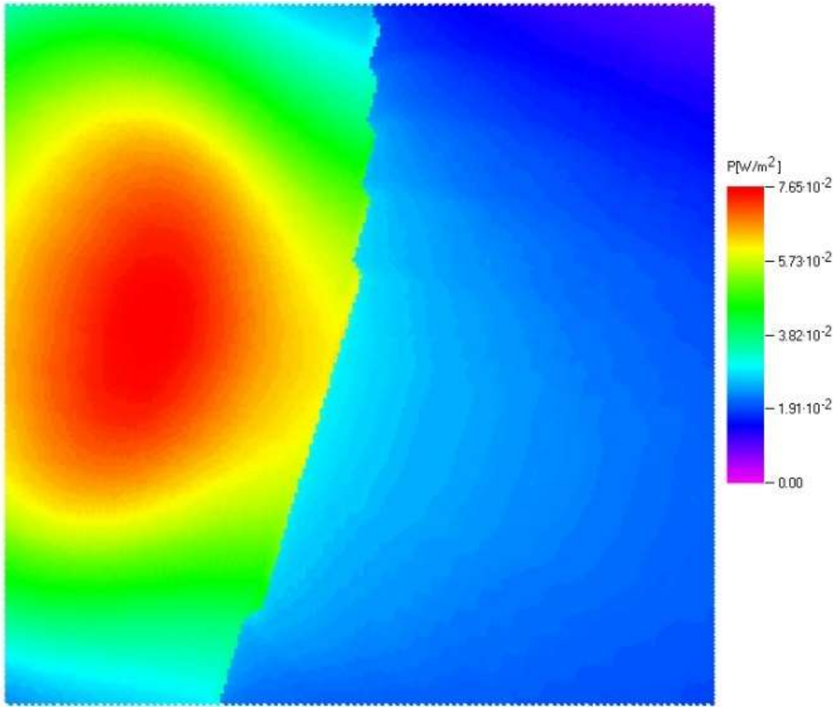

2D power density distribution of calculated SXR emission

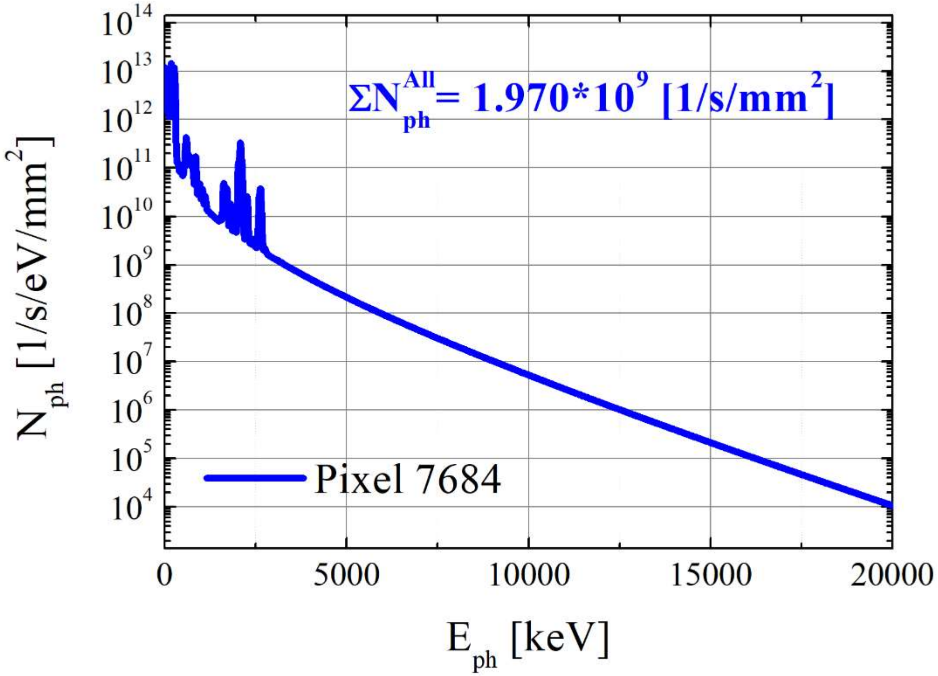

Spectrum for the most irradiated pixel

Design and development of imaging system (COMPASS U, TJ-II)

- TJ-II as a testing machine

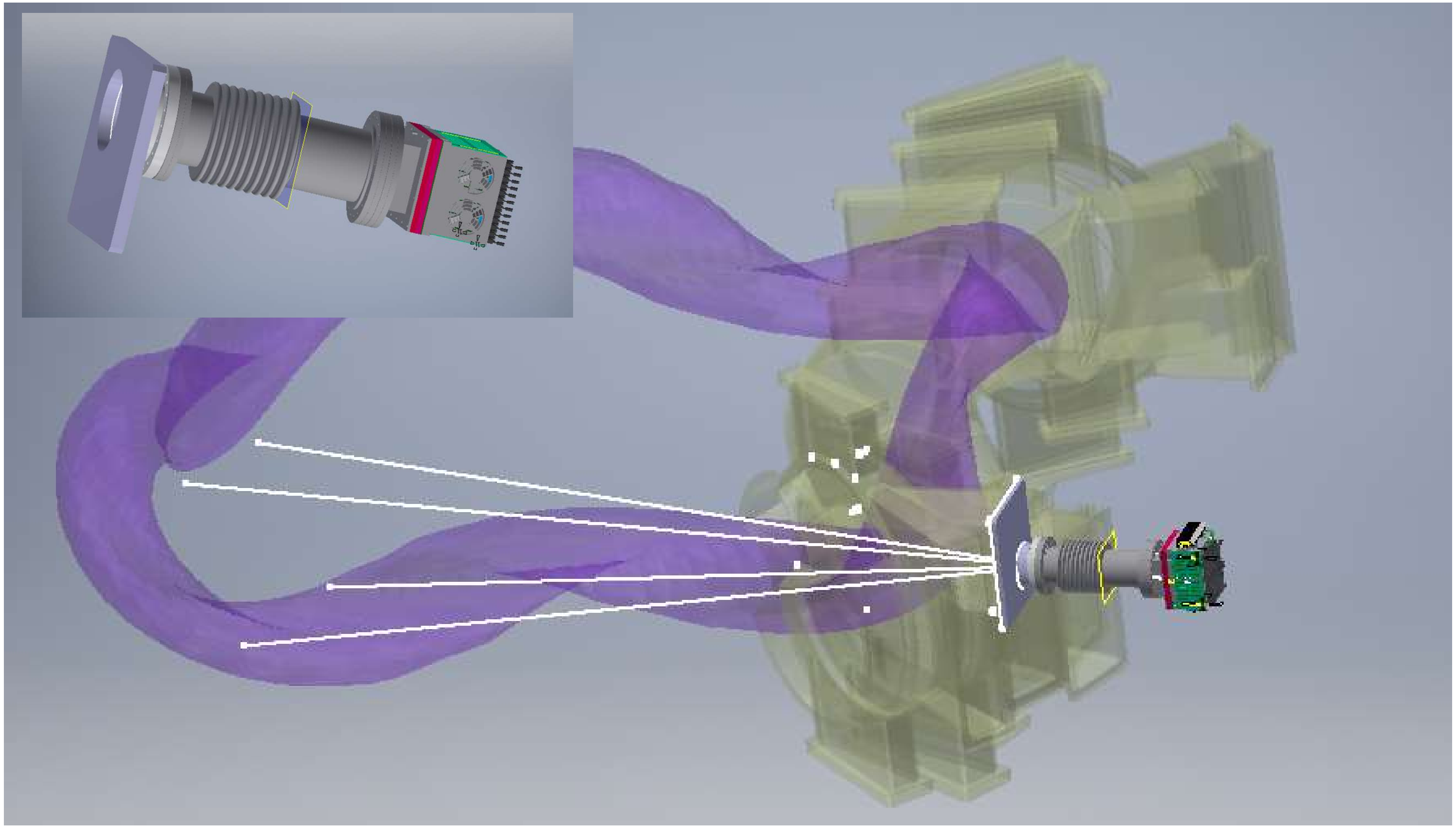

Design and development of imaging system (COMPASS U, TJ-II)

TJ-II as the first testing machine (!)

X-ray quantum spectra of maximum intensity for the case of pure hydrogen plasma and hydrogen plasma with impurities:

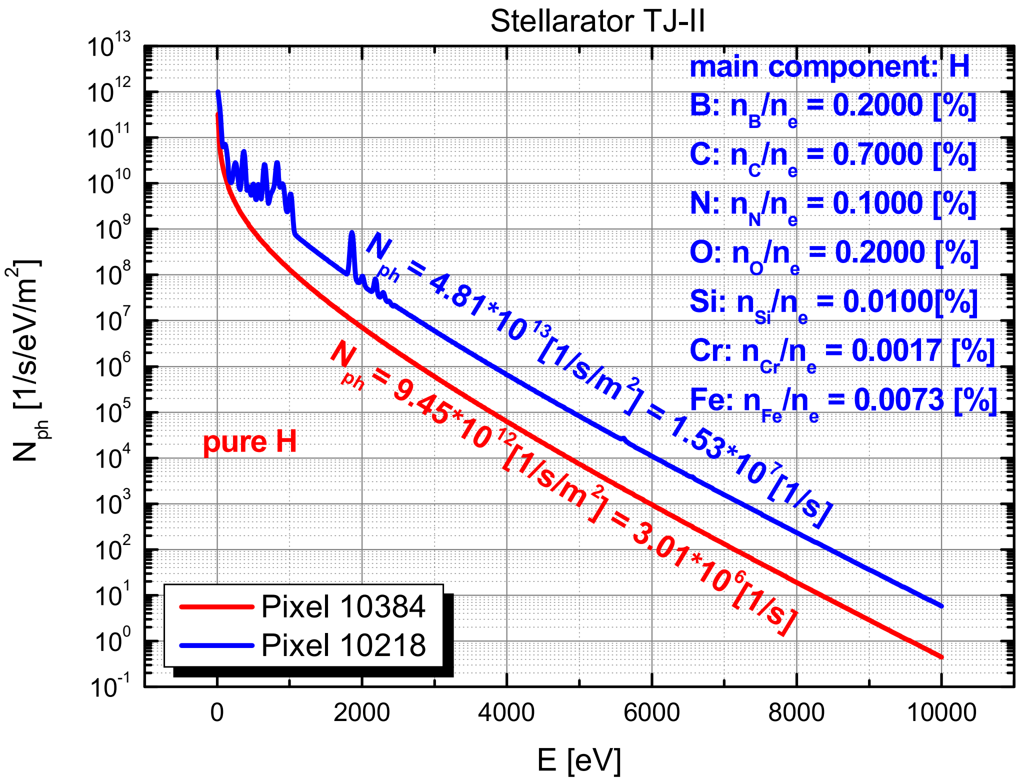

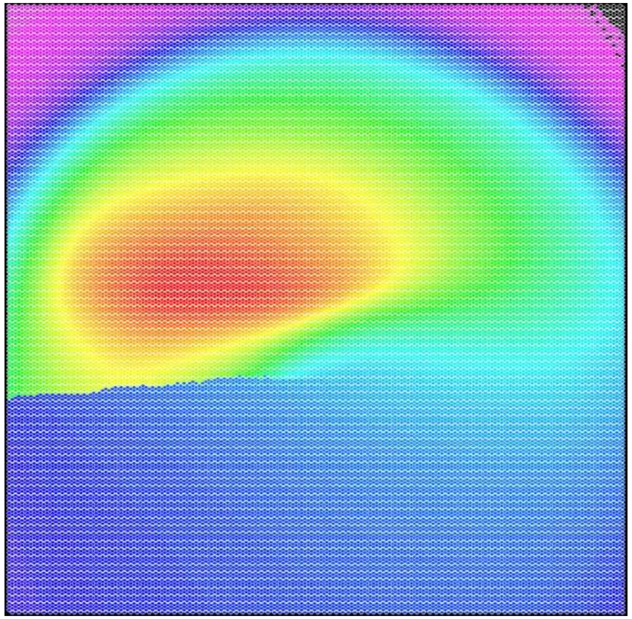

X-ray power distribution on the GEM matrix (plasma: H, B, C, N, O, Si, Cr, Fe)

Design and development of imaging system (COMPASS U, TJ-II)

Plasma composition adopted in the simulations: H, B(0.2%), C(0.7%), N(0.1%), O(0.2%), Si(0.01%), Cr(0.0017%), Fe(0.0073%). $T_{e,max}$= 0.6keV, $n_{e,max}$= $3.9*10^{19}m^{-3}$

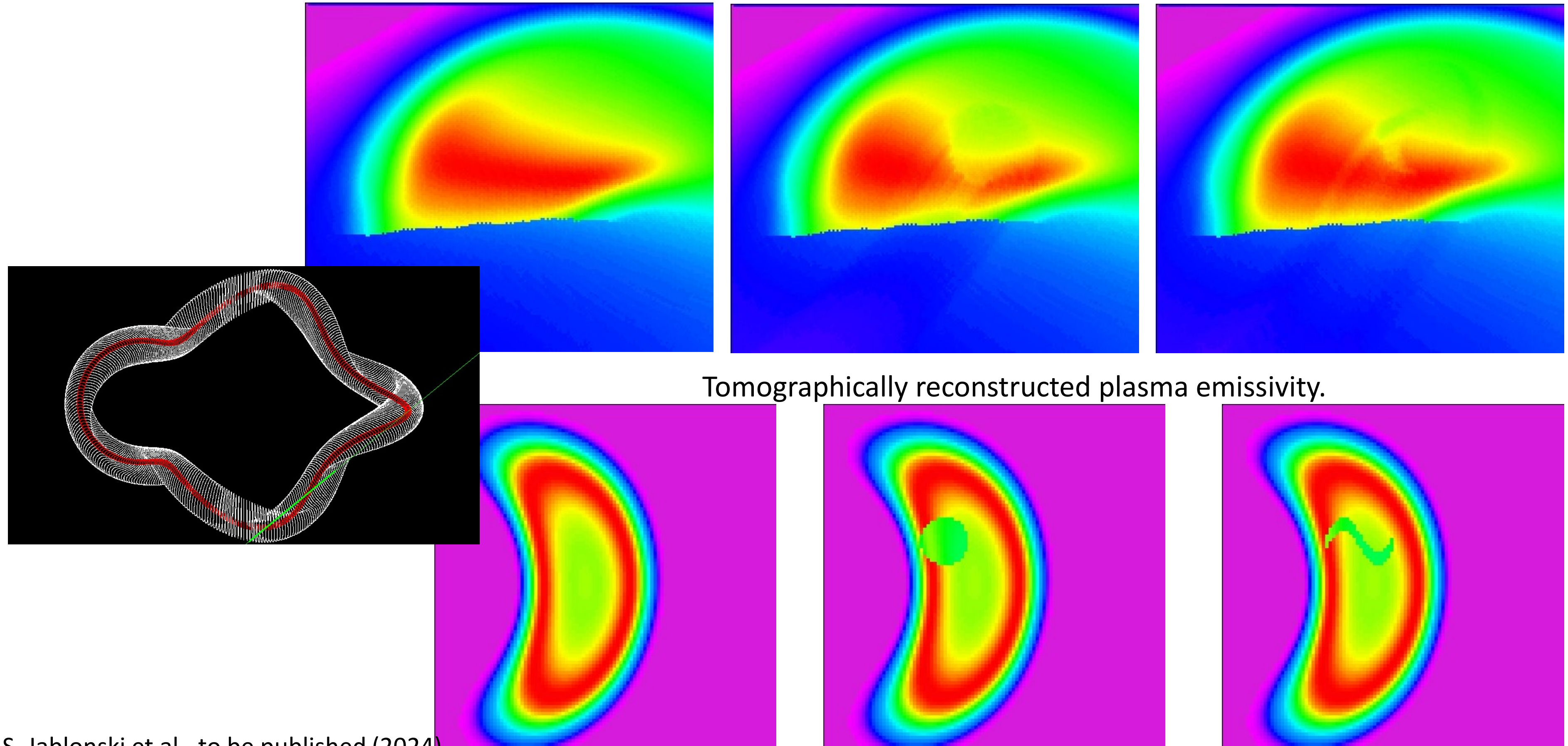

Tomographically reconstructed plasma emissivity.

S. Jablonski et al., to be published (2024)

Design and development for JET tokamak

W. Dominik[1], M. Chernyshova[2], T. Czarski[2], K. Jakubowska[2], J. Rzadkiewicz[2], M. Scholz[2], L. Karpinski[2], K. Pozniak[3], G. Kasprowicz[3], W. Zabolotny[3], A. Wojeński[3], A. Shumack[4], H. Czyrkowski[1], R. Dabrowski[1], I.K. Kierzkowski[1], Z. Salapa[1]

[1]Warsaw University, Faculty of Physics, Institute of Experimental Physics, 00-681 Warsaw, Poland

[2]Institute of Plasma Physics and Laser Microfusion, Warsaw, Poland

[3]Warsaw University of Technology, Institute of Electronic Systems, Warsaw, Poland

[4]Culham Centre for Fusion Energy, Culham, UK

Development since 2011

IFPiLM

Design and development for JET tokamak

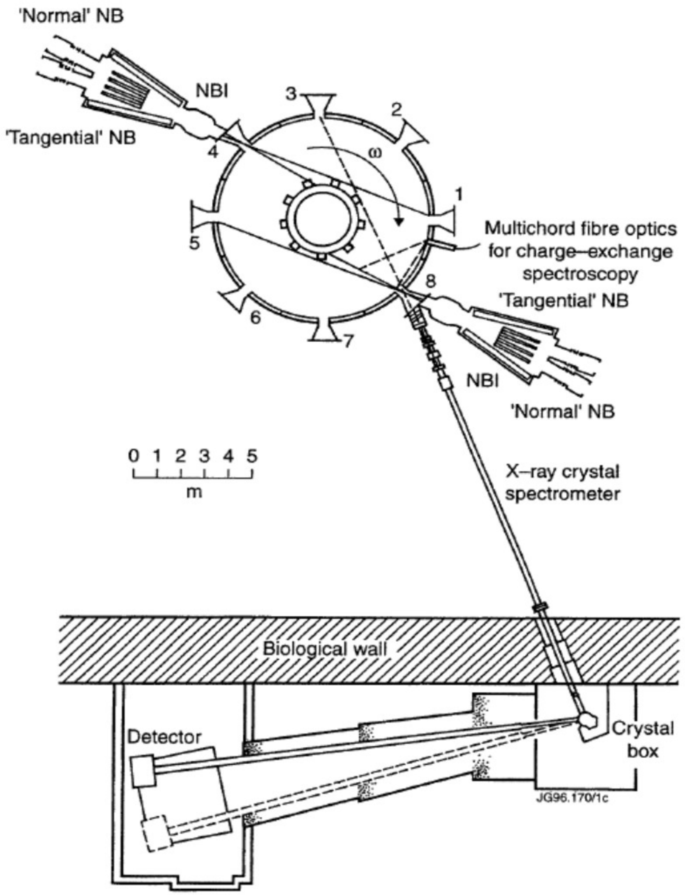

High-resolution X-ray crystal spectrometer at JET

L.-G. Eriksson et al., PPCF **39** (1997) 27

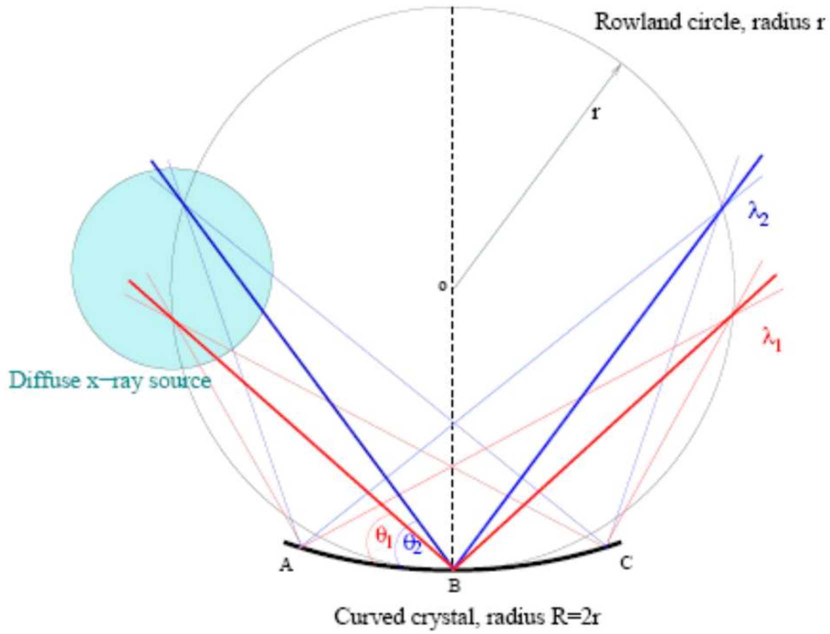

High-resolution Johann curved crystal X-ray geometry

M. Nelson PhD 2006

Design and development for JET tokamak

Objectives of high-resolution X-ray diagnostics at JET:

Monitoring of the radiation emitted by Ni^{26+} and W^{46+} at 2.4 keV and 7.8 keV from the central plasma; providing also information on the continuous radiation.

The final design of the position sensitive GEM X-ray detectors driven by the following assumptions:

- Large detection area (20 x10 cm^2),
- High charge gain possibility,
- Detection stability for a wide range of photon rates,
- Reasonable energy resolution.

Operational 1986- ~2006

Observed the resonance $1s^2p\ [^1P_1] - 1s^2\ [^1S_0]$ line of He-like nickel at 1.5856 Å (7819.4 eV), the most prominent metal in JET inconel wall material (~72%), with the highest impurity concentration in the central plasma and the largest effective emissivity for the high temperature JET plasmas.

Parameters calculated: Ion temperature, Toroidal rotation, Nickel concentration

Design and development for JET tokamak

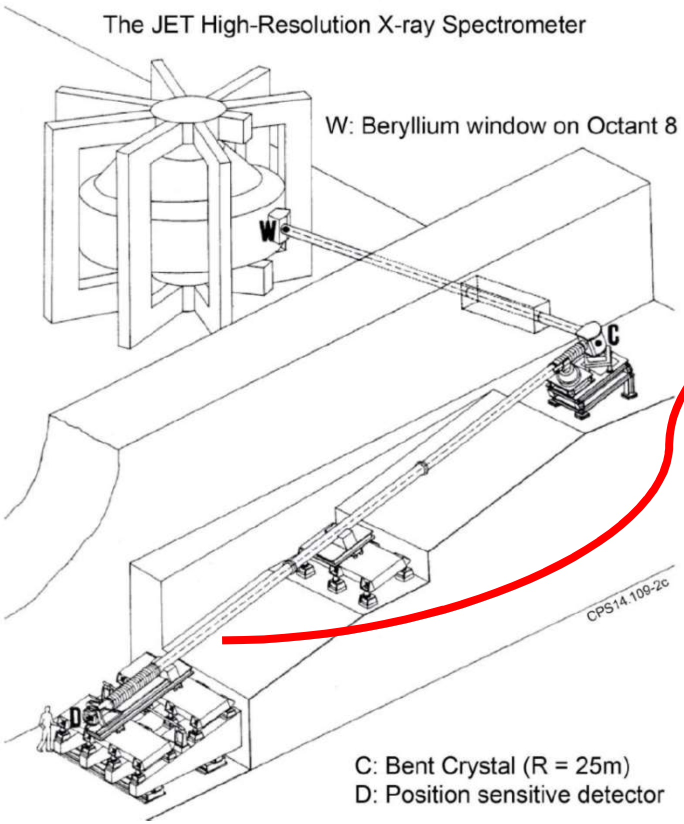

R. Bartiromo et al., RSI **60** (1989) 237

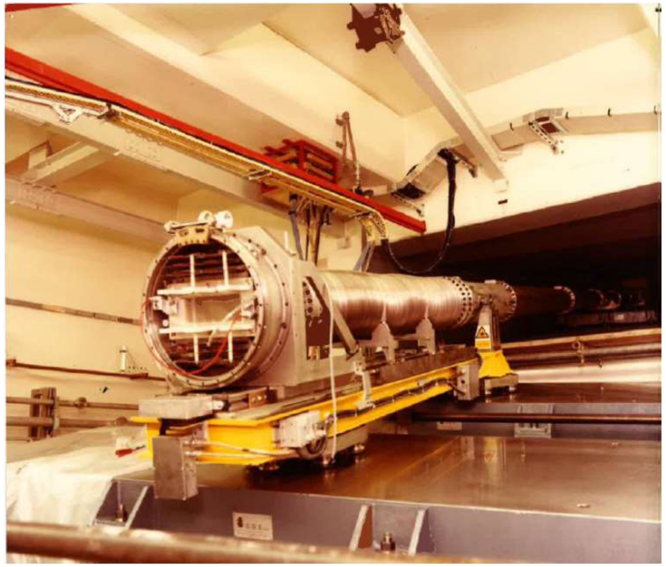

Spectrometer upgrade for core W concentration measurement:

- **New SiO_2 crystal**
- **GXS Project 2010 *(GEM detector for X-ray crystal Spectrometry)***

The geometrical factors of the spectrometer together with the detector anode structure make possible to obtain an excellent energy resolution $\Delta\lambda/d\lambda$ = 20 000 (corresponding to changes in the rotation velocity of ~10 km/s) being crucial for the precise line-shape analysis.

Design and development for JET tokamak

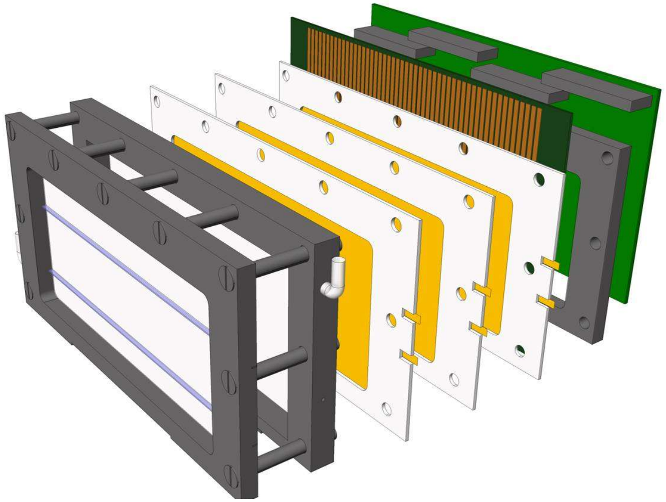

Structure of the T-GEM X-ray detector.

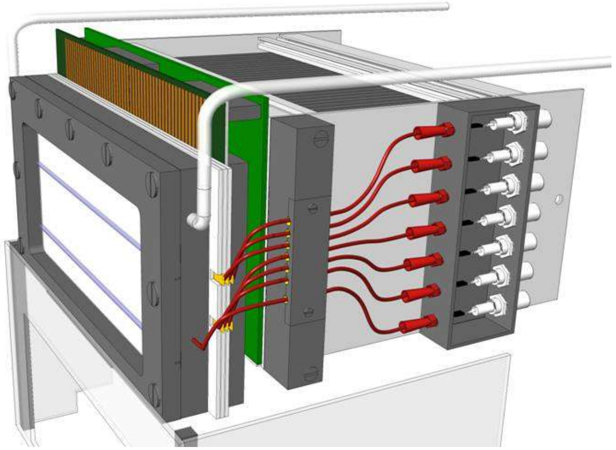

View of the assembled final T-GEM module.

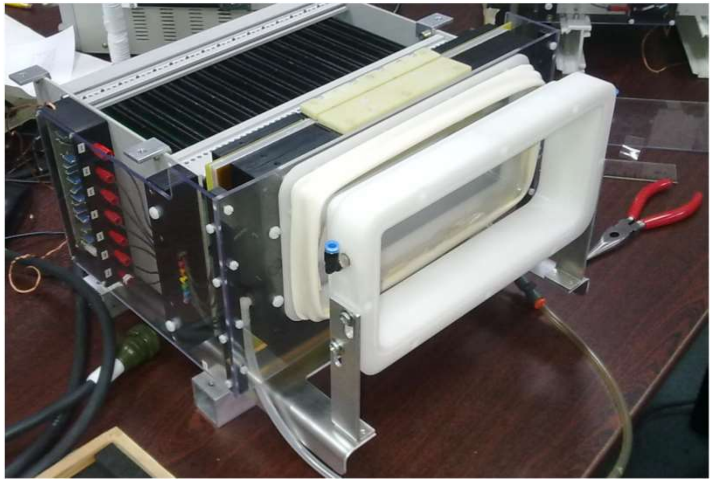

Photo of the assembled final T-GEM module with He buffer fitting.

Design and development for JET tokamak

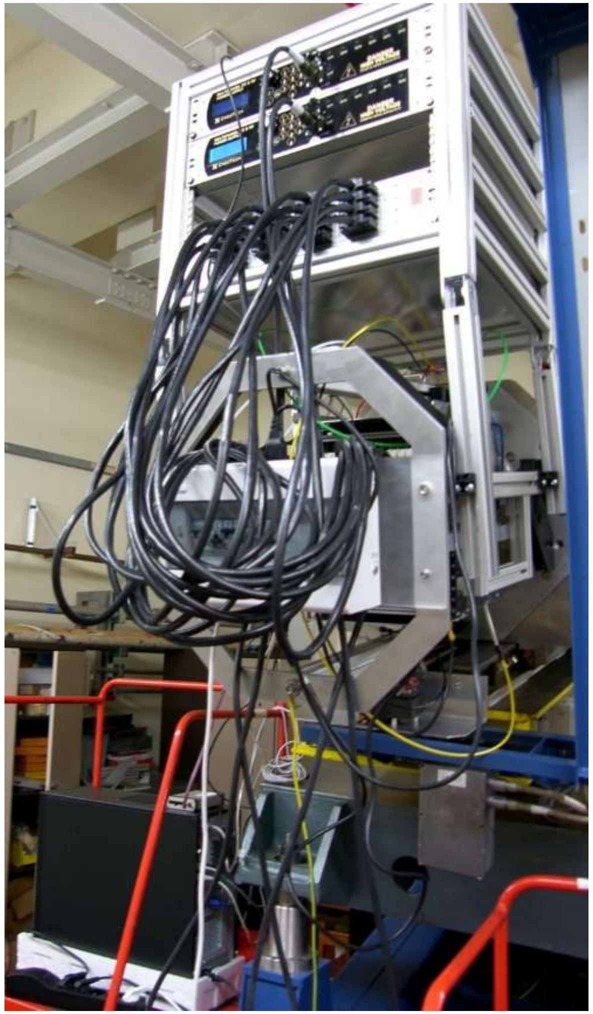

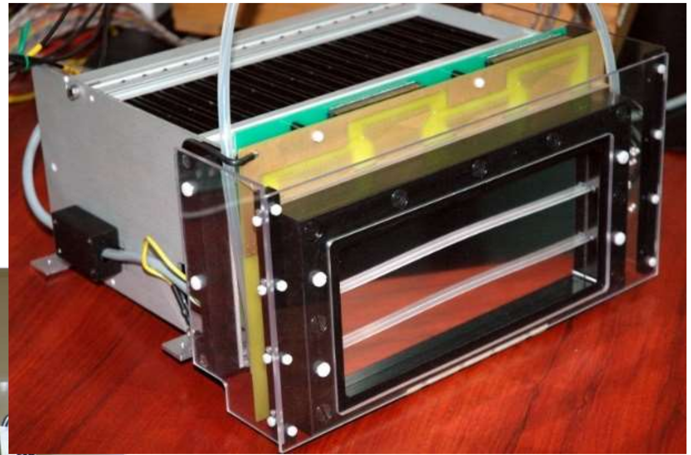

Design and development for JET tokamak

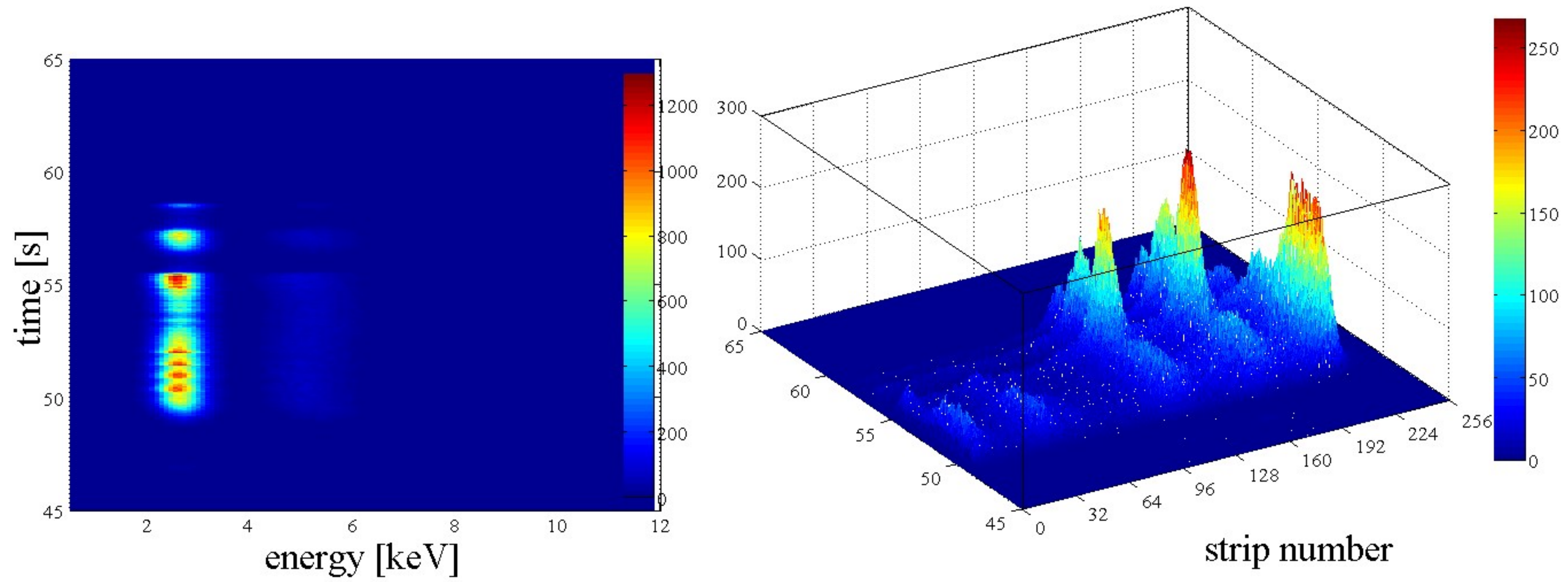

Photon intensity time evolution (left) and 3D view of individual histograms (right) for each strip irradiated at JET pulse with 10 ms integration time. #9019093.

M. Chernyshova et al., JINST 9 (2014) C03003

Design and development for JET tokamak

'Ni detector' results:

Spectrum range Δλ=1.3 pm

Ni^{26+}(w) = 1.59 Å, 7.8194 keV

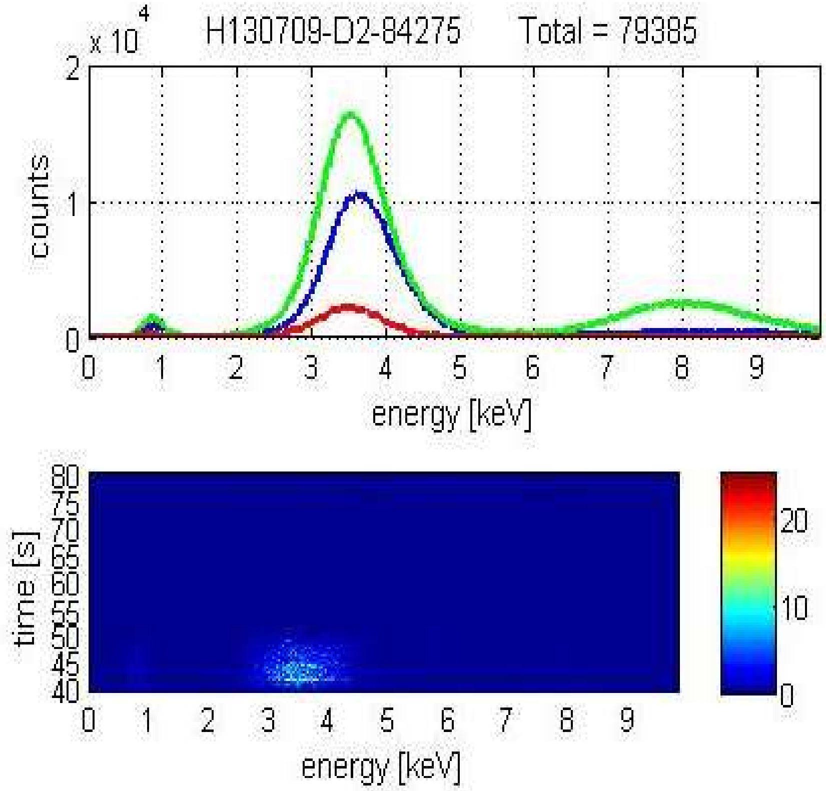

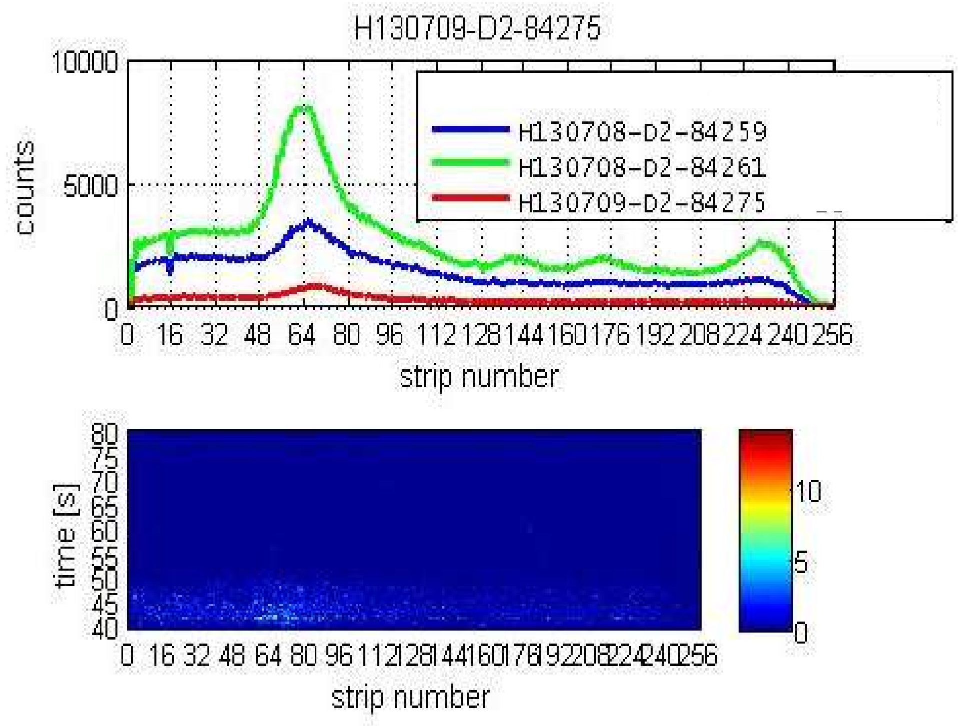

GEM detectors for X-ray crystal spectrometry at JET: results

Fitting of Ni spectra

Voigt function

Gaussian functions

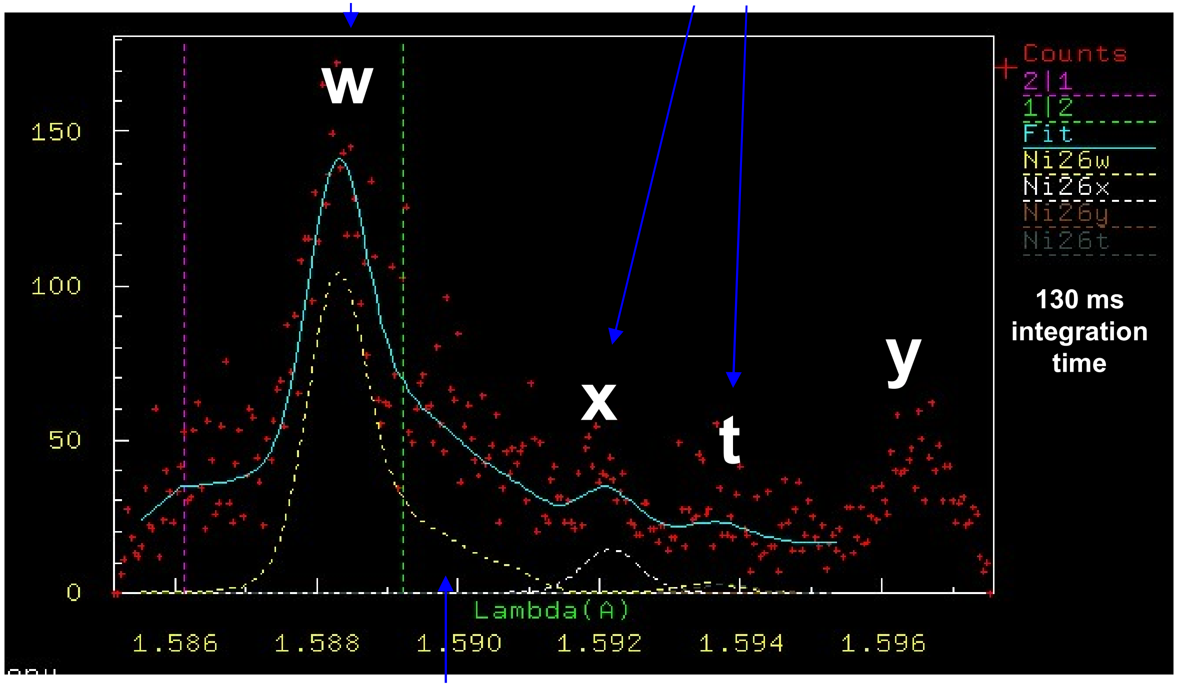

Feature consisting of dielectronic satellites, fit with function depending on T_e

Ni^{26+} spectral lines

w: 1s2p $^1P_1$ -> $1s^2$ $^1S_0$

x: 1s2p $^3P_2$ -> $1s^2$ $^1S_0$

y: 1s2p $^3P_1$ -> $1s^2$ $^1S_0$

Dielectronic satellite line n=2

t: 1s2s2p $^2P_{1/2}$ -> $1s^2 2s$ $^2S_{1/2}$

Feature dielectronic satellite lines

n>=3.

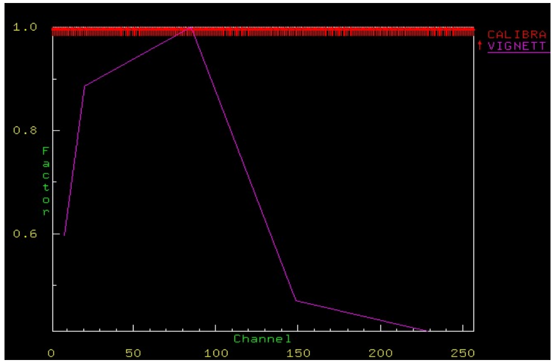

- Divide by vignetting function
- Least squares fit

→ T_i, $\omega_{Ni^{26+}}$, Ni concentration

Design and development for JET tokamak

‘Ni detector’:

PPF data production for He-like Ni spectra: finalized Nov 2013

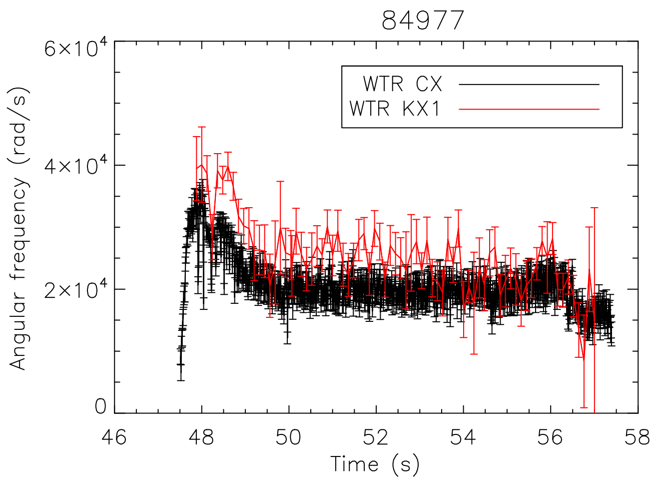

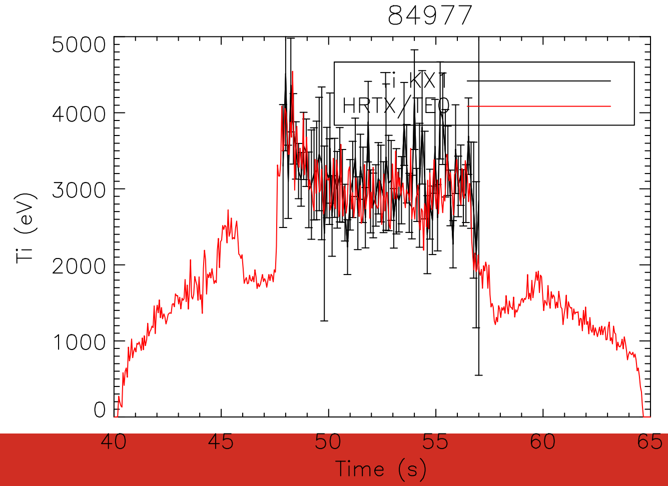

- KT2 data (Ni^{25+}) – only relative data - r/a = 0.3-0.5
- KX1 data (Ni^{26+}) - r/a ~ 0.2-0.4

CNC: ~ 10% underestimation due to escape peak from 2nd order of diffraction in 1st order

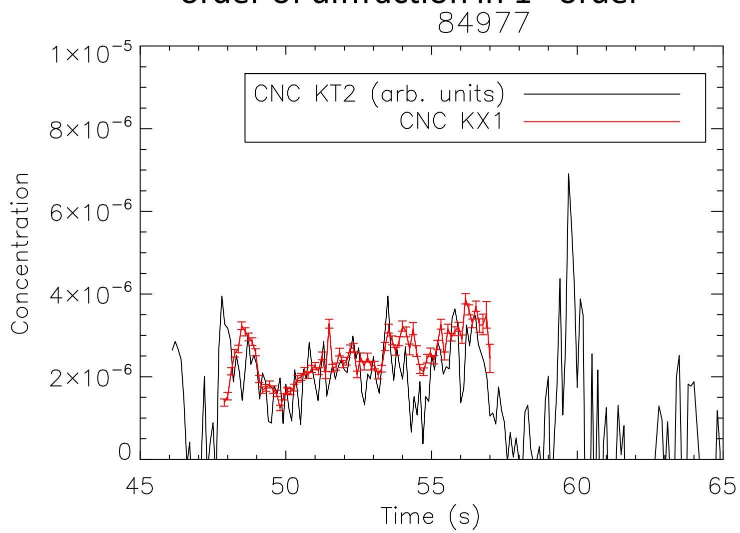

Private PPFs created for KX1 He-like Ni spectra for ion temperature, rotation frequency and Ni concentration. Reasonable agreement in trends with data from KS5, KT2 and HRTS.

Design and development for JET tokamak

‘W detector’:

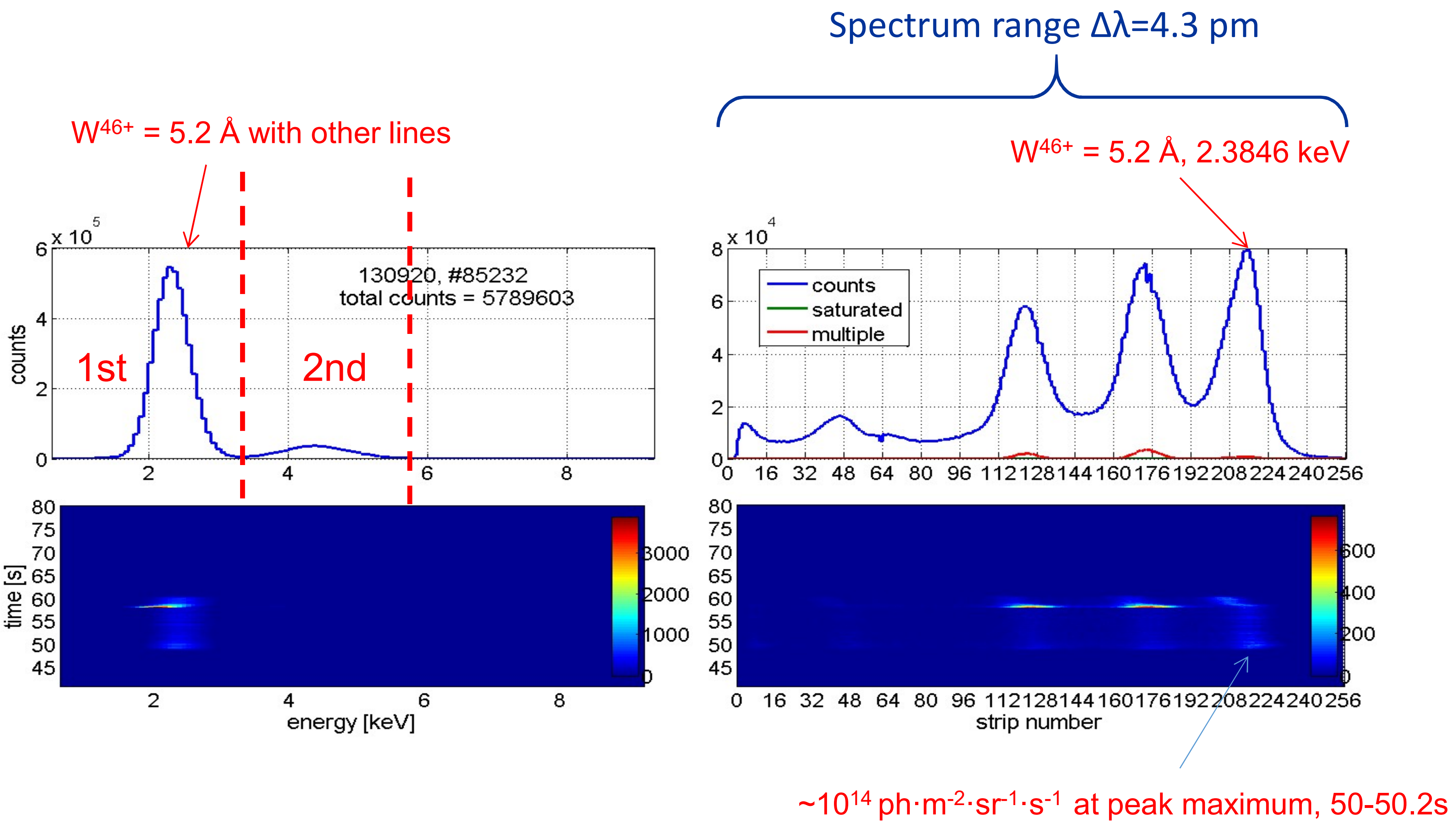

Design and development for JET tokamak

'W detector' spectra: line identification needed

crystal box potentiometer ➡ ~5.17-5.22 A, data with LBO

W LBO at 58 s

max T_e ~4keV

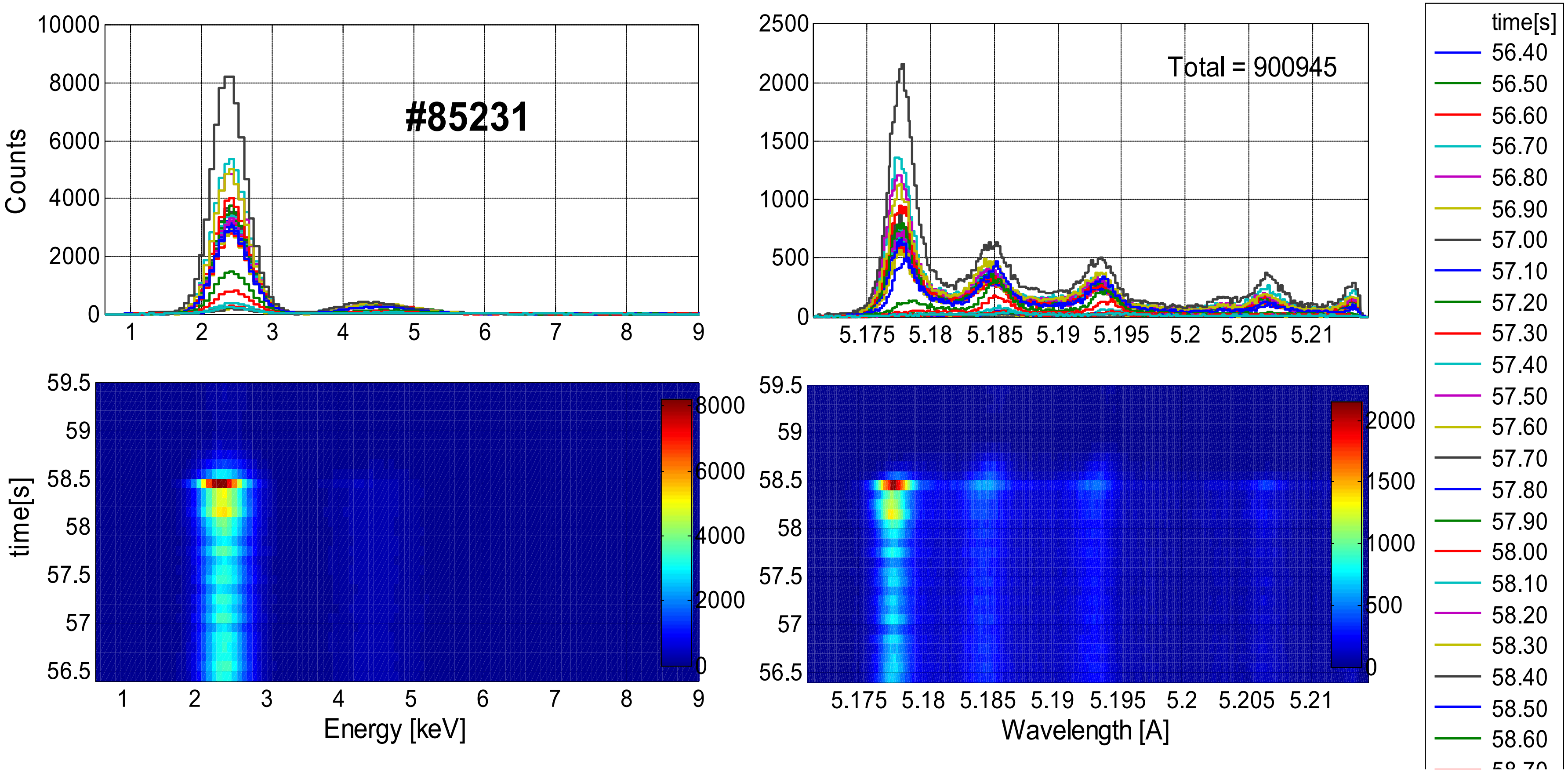

Design and development for JET tokamak

'W detector' spectra: line identification needed

crystal box potentiometer ➡ ~5.17-5.22 A, data with LBO

W LBO at 58 s

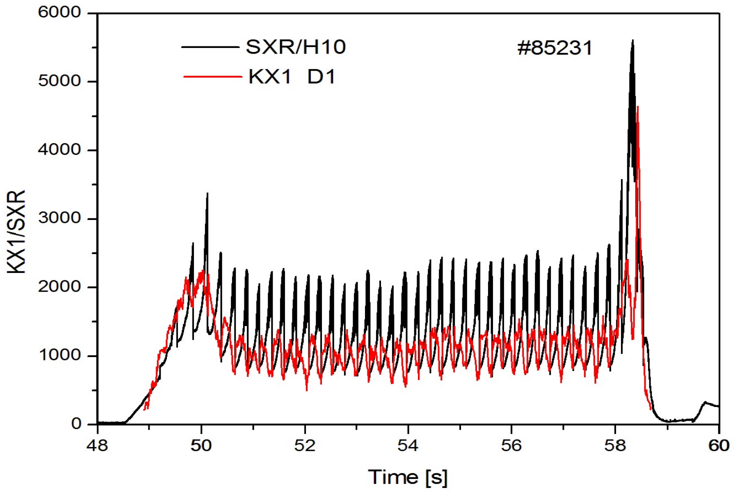

Peak area for W line (Voigt fit) vs time with a set of important parameters for #85231 discharge.

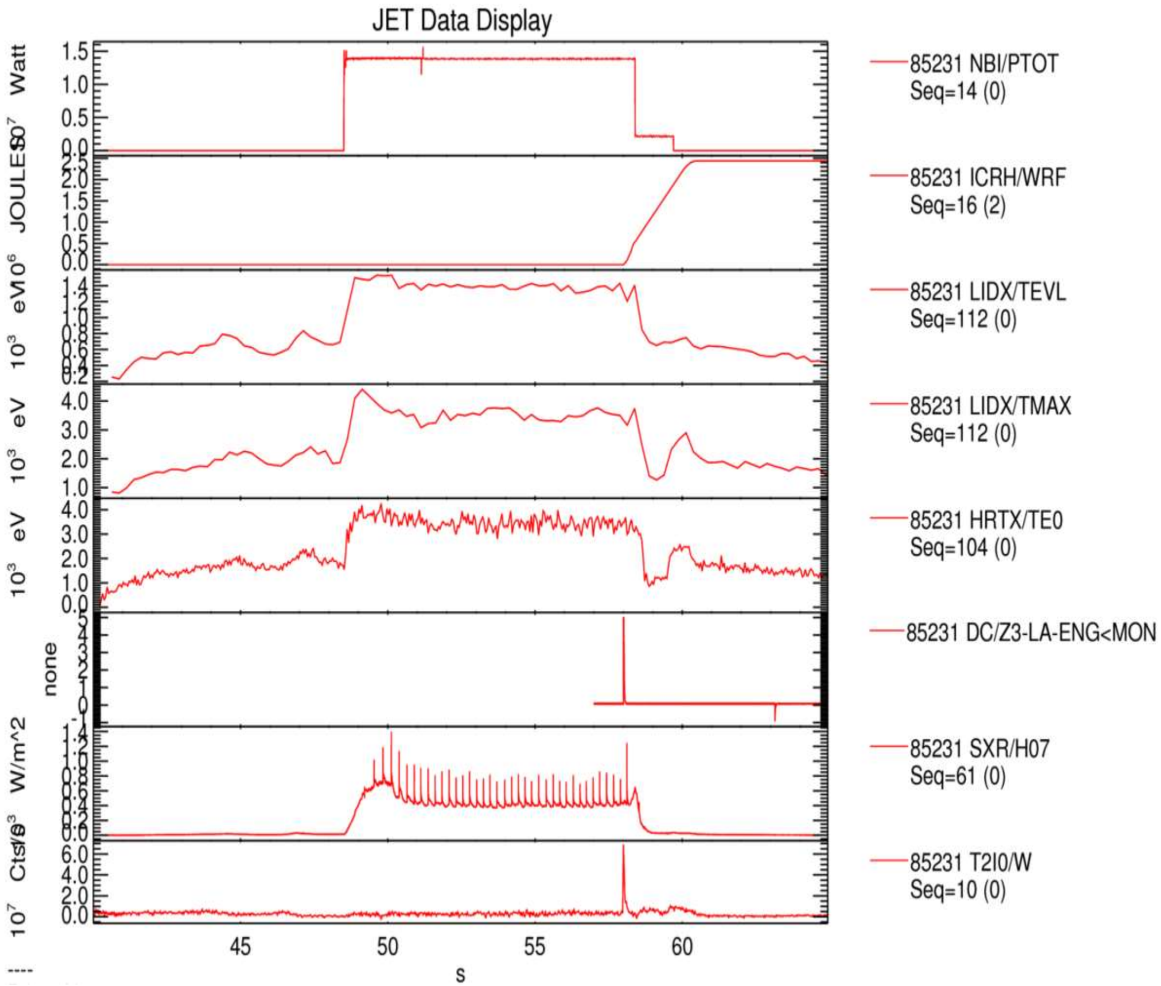

IFPiLM

Design and development for JET tokamak

'W detector' spectra: line identification needed

crystal box potentiometer ➡ ~5.17-5.22 A, data with LBO

Mo LBO at 58 s
max T_e ~4keV

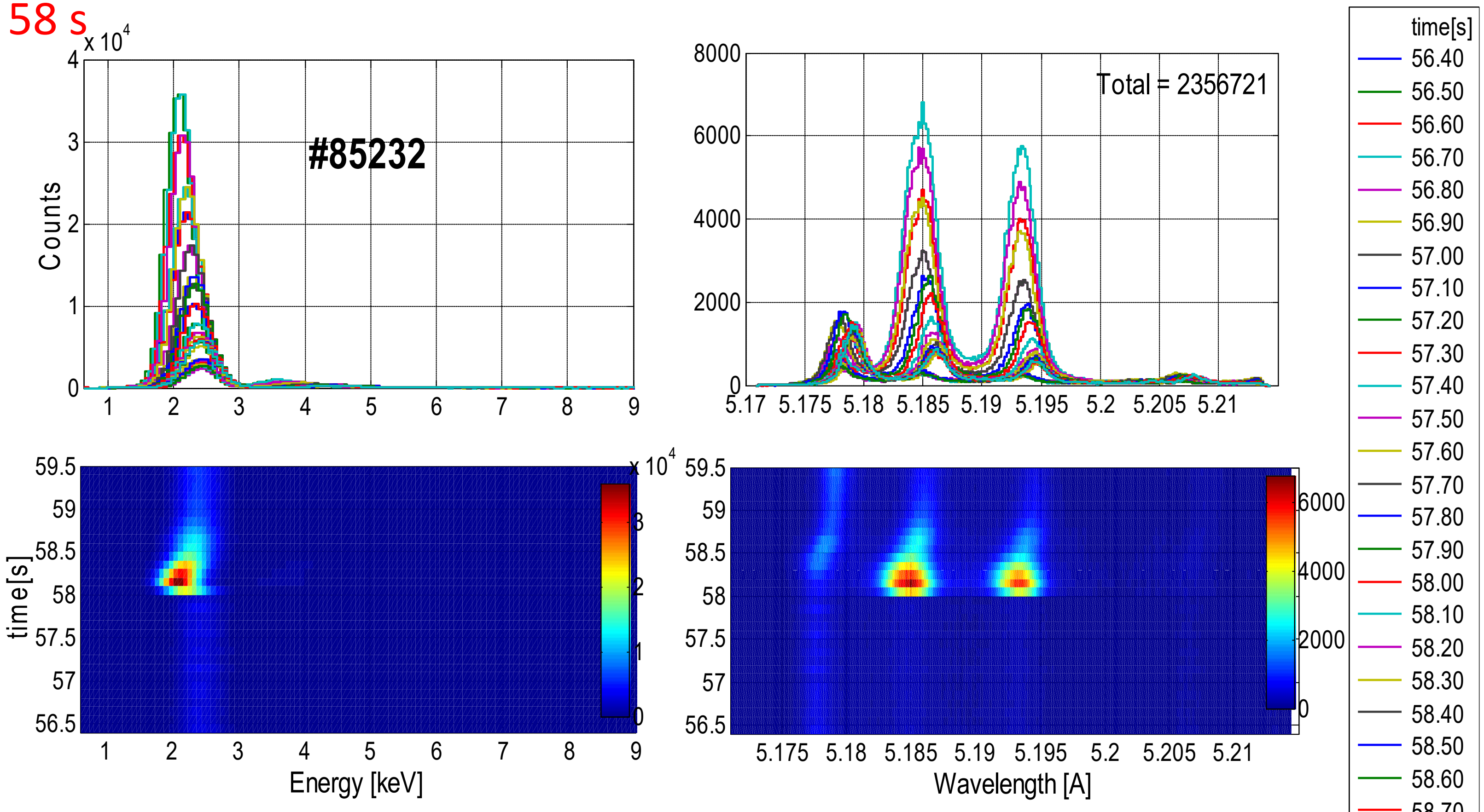

‘W detector’ spectra identification

Comparison of the experimental (circles) and theoretical (lines) spectra:

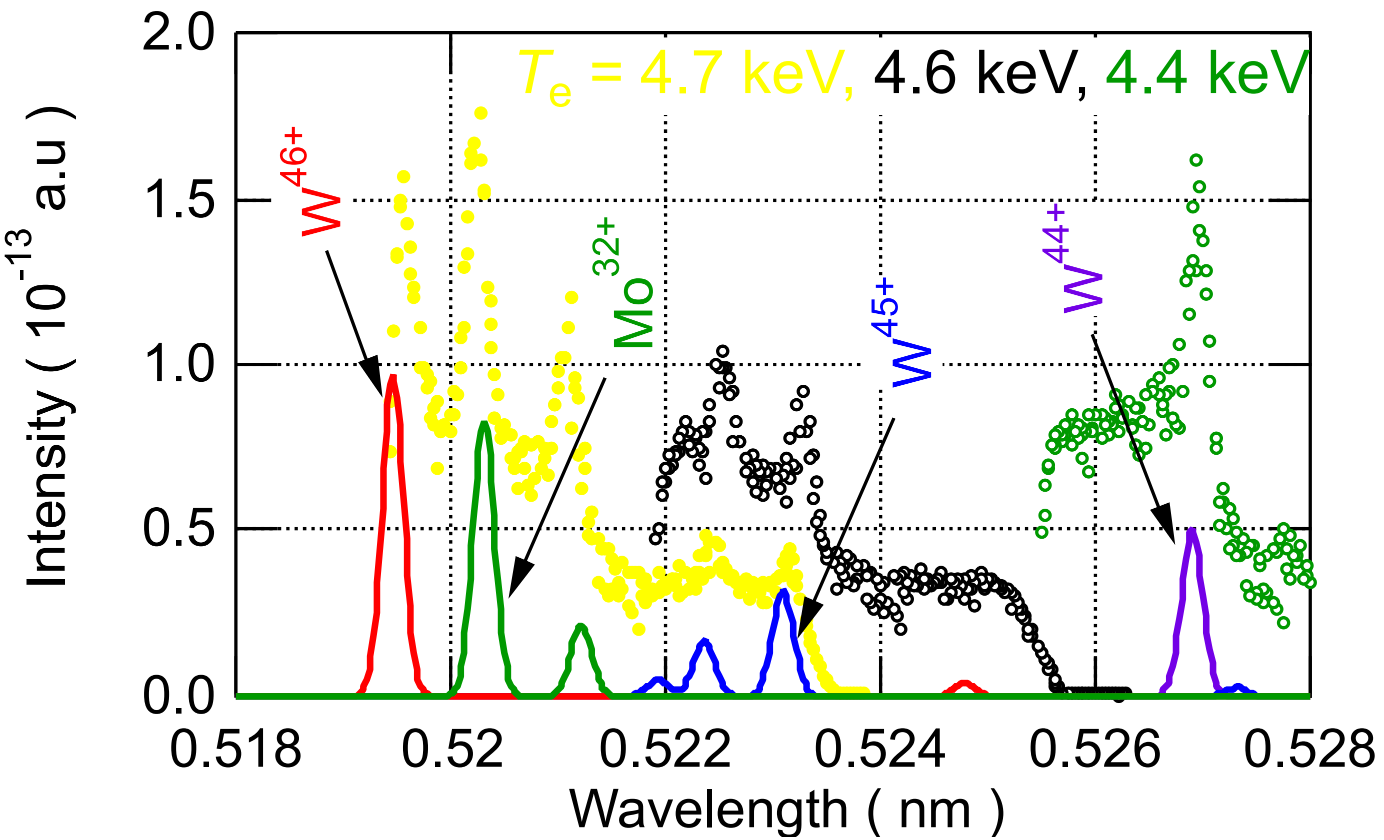

Mo and W lines can be measured simultaneously in the same detector!

T. Nakano et al., J. Phys. B: At. Mol. Opt. Phys. 48 (2015) 144023

Summary

- **The results are obtained** using the recently developed SXR diagnostics for the WEST project:
  - it was possible to collect calibrated data with **both spatial and spectral resolution,**
  - the **measured spectra represent the combined contribution from both SXR and high energy ionising radiation**, comparison with other WEST diagnostics shows good agreement in the trends,
  - in the present scenarios the system detects a sufficiently high energy part of X-rays and is sensitive to high ionising radiation,
  - measurements have been successfully performed on long pulses (up to and longer than 60 s), validation and commissioning of the diagnostics is underway;
- **Dev**elopment of **the radiation power** diagnostics for DEMO has started:
  - First simulations and analyses of its performance have been carried out,
  - Initial evaluation of the accuracy of the relative differences has been carried out,
  - The first **prototype** is on its way.
- **A 2D imaging system** using GEM technology based on advanced readout structure and optimised amplification stage geometry is in preparation;
- The detection part of **the high-resolution crystal spectrometer** in JET has been fully designed and built, in use from 2013 to the present/end of JET.